2007

All-optical Regeneration For Phase-shift Keyed Optical Communication Systems

Kevin Croussore
University of Central Florida

ALL-OPTICAL REGENERATION FOR PHASE-SHIFT KEYED OPTICAL COMMUNICATION SYSTEMS

by

KEVIN CROUSSORE

B.S. University of North Carolina at Charlotte, 2000
M.S. University of North Carolina at Charlotte, 2002

A dissertation submitted in partial fulfillment of the requirements
for the degree of Doctor of Philosophy in Optics
in the Department of Optics
in the College of Optics and Photonics
at the University of Central Florida
Orlando, Florida

Fall Term
2007

Major Professor: Guifang Li

ABSTRACT

All-optical signal processing techniques for phase-shift keyed (PSK) systems were developed theoretically and demonstrated experimentally. Nonlinear optical effects in fibers, in particular four-wave mixing (FWM) that occurs via the ultra-fast Kerr nonlinearity, offer a flexible framework within which numerous signal processing functions can be accomplished. This research has focused on the regenerative capabilities of various FWM configurations in the context of processing PSK signals. Phase-preserving amplitude regeneration, phase regeneration, and phase-regenerative wavelength conversion are analyzed and demonstrated experimentally.

The single-pump phase-conjugation process was used to regenerate RZ-DPSK pulse amplitudes with different input noise distributions, and the impact on output phase characteristics was studied. Experiments revealed a limited range over which amplitude noise could effectively be suppressed without introduction of phase noise, particularly for signals with intensity pattern effects.

Phase regeneration requires use of phase-sensitive amplification (PSA), which occurs in nonlinear interferometers when the pump and signal frequencies are degenerate (NI-PSA), or in fiber directly through single-stage (degenerate) or cascaded (non-degenerate) FWM processes. A PSA based on a Sagnac interferometer provided the first experimental demonstration of DPSK phase and amplitude regeneration. The phase-regenerative capabilities of the NI-PSA are limited in practice by intrinsic noise conversion (amplitude to phase noise) and to a lesser extent by the requirement to modulate the pump wave to suppress

stimulated Brillouin scattering (SBS). These limitations are relaxed in novel materials with higher SBS thresholds and nonlinearities. Degenerate FWM provides PSA in a traveling-wave configuration that intrinsically suppresses the noise conversion affecting the NI-PSA, while providing stronger phase-matched gain. Experiments confirmed superior phase-regenerative behavior to the NI-PSA with simultaneous reduction of amplitude noise for NRZ-DPSK signals.

Phase-regenerative wavelength conversion (PR-WC) provides the regenerative properties of PSA at a new wavelength, and was proposed and demonstrated for the first time in this research. The parallel implementation of two FWM processes, phase-conjugation and frequency conversion, provides two idlers which exhibit interesting and useful regenerative properties. These were investigated theoretically and experimentally. Ideal phase-regenerative behavior is predicted when the contributing FWM processes are equally phase-matched, which can be maintained over any interaction length or wavelength shift provided the pump powers are properly adjusted. Depleted-pump regime PR-WC provides simultaneous phase and amplitude regeneration. Experiments confirmed regenerative behavior for wavelength shifts of the idlers up to 5 nm.

Two techniques for phase regeneration of 4-level PSK signals were developed and evaluated. The first is based on parallel operation of PSAs suitable for processing 2-level PSK signals, where phase projection and regeneration are combined to recover the input data. Analysis of this scheme outlined the conditions required for effective phase regeneration and for practical implementation using known PSAs. A novel process based on FWM (parallel

phase-conjugation followed by PSA) was developed and analyzed, and demonstrated using numerical simulations. These studies provide a basis for further work in this area.

ACKNOWLEDGMENTS

I would like to acknowledge my advisor, Dr. Guifang Li, for providing an exceptional learning environment. Throughout my tenure as a graduate student I was afforded continuous support, patience and honesty, and given opportunities for personal and academic advancement that are unsurpassed in my experience.

It has been particularly rewarding to work with members of the OFC group. All of those who have come and gone and who still remain are excellent scientists and colleagues, and all have at one time or another made important contributions in this experience. I would especially like to acknowledge contributions to my work from Dr.'s Inwoong and Cheolhwan Kim, whose assistance in the lab has been invaluable. Particular thanks also go to Gilad Goldfarb, with whom I engaged in colorful discussions which were often animated, always rewarding and fruitful, and always served to refresh our collective sanity.

The greatest debt of gratitude is owed to my wife LaShaunda, who has endured the past five years without loosing sight of the greater goals in our lives. Her continuous love and support has been my source of strength, stability and purpose, and I love her very much. Finally, but not least, I am forever indebted and grateful to my parents. They long ago gave up asking 'how much longer,' but never wavered in their support, love or understanding.

TABLE OF CONTENTS

LIST OF FIGURES

LIST OF ACRONYMS AND ABBREVIATIONS

2R	Re-amplify, re-shape
3R	Re-amplify, re-shape, retime
All-R	Re-amplify, re-shape, retime, re-phase
AN	Amplitude noise
AR	Amplitude regeneration
ASE	Amplified spontaneous emission
Bi-HNLF	Bismuth-oxide-based highly-nonlinear fiber
BPSK	Binary phase shift keying
BS	Bragg-scattering
CD	Coherent detection
CP(P)R	Carrier phase (and polarization) recovery
CSRZ	Carrier-suppressed return-to-zero
CW	Continuous wave
CPM	Cross-phase modulation
DD-PLL	Decision-driven phase lock loop
DFWM	Degenerate four-wave mixing
DPSK	Differential phase shift keying
DSF	Dispersion shifted fiber
DSP	Digital signal processing
DWDM	Dense wavelength division multiplexing
EDFA	Erbium-doped fiber amplifier
FBG	Fiber Bragg gratings

FC	Frequency conversion
FOPA	Fiber optical parametric amplifier
FWM	Four-wave mixing
Gb/s	Giga bit per second (Giga = 10^9)
GHz	Gigahertz (=10^9 Hz)
HNLF	Highly nonlinear fiber
LO	Local oscillator
NDFWM	Non-degenerate four-wave mixing
NF	Noise figure
N(F)I	Nonlinear (fiber) interferometer
NLPN	Nonlinear phase noise
nm	Nanometer (10^{-9} meters)
MZI	Mach-Zehnder interferometer
NOLM	Nonlinear optical loop mirror
NRZ-BPSK	Non-return-to-zero Binary phase shift keying
NRZ-DPSK	Non-return-to-zero differential phase shift keying
OEO	Optical-electronic-optical
OOK	On-off keying
OPO	Optical parametric oscillator
OSNR	Optical signal-to-noise ratio
OTDM	Optical time-division multiplexing
PC	Phase-conjugation
PN	Phase noise

PLL	Phase-locked loops
PRBS	Pseudo-random binary sequence
PSA	Phase sensitive amplifier
PSG	Phase-sensitive gain
PSK	Phase shift keying
PSO	Phase-sensitive oscillator
PPAR	Phase-preserving amplitude regeneration
PR	Phase regeneration
PR-WC	Phase-regenerative wavelength conversion
QPSK	Quadrature phase shift keying
RFSA	Radio-frequency spectrum analyzer
RZ-DPSK	Return-to-zero differential phase shift keying
SBS	Stimulated Brillouin scattering
SNR	Signal-to-noise ratio
SOA	Semiconductor optical amplifier
SPM	Self-phase modulation
SP-PSA	Symmetric-pump phase-sensitive amplifier
SSMF	Standard single-mode fiber
WDM	Wavelength division multiplexing

CHAPTER ONE: INTRODUCTION

1.1. Historical Perspective

Optical fiber communications systems form the backbone of the global telecommunications network. In the late 1970s fiber transmission systems operating in the 800 nm wavelength region began replacing aging microwave systems that operated with gigahertz carrier frequencies. The push to use optical frequency carriers (terahertz waves) was driven by the ever present demand for increased information capacity, and enabled by two key technologies that were realized nearly simultaneously: optical fibers with per-kilometer losses less than 20 dB in the wavelength region near 1 μm were developed [1], providing a suitable transmission medium, while Gallium Arsenide (GaAs) semiconductor lasers provided a cost-effective, compact optical source [2]. These developments provided the first real impetus for a global expansion of fiber optic networks [3], however the maximum transmission distance was limited by fiber loss and detector sensitivity to around 10 km. This required spacing electronic repeaters (optical-electronic-optical, or OEO regenerators) every 10 km to bridge longer transmission distances. A transition to the lower loss window near 1.3 μm (loss < 1 dB/km) was enabled by development of InGaAsP diode lasers and detectors. Along with realization of single mode optical fibers to eliminate the problem of modal dispersion, this allowed transmission distances to expand to about 50 km with data rates approaching 2 Gb/s [4]. Transmission distances were still fundamentally limited by the fiber loss, which was pushed to a minimum of about

0.2 dB/km near 1.5 μm [5]. A transition to this operating window was delayed by the relatively large fiber dispersion, which was an issue due to the large spectral width of early transmitter lasers. Development of narrow-linewidth sources and dispersion shifted fibers (with reduced dispersion near 1.5 μm) eventually allowed transmission of data rates approaching 10 Gb/s over nearly 100 km [6]. With fiber loss effectively minimized, there was initially a push to develop coherent detection technologies, which would improve receiver sensitivity and increase repeater spacing. However commercialization of the erbium doped fiber amplifier (EDFA) in 1990 removed the immediate need for more complex detection schemes. OEO repeaters spaced every 60-70 km were replaced by more simple and cost-effective EDFAs, removing fiber loss as a limitation to transmission distance [7]. The advent of the EDFA, with its amplification bandwidth of nearly 40 nm, also enabled the broad transition from single to multi-channel (wavelength division multiplexed, or WDM) systems and an associated rapid growth of transmission capacity. By the year 2000, commercial systems with 1.6 Tb/s total capacity were deployed using 10 Gb/s data rates [7], while research systems could reach 11 Tb/s over limited transmission distances [8]. With an increase of the per-channel data rate to 40 Gb/s, the total capacity (at a commercial level) was expanded to 6.4 Tb/s shortly thereafter.

WDM systems push for higher information capacity through diverse techniques. The initial approach of simply increasing the channel count adds considerable complexity at each network site that requires signals to be separated and processed independently, as is the case for OEO repeaters.

However WDM systems have progressively moved to reduced channel spacings and higher channel counts, and new amplification techniques such as Raman have been studied to open transmission windows outside the conventional (C-band) window that ranges from 1530 to 1570 nm. Such systems could potentially support thousands of WDM channels ranging in wavelength from 1300 to 1700 nm where fiber loss remains consistently below 1 dB/km [7]. While exploitation of the entire fiber bandwidth may eventually be required to reach the ultimate system capacity, the dramatic increase in complexity associated with management of so many wavelengths on a single fiber has recently prompted other avenues of research aimed at increasing the per-channel symbol rate and spectral efficiency.

Per-channel bit rates have increased from 10 Gb/s to 40 Gb/s in commercial systems, and the use of optical time division multiplexing (OTDM) has produced aggregate channel symbol rates of 160 and 320 Gb/s [9, 10]. Such systems rely, at the commercial level, primarily on intensity modulation (IM, referred to as on-off-keying or OOK) to transmit information, although recent commercial systems and a number of research-level systems have used phase-shift keyed (PSK) signals. Currently, 40 Gb/s direct intensity modulation of semiconductor transmitter lasers is feasible for dense WDM applications. Higher pulse rates are possible using mode-locked semiconductor or fiber lasers (beyond 80 GHz), although direct modulation beyond 40 Gb/s is currently difficult.

An alternative to simply increasing the symbol rate is the use of multi-level modulation to increase the bit rate. In addition to IM, the phase and polarization of light may also be modulated in an information-bearing manner to transmit more than one bit per symbol. Although two or more parameters can be modulated simultaneously, the most straightforward techniques rely on increasing the number of modulation levels of a single parameter. Recently both 4- and 8-level PSK transmission have been successfully demonstrated with record spectral efficiencies of 2 b/s/Hz or greater [11, 12]. Spectrally efficient transmission offers other benefits, including better tolerance to fiber chromatic and polarization mode dispersion [13] due to the reduced spectral width, at the expense of more complex transmitter and receiver structures.

The drive to increase system capacity is always balanced against the need to transmit information over reasonable distances, ranging from hundreds of kilometers for metropolitan networks to tens of thousands of kilometers for ultra-long haul applications, such as trans-oceanic. Compensation of fiber loss through amplification inherently degrades the signal-to-noise ratio (SNR) through addition of spontaneous emission noise. Signals with faster symbol rates are less tolerant to both chromatic and polarization mode dispersion because of closer symbol proximity in the time domain. Dispersion management using dispersion compensating fiber is a well established technique for handling chromatic dispersion, but at symbol rates of 40 Gb/s and above polarization mode dispersion becomes a serious issue [14, 15]. Additionally, nonlinearities seeded by random amplifier noise become significant when the total transmission

distance ranges in the thousands of kilometers. Of particular importance are four-wave mixing (FWM) between neighboring WDM channels, intra-channel self-phase modulation (SPM) and inter-channel cross-phase modulation (CPM). The latter impairments are most important for PSK signals, while FWM inhibits transmission of both OOK and PSK signals. More advanced modulation formats, particularly those that combine for example amplitude and phase shift keying, are inherently less tolerant to noise and nonlinear impairments. Ultimately, the OEO repeater spacing in a transmission link is determined by these factors. Fiber systems deployed to this point continue to rely on such electronic regenerators.

1.2. Differential Phase-Shift Keying Transmission

Over the past few years, WDM systems based on OOK have reached record capacities with innovations such as forward error correction (FEC), distributed Raman amplification (with lower noise figure than EDFAs) and more advanced, dispersion managed fibers [16]. However research has shown other modulation formats, in particular binary or differential phase-shift-keying (BPSK or DPSK), offer superior transmission characteristics in certain regimes of operation. DPSK can tolerate a 3-dB lower optical signal to noise ratio (OSNR) than OOK, because the separation of the “on” and “off” states is intrinsically increased. Figure 1.1 shows a simplified schematic of the OOK and DPSK signal constellations and receiver implementations. For the same average power, the peak power of each DPSK pulse is lower by 50% while the binary symbols are spaced further apart by a factor $\sqrt{2}$. For DPSK with balanced detection, this

factor alone should double the reach of a transmission system because of the enhanced tolerance to amplifier spontaneous emission noise [16]. Additionally, it is evident from Figure 1.1 that the decision threshold for DPSK remains independent of the average received power, rendering DPSK with balanced detection less sensitive to slow signal power fluctuations.

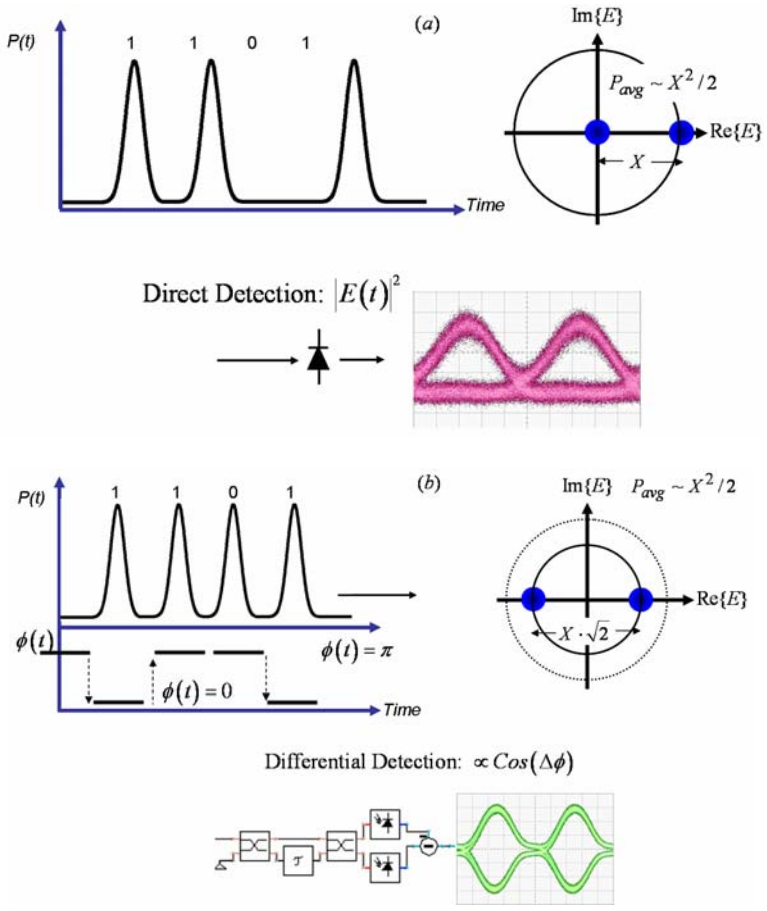

Figure 1.1. Signal constellations and receiver implementations. (a) OOK and (b) DPSK with balanced detection.

Fiber nonlinearities play a prominent role in determining which modulation format is superior under specific system configurations. Important nonlinearities are inter-channel FWM, SPM and CPM, and intra-channel FWM and CPM.

Careful management of fiber dispersion and channel separation can usually be used to reduce the effects of inter-channel FWM in both OOK and DPSK systems [17]. However both SPM and CPM play important roles and affect OOK and DPSK signals differently. In single-channel 10G systems, SPM combines with dispersion to broaden both OOK and DPSK pulses. DPSK signals suffer an additional penalty in the form of nonlinear phase noise (NLPN), whereby intensity fluctuations are converted to phase fluctuations through the fiber's Kerr nonlinearity (the so called Gordon-Mollenauer effect) [18-20]. CPM combined with intensity noise causes an additional penalty of this form for DPSK signals [21-23], while leading to timing jitter when combined with dispersion for OOK signals (for DPSK, the nearly constant per-channel amplitude largely mitigates the primary CPM effect of timing jitter [24-27]). Depending on system parameters (e.g. launch power per span, optical filtering bandwidth), OOK can out-perform DPSK in single-channel, long haul communications systems due to the susceptibility of DPSK to Gordon-Mollenauer phase noise [28]. In WDM systems with narrow channel spacings, DPSK will usually out-perform OOK due to its robustness to the primary effects of inter-channel CPM [28, 29]. At higher bit rates intra-channel nonlinearities (FWM and CPM) limit transmission of both OOK and DPSK [30]. Intra-channel FWM between pulses with the same spectrum produces both amplitude and phase fluctuations, while CPM leads to phase modulation dependent on the pulse amplitudes. For both OOK and DPSK timing jitter results (when combined with dispersion), while DPSK also suffers from induced phase fluctuations (in the presence of pulse to pulse intensity

fluctuations. However the more even power distribution of DPSK compared to OOK serves to reduce the effects of intra-channel nonlinearities [31]. There is also evidence that the induced nonlinear phase shifts for DPSK can be partially correlated, leading to reduced penalties when differential detection is employed [32]. Experiments have consistently shown that at 40G data rates DPSK out-performs OOK in both single channel and WDM implementations [16]. In fact, in certain regimes, the sensitivity improvement of DPSK compared to OOK can be as much as 5 dB [33]. These realizations have cemented DPSK as a choice for long-haul networking applications and led to a surge of interest in associated technologies, including optical signal processing and regeneration.

1.3. All-Optical Regeneration

1.3.1. Review

Fiber-based light wave communications systems suffer from impairments that limit the un-regenerated transmission distance. Among these are amplified spontaneous emission noise, chromatic and polarization-mode dispersion, and nonlinear effects such as FWM, SPM and CPM, and intra-channel FWM and CPM (IFWM and ICPM). Nonlinearity-induced impairments are seeded by amplifier noise and dispersion, which produce random and pattern-dependent noise, respectively. Nonlinear processes also combine with dispersion to produce timing jitter, which is an important factor in both OOK and PSK systems. Dispersion can be managed through use of DCF, but other transmission penalties require more complex solutions. Despite the fact that WDM systems

may now span trans-oceanic distances without OEO regeneration, this process is still required in many instances, especially when signals pass through several networking nodes during transmission. OEO regeneration is inherently a parallel process, in which the entire set of channels must be demultiplexed, detected and re-transmitted, possibly with new wavelength allocation. This leads to enormous complexity and cost as the total number of channels increases, providing the motivation for reducing the channel count and increasing the bit rate.

An alternative to electronic regeneration, and to electronic signal processing in general, is to keep signals in the optical domain throughout transmission. In the past few years all-optical signal processing and regeneration have received considerable attention. Among the potential benefits of all-optical networking are elimination of expensive, complex and power-consuming WDM receiver and transmitter units (required for OEO regeneration), transparency of the system to the bit rate, amplitude, wavelength and modulation format, and little or no latency because of the removal of time-consuming OEO conversion [34, 35]. Additionally, some implementations of all-optical regeneration may offer the prospect of multi-channel operation, which is not possible using OEO regeneration [36]. Figure 1.2 compares OEO and all-optical regeneration schemes. Many signal processing functions (wavelength conversion, switching, optical labeling and erasure and data storage or buffering) will have to be developed in order to build truly transparent optical networks, and considerable research has gone into these areas.

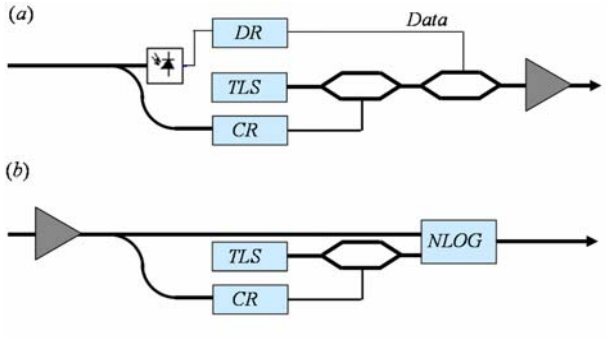

Figure 1.2: Comparison of OEO (a) and all-optical (b) regeneration.

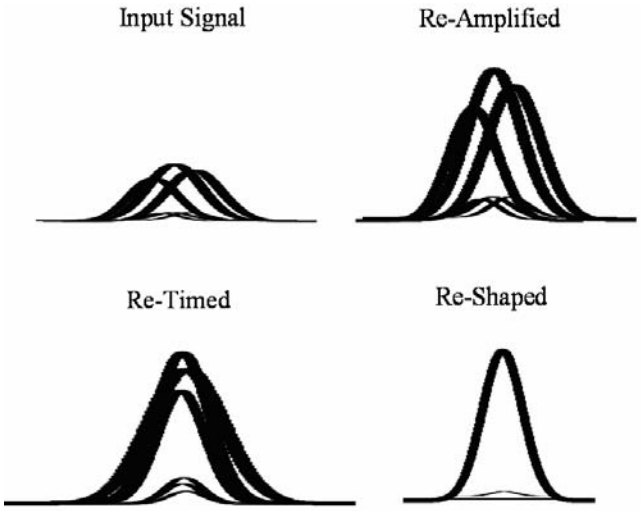

Figure 1.3: All-optical regeneration for OOK.

All-optical regeneration refers to restoration of signal properties to the initial state at the transmitter. For OOK signals, this entails amplification, restoration of the pulse shape, removal of noise in “0’s”, and equalization of pulse amplitudes (called re-shaping) and removal of accumulated timing jitter (re-timing). A regenerator providing all three functionalities is called an optical 3R regenerator. Figure 1.3 shows an OOK signal at the various stages of the all-optical regeneration process. The degraded signal is first amplified, and then

divided so that an optical clock can be extracted through an electronic or all-optical process as shown in Figure 1.2(b). The resulting clock is used to drive a nonlinear optical gate that provides the pulse re-shaping (noise suppression) functions; use of the re-timed clock removes timing jitter. Several factors determine how well a particular regeneration process will function in a system, including regenerated pulse width (which can usually be tailored through proper clock generation) and the introduction of chirp.

Because of the initial dominance of OOK in WDM system demonstrations, OOK regeneration was studied extensively over the past two decades. All aspects of all-optical regeneration for OOK have been successfully demonstrated, although no single technology has emerged as the dominate candidate for use in next generation, all-optical networks. Most of the wide range of devices and processes employed can be loosely divided into two categories. Those based on semiconductor technology (usually semiconductor optical amplifiers (SOAs), electro-absorption modulators (EAMs) and saturable absorbers, or SAs) rely on cross-gain modulation (XGM), CPM, FWM and nonlinear polarization rotation (NLPR) [37]. Semiconductor-based devices have been used to successfully demonstrate high speed all-optical clock recovery [9, 35, 36, 38-40] as well as full 3R regeneration, at bit rates up to 80 Gb/s [35, 36, 41-44]. It can be argued [35, 45] that the possibility of building a fully integrated, 3R regenerator on a single silicon structure makes the semiconductor technology preferable. However speed limitations of SOAs open the door to hybrid

(semiconductor and fiber) as well as ultra-fast all-fiber devices relying on the Kerr nonlinearity, with femtosecond response times.

Considerable research has gone into developing fiber-based devices for optical signal processing and regeneration. Although the material nonlinearity of fused silica fiber is small (n_2 = 2.2 – 3.4 x 10^{-20} m^2/W), the strong confinement combined with long interaction lengths allows for efficient nonlinear interactions, provided phase-matching can be achieved. Clock recovery and generation of re-timed pulses has been achieved in fiber directly using techniques such as active mode-locking [46-53], at both sub-harmonic (for OTDM systems) and aggregate line rates. The remaining regeneration functions of extinction ratio improvement and pulse amplitude equalization have been demonstrated through several effects. Fiber optical parametric amplifiers (FOPAs) operating in the depleted pump regime exhibit nonlinear (input-output signal) power transfer functions suitable for simultaneously improving the extinction ratio (ER) and equalizing pulse amplitudes. Level equalization was studied first by Inoue [54, 55], through measurement of the power transfer function. Later experiments showed advantages of using higher order FWM products as the regenerated output [56-60], effectively combining regeneration with wavelength conversion, and investigated use of a two-pump FOPA configuration [57, 58]. Alternative implementations include using the noisy data as the pump and achieving regeneration through a combination of FWM and SPM-induced spectral broadening [61, 62], and selecting the pump as the regenerated output, which produces data inversion [63].

An important class of 2R regenerators is based solely on SPM-induced spectral broadening combined with offset spectral filtering, first proposed by Mamyshev [64] and subsequently analyzed and demonstrated by others [65-68]. This technique offers relatively small signal quality improvements, but has the advantage of simplicity and the potential for multi-wavelength operation [69-71]. Several improvements to the scheme have been proposed, including bi-directional operation in a fiber loop [72] and addition of a saturable absorber to increase ER improvement [73, 74]. A variety of other fiber-based regenerators have been demonstrated based on several effects, including CPM-induced nonlinear polarization rotation [75], synchronous modulation [46], CPM-induced wavelength translation [76] and using nonlinear Sagnac interferometers [77, 78].

1.3.2. Regeneration of DPSK Signals

Phase shift keyed signals are degraded by the addition of linear phase noise (arising from ASE, modulation imperfections and dispersion) and nonlinear phase noise that arises from nonlinearities (SPM and CPM). Neglecting effects of timing jitter, these pose the fundamental limit to DPSK transmission length [79]. In un-regenerated systems NLPN, which is seeded by amplitude noise from ASE, dispersion and FWM, produces cubic growth of the phase noise variance with distance [22]. Owing partly to the differential nature of the detection process, DPSK is somewhat insensitive to accumulated amplitude noise at detection; however it is clear the amplitude noise must be managed in order to restrict growth of NLPN. In addition to the functionalities previously mentioned for

OOK regeneration, an all-optical regenerator for DPSK signals must restore encoded differential phase shifts (phase regeneration). All-optical regeneration of a DPSK signal is summarized in Figure 1.4. The robust performance of PSK systems comes with a price in terms of complexity: the most successful regeneration techniques to date (those discussed in this research) require carrier phase and polarization recovery (CPPR) in order to generate optical pumps that can be phase-locked to the incoming signal, for operation of the nonlinear-optical gate.

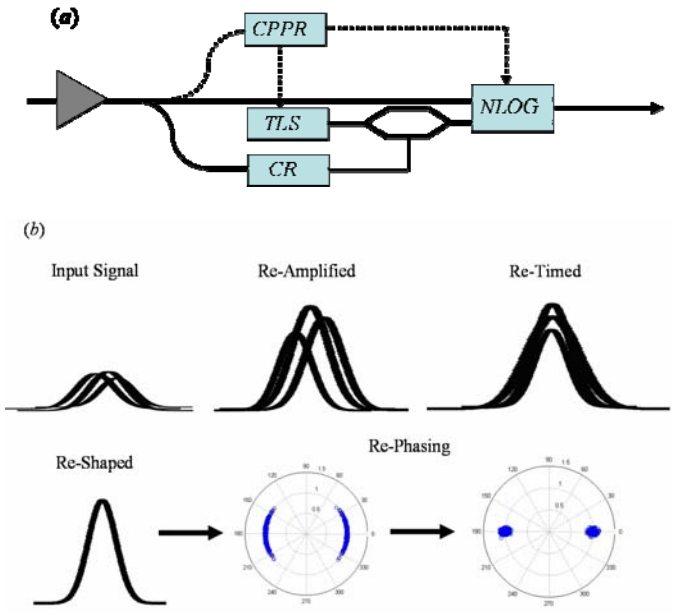

Figure 1.4: Phase and amplitude regeneration for DPSK signals. (a) Circuit diagram. CPPR: carrier phase and polarization recovery. The NLOG must perform re-phasing as well as the usual 3R re-shaping. (b) Depiction of pulses at various stages of regeneration. The re-phasing process is represented using polar plots.

Following the technique of dispersion management using dispersion-compensating fibers, nonlinearity management based on use of materials with

negative nonlinear coefficients was proposed as a means to compensate nonlinear processes in fiber transmission systems [80, 81]. Thus far, such techniques have not been deployed. An alternative for compensation of accumulated phase jitter is spectral inversion through phase conjugation [82, 83]. For effective nonlinearity compensation PC should be applied at the midpoint of a symmetric transmission system, rendering this technique most suitable for single long-haul links rather than networks in which the transmission distance can change depending on routing. Additionally, PC shifts the entire spectrum, which may be unsuitable for some WDM applications. Post-transmission nonlinear phase shift compensation has been implemented using data driven phase modulation [84-87]. Experimental results showed effective compensation of nonlinear phase noise from SPM in single-channel systems, where the received pulse amplitude is a good indicator of the accumulated phase shift. However operation in multi-channel systems is impaired by effects of FWM and CPM, and in single-channel systems linear contributions to phase noise persist.

One approach to regenerating the phase of DPSK signals is to convert the phase noise into amplitude noise, and then perform less complex amplitude regeneration. A suitable method for all-optical phase encoding must then be employed. In a first experiment, a SOA was placed asymmetrically in a Sagnac interferometer that followed standard DPSK demodulation [88, 89]. Later analysis confirmed the reduction of differential phase noise was due to phase noise averaging, which improves correlation of neighboring phase shifts [90]. The averaging, and thus phase regeneration, is thus performed initially where the

pulse train is demodulated, while subsequent amplitude regeneration prevents this averaging from being destroyed when the pulse trains are re-combined to recover the original, phase-modulated data. Phase noise averaging based on phase-sensitive amplification has also been proposed [91]. Analysis has shown the maximum reduction of phase noise variance is ½ [90].

Other approaches involve amplitude regeneration of the complimentary OOK pulse trains created by DPSK demodulation, followed by all-optical phase modulation [92]. This technique has not been implemented experimentally.

Phase-regenerators based on amplitude regeneration require a method of phase-preserving amplitude regeneration (PPAR). The most promising techniques studied for OOK regeneration (for example those based on SPM combined with filtering) intrinsically distort phase information, however those based on gain saturation in FWM do not [93, 94]. Phase-preserving amplitude regenerators are also useful for suppression of the build up of nonlinear phase noise [95-97]. Besides FWM, PPAR has been proposed (but not demonstrated) using a modified NOLM [98] and using CPM-induced spectral broadening combined with offset filtering [99]. In this work, PPAR based on gain saturation in FWM is studied experimentally [100], with particular attention paid to introduction of nonlinear phase noise during the regeneration process.

The most effective means for suppression of phase noise in DPSK systems is provided by phase-sensitive amplification. PSAs have been proposed [101] and demonstrated experimentally [102] to provide simultaneous phase and

amplitude regeneration for RZ-DPSK signals. Later research demonstrated phase noise reduction of NRZ-DPSK signals as well [103].

1.4. Statement of Dissertation

This Dissertation presents analytical and experimental studies of regeneration techniques for PSK systems. Unlike phase noise management schemes that must be deployed in well-defined, symmetric systems, regenerative devices are more suitable for flexible deployment. These should offer good performance over a range of input signal conditions, allowing them to be placed in both long-haul links as well as at networking sites. Four distinct areas were addressed.

1.4.1. Phase-Preserving Amplitude Regeneration

Several regeneration techniques proposed after the first demonstration of PSA for phase regeneration require use of phase-preserving amplitude regenerators. However an extensive experimental study of these devices was lacking, although preliminary research had been conducted. Of particular interest is the amount of input amplitude noise the device can tolerate without significant introduction of nonlinear phase noise, arising through SPM and CPM. Phase-preserving amplitude regeneration using gain saturation in FWM was studied experimentally, using different noise distributions. The results suggest a limited range of input signal amplitude noise over which the penalty resulting from NLPN is negligible [100].

1.4.2. Phase regeneration of DPSK signals

The most fundamental advance towards an all-optical DPSK network is the realization of optical phase regeneration. Prior to the present research, this topic was addressed in a limited manner. Realization of previous nonlinearity management schemes does not mitigate the requirement for flexible optical phase regenerators. This research has demonstrated use of PSAs, in different implementations, as an effective means of DPSK phase. It has also shown that the PSA can simultaneously provide amplitude regeneration and pulse re-shaping [101-104].

1.4.3. Phase-Regenerative Wavelength Conversion

A key function for optical networks is wavelength conversion (WC), which can eliminate wavelength blocking. Generally wavelength conversion degrades signal quality due to the introduction of noise. A suitable method of WC that can improve signal quality would therefore be beneficial. In this research a novel phase-regenerative wavelength conversion process based on an existing PSA architecture was investigated. The results obtained provide the first conclusive demonstration of phase-regenerative wavelength conversion and open the door to further studies based on the same technique.

1.4.4. Regeneration of Quadrature-Phase-Shift-Keying Signals

A QPSK signal carries twice the information of DPSK at the same symbol rate. However all-optical processing becomes more complicated because of the need

to preserve more complex phase information. The phase-regeneration techniques discussed previously apply solely to DPSK (or BPSK) signals, but they provide a basis for studying phase regeneration of QPSK signals. Two methods for QPSK regeneration were analyzed and evaluated for their practical realization, expanding on the principles of DPSK phase regeneration.

1.5. Outline of Dissertation

This dissertation is organized as follows. In Chapter 2 phase-preserving amplitude regeneration of DPSK using FWM in fiber is studied experimentally. Chapter 3 introduces phase sensitive amplification, offers a brief historical perspective and reviews previous work within the field. Particular attention is paid to recent work relevant to all-optical communications. Chapter 4 presents RZ-DPSK phase and amplitude regeneration using a PSA based on a nonlinear fiber interferometer (NFI). Both simulations and experiments are reviewed. Chapter 5 provides a brief review of theory and the experimental demonstration of NRZ-DPSK phase regeneration followed by combined phase-and-amplitude regeneration using a PSA based on FWM in fiber directly. Performance of these two PSA implementations is briefly compared. In Chapter 6 phase-regenerative wavelength conversion using parallel FWM processes in a single stage is first developed analytically and then demonstrated experimentally. The unique properties of this process are elucidated. Chapter 7 extends the concept of PSK regeneration to quadrature-phase-shift keyed (QPSK) signals and reviews two

possible techniques for all-optical implementation. Chapter 8 contains conclusions.

CHAPTER TWO: PHASE PRESERVING AMPLITUDE REGENERATION

2.1. Introduction

Phase-preserving amplitude regeneration allows management of nonlinear phase noise, and is a key technique for phase-regeneration schemes that function by first converting phase noise into amplitude noise. The most suitable method for DPSK amplitude regeneration is to exploit gain saturation in FWM without wavelength conversion, since the output signal does not acquire phase noise from the pump, while an output idler will. This requires the combination of large pump and signal powers inside highly nonlinear fibers (HNFs), which has the potential to introduce excess NLPN that one seeks to avoid through regeneration. A systematic experimental study of phase-preserving amplitude regeneration using FWM is therefore of interest.

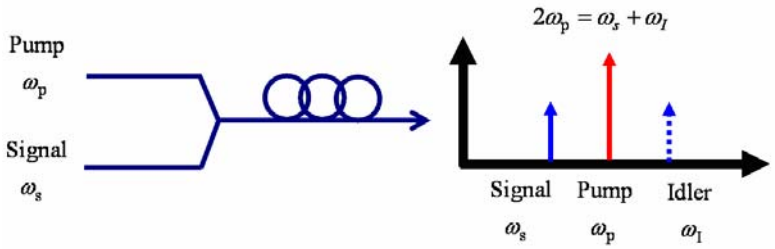

Figure 2.1: Single-pump phase-conjugation schematic and frequency arrangement.

A schematic of the single pump PC process is given in Figure 2.1. A strong pump amplifies a signal (an input to the process) and a phase-conjugate idler that is generated in the process. The pump, signal and idler obey the

frequency relationship $\omega_p = (\omega_s + \omega_I)/2$. Propagation of the waves in fiber can be described approximately by three coupled mode equations,

$$\partial_z A_p = i\gamma\left(|A_p|^2 + 2|A_s|^2 + 2|A_I|^2\right)A_p + i2\gamma A_s A_I A_p^* e^{i\beta z} \quad (2.1a)$$

$$\partial_z A_{s,I} = i\gamma\left(2|A_p|^2 + 2|A_{I,s}|^2 + |A_{s,I}|^2\right)A_{s,I} + i\gamma A_{I,s} A_p{}^2 e^{-i\beta z} \quad (2.1b,c)$$

where A_j represents a complex amplitude (normalized to units of W^{-1}), γ is the fiber nonlinear coefficient in $W^{-1}km^{-1}$ and $\beta = k_s + k_I - 2k_p$ is the linear wave-vector mismatch. Equations 2.1 include effects of the primary FWM process, SPM and CPM, but neglect generation of higher order FWM products which can impact the overall noise performance and signal gain. It is customary to solve equations 2.1 in the un-depleted pump (UDP) regime (A_p = constant) neglecting signal/idler SPM as well as CPM of the pump by the weaker waves. Such a solution does not apply to the regeneration process since this requires depletion of the pump but does offer physical insights. In this regime the signal and idler outputs are given by $A_{s,I}(z) = \mu(z)\cdot A_{s,I}(0) + \nu(z)\cdot A_{I,s}^*(0)$, where the auxiliary functions

$$\mu(z) = e^{i(\beta_n/2 + 2\gamma P_p)z}\left(\cosh(gz) - i\frac{\beta_n}{2g}\sinh(gz)\right) \quad (2.2)$$

$$\nu(z) = ie^{i(\beta_n/2+2\gamma P_p)z} \cdot \frac{2\gamma}{g} A_p{}^2 \sinh(gz) \tag{2.3}$$

and $\beta_n = \beta - 2\gamma P_p$ is the net wave-vector mismatch, incorporating SPM of the pump and CPM of the signal and idler. Equations 2.1 – 2.3 illustrate the idler acquires phase noise from the pump but the signal does not, making the signal the logical choice of outputs despite the fact that the idler may exhibit a superior input-output power transfer function. Accordingly, the pump phase can be freely modulated for suppression of stimulated Brillouin scattering.

In the UDP regime the signal phase is governed by its input phase and by CPM from the pump (eqs. 2.2-2.3). In general SPM and CPM both play a role in determining the signal phase, as suggested in equations 2.1. In the depleted-pump regime signal power fluctuations transfer to phase fluctuations in the same manner as in transmission fibers; however the process can be exacerbated in the FPA if the signal launch power is high. This is illustrated in the experimental results below.

2.2. Experimental Setup and Results

Figure 2.2 shows the experimental setup for amplitude regeneration tests. An RZ-DPSK pump is derived from a phase modulator and pulse carver at 10 Gb/s data rate. The pump was amplified and filtered for ASE before being coupled into the 6 km high-confinement fiber (HCF). An RZ-DPSK signal was generated and passed through an optical SNR adjustment circuit consisting of attenuation followed by amplification using EDFAs. By adjusting the amount of attenuation

and the number of EDFAs, the SNR could be freely varied. The degraded signal was amplified, filtered and launched co-polarized with the pump into the HCF. The fiber had an effective nonlinearity of 11/W/km, zero-dispersion wavelength near 1552 nm and dispersion slope of 0.017 ps/nm^2/km. The output of the FPA was filtered and divided for direct and differential detection. The typical pump wavelength was 1552 nm, and the signal wavelength was varied between 1548 and 1551 nm.

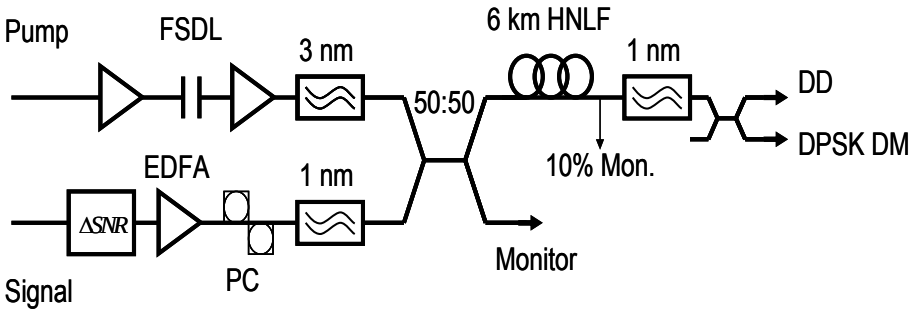

Figure 2.2. Setup for amplitude regeneration experiments. FSDL: free-space optical delay line. DD: direct (intensity only) detection. DPSK DM: differential detection. ΔSNR : ASE addition or modulation for addition of amplitude noise.

The input-output power transfer function for the amplified signal was characterized for several pump powers by changing the launched signal power from -4 to 14 dBm, the maximum available launch power. The results shown in Figure 2.3(a) indicate limiting amplification could be obtained at approximately 8 dBm signal power with pump powers around 24 dBm (approximately 250 mW). Note powers quoted are average values for the signal, but the pump peak powers were calculated assuming ~50% duty cycle. The pump power was increased to a maximum value of 283 mW (24.5 dbm), limited by the onset of

SBS despite binary phase modulation of the pump, lowering the threshold of limiting amplification to approximately 7 dBm. Figure 2.3(b) is the detailed plot from Figure 2.3(a) for the highest pump power. In Figure 2.3(c), the intensity waveform is shown at four different signal launch powers, denoted by the arrows (in order) in Figure 2.3(b). The lowest signal power does not fully deplete the pump; consequently intrinsic ASE noise is preserved and the output SNR is slightly degraded (for these measurements, input noise results from both modulation and amplification). The second waveform shows the regenerative characteristics of the depleted pump FPA. The last two diagrams reveal that although the average power is stabilized (Figure 2.3a,b), the pulses beyond the saturation point are distorted due to the combination of CPM and FWM. Consequently, the apparent dynamic range of the regenerator (approaching 5 dB in Figure 2.3b) can not be fully utilized. In the following experiments the range of signal power variation (maximum/minimum peak power) was generally limited to 3 dB.

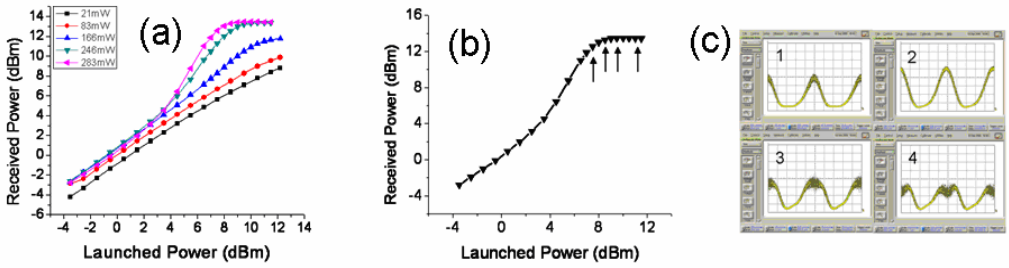

Figure 2.3. (a) Measured input-output signal power transfer function for the FPA for increasing pump powers. (b) From part (a), highest pump power. Arrows correspond to ordered points (1,2,3,4) in part (c). (c) Intensity waveforms at various points of the input-output power characteristic, denoted by arrows in (b).

Figure 2.4 shows the FWM spectrum at pump depletion and a detailed spectrum for the output signal under different conditions. Of interest is the amount of spectral broadening of the signal, which results from CPM by the pump. The growth of pump and signal sidebands is similar to MI, which can be induced by CPM in any dispersion regime [105], but not phase-matched. Note the same signal spectrum is obtained when the pump and signal polarizations are orthogonal. This severe spectral broadening should be avoided in practical circumstances.

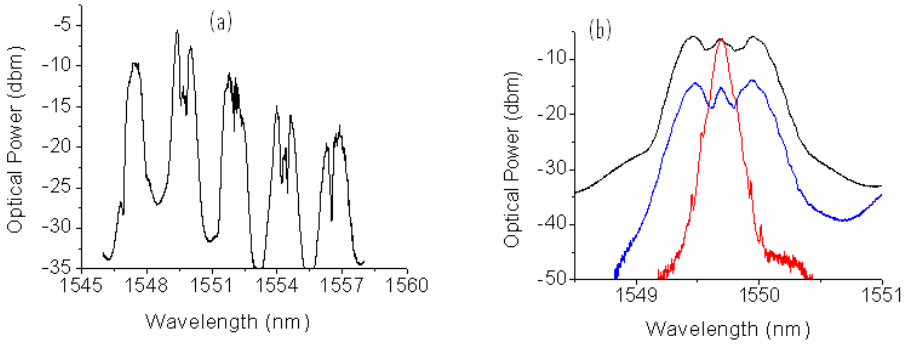

Figure 2.4. (a) Full spectrum at pump depletion. (b) Detailed signal spectrum at two launch power levels (black: 12.5 dBm, blue: 5.5 dBm) and with the pump absent (red).

Amplitude regeneration was tested with deterministic distortions introduced, emulating a signal degraded by FWM or dispersion. The results are summarized in Figure 2.5. The un-regenerated signal is shown on the left, after direct detection (top) and differential detection (bottom). Note that even high-frequency AN (in this case the modulator is driven at approximately 6 GHz) does not close the eye at detection. The regenerated waveform is shown on the top

right, revealing excellent pulse-amplitude equalization. After demodulation significant distortion exists, indicating adverse affects on the signal phase in the regeneration process. In this case, signal SPM is significant due to high launched signal power (in excess of 15 dBm). Reducing this effect by increasing the pump power led to less efficient amplitude equalization. The amount of eye closure in Figure 2.5 is prohibitive for practical implementations, indicating FPA-based regeneration should be applied after dispersion compensation.

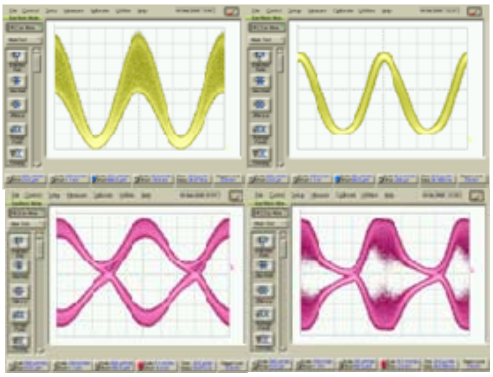

Figure 2.5. Amplitude regeneration under the addition of sinusoidal amplitude distortions. Left: back-to-back intensity waveform (top) and eye after differential detection (bottom). Right: corresponding figures after amplitude regeneration.

The AR properties of the FPA were tested for signals degraded by varying levels of ASE noise. Results are characterized by comparing the normalized intensity noise of the input to that of the output. The normalized intensity noise $\sigma_N = \sigma / \overline{P_{peak}} \cdot 100$, where σ and $\overline{P_{peak}}$ are the standard deviation and mean value of the signal peak power, respectively. These can be measured using the histogram function of the sampling oscilloscope after direct detection (e.g. Figure 2.6a). Without direct measurements of the electric field it is more difficult to

ascertain the degree of phase diffusion introduced by FPA-based AR. Measurements of the demodulated eye Q-factor (DEQF), defined as $DEQF = 10 \cdot \log\left((P_1 - P_0)/(\sigma_1 + \sigma_0)\right)$, give some insight when combined with precise amplitude noise measurements; however after demodulation both AN and PN contribute to eye closure. For this reason, only qualitative statements about the relative PN values of the input and output (regenerated) signal can be made. The powers P_1 and P_0, and noise variances σ_1 and σ_0 are measured in the same manner for differential and direct detection.

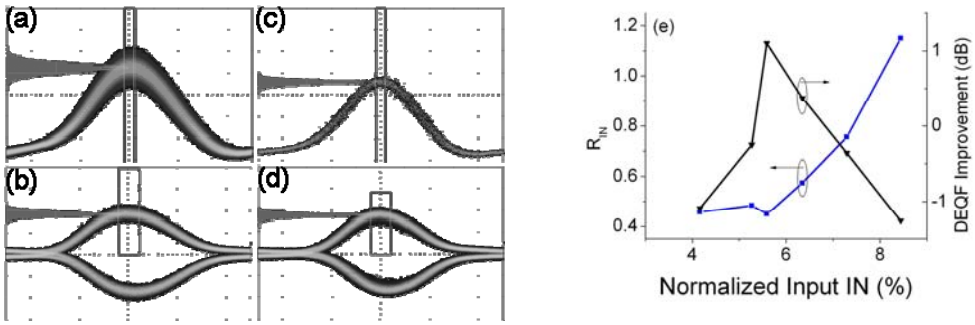

Figure 2.6. Intensity waveform eye diagrams before (a) and after (c) amplitude regeneration. Corresponding demodulated eye diagrams are shown in (b) and (d), respectively. (e): Normalized intensity noise and demodulated eye Q-factor improvement for various input noise values. Circled points correspond to data of Figure 2.6(a-d).

Figure 2.6 shows typical back-to-back (a, b) and regenerated (c, d) intensity waveforms and demodulated eye diagrams. The rectangles define sampling windows for noise and peak power measurements. The reduction of AN is evident, while the demodulated eyes appear similar indicating only small PN is introduced. In fact, depending on the level of AN reduction, the eye opening after demodulation can actually be increased despite the fact that FPA can only

increase phase noise. This is confirmed by the data of Figure 2.6(e), which compares the relative values of normalized intensity noise ($R_{IN} = \sigma_{N,out} / \sigma_{N,in}$) for continuously increasing input noise added by ASE, as well as the DEQF values at each point. The AR performance behaved in an un-interesting manner, with R_{IN} almost continuously increasing for larger input noise values. Above the normalized noise value of 8.5% AN at the output exceeded that of the input. However the DEQF improvement was optimized (*DEQF* > 0 dB) for moderate values of input noise. In this regime, the reduction of amplitude noise counteracts eye closure due to added phase noise. At smaller input noise values, even though AN is reduced, the initial eye closure due to AN is so small that the introduced PN leads to eye closure. At larger input noise values, AR performance diminishes while phase diffusion resulting from AN→PN conversion through nonlinearity increases. These results indicate limitations on the number of spans DPSK signals should be transmitted before amplitude regeneration will result in positive power penalties.

CHAPTER THREE: PHASE-SENSITIVE AMPLIFICATION

3.1. Introduction

Parametric processes occurring in nonlinear materials are inherently phase-sensitive: the growth or attenuation of a particular wave is determined by the relative phasing of all the waves. Usually in parametric processes not all of the waves involved are present at the input. For example, two strong pumps may be used to amplify a very weak signal in a FWM arrangement. The fourth wave, called the idler, grows from noise. In such an experiment propagation of four distinct waves is governed by a set of equations relating the complex amplitudes A_j (in the frequency domain):

$$\frac{\partial A_1}{\partial z} = i2\gamma A_2 A_3 A_4^* \cdot e^{i\beta z}, \qquad \frac{\partial A_2}{\partial z} = i2\gamma A_1 A_4 A_3^* \cdot e^{-i\beta z}$$

$$\frac{\partial A_3}{\partial z} = i2\gamma A_1 A_4 A_2^* \cdot e^{-i\beta z}, \qquad \frac{\partial A_4}{\partial z} = i2\gamma A_2 A_3 A_1^* \cdot e^{i\beta z}$$

These equations describe the FWM interaction in which $\omega_1 + \omega_4 = \omega_2 + \omega_3$. If waves 1 and 4 are the pumps, wave 2 is the signal and wave 3 (which is not an input) is the idler. This process is called phase-conjugation (PC). Using the relationship $\partial_z I_j = A_j \cdot \partial_z A_j^* + A_j^* \cdot \partial_z A_j$ produces a differential equation for the optical intensity. For example, the propagation equation for signal intensity is given by $\partial_z I_2 = -4\gamma\sqrt{I_1 I_2 I_3 I_4} \cdot \sin(\theta)$ where $\theta = \phi_1 + \phi_4 - \phi_3 - \phi_2 - \beta z$. For θ = -π/2, the signal

and idler will be amplified, and for θ = π/2 they will be attenuated. These conditions require a definite phase for each wave.

An initial idler is always provided by optical noise (either ASE or vacuum fluctuations). In this sense the aforementioned FWM process is always phase-sensitive, although the phase-sensitivity can be vanishingly small. Optical noise weakly drives the linear material polarization (at frequency ω_3). The nonlinear polarization resulting from interaction of waves 1, 2 and 4 allows a strong idler to grow with a phase defined by the other waves, such that the condition θ = -π/2 is satisfied. Growth of the signal and idler continues until θ deviates significantly from its initial value: the linear phase mismatch term βz eventually detunes the interaction. Nonlinear phase shifts of the waves, from SPM and CPM, can either advance or retard the detuning rate.

Phase-sensitivity is apparent when an idler is initially provided (i.e. a laser at frequency ω_3). In that case, both linear and nonlinear polarizations are driven. In general if one can control the initial phases of the waves, the signal can be freely amplified or attenuated. For the phase-sensitive process to be useful, clearly defined phase relationships must exist between the input waves. Finally, from the relationship $\theta = \phi_1 + \phi_4 - \phi_3 - \phi_2 - \beta z$ it is apparent only one condition exists for maximum signal amplification (θ = -π/2). Free variation of a single parameter (e.g. signal phase, with others constant) allows this condition to be satisfied for only one value of that parameter. If two of the parameters are correlated (signal and idler phase) the condition for maximum gain can be satisfied at two points. The latter case is important for the DPSK signal

processing techniques described subsequently, and is achieved by operating with the partial frequency degeneracy $\omega_2 = \omega_3$.

3.2. Review

Phase-sensitive amplifiers (PSA's) are important devices for studying fundamental physics and for practical applications. Historically PSA's have been interesting since they can produce non-classical states of light such as amplitude-squeezed states. From a quantum-optics perspective, the phase-sensitive amplifier performs a squeezing transformation on one mode or on coupled modes of the electromagnetic field [106]. Such transformations are described by a particular phase-dependence of the amplification processes, with a corresponding phase-dependent re-distribution of quantum noise. In this text a reference to squeezing is taken to be synonymous with observation of PSA. When the input field can be described classically a similar re-distribution of noise occurs, but non-classical fields can not be produced from classical inputs by PSA [107].

The squeezing transformation derives its name from the effects of PSA on coherent-state inputs in quantum optics. A mode of the electromagnetic field can be written $E = Eo \cdot \left(X_1 \cdot \cos\left(\omega \cdot t\right) + X_2 \cdot \sin\left(\omega \cdot t\right)\right)$. Each of the quadrature amplitudes has an associated noise variance ΔX, where in quantum optics the uncertainty product must satisfy $\Delta X_1 \cdot \Delta X_2 \geq 1/4$ in accordance with the uncertainty principle. In its simplest form the squeezing transformation is expressed as $E_{s,out} = G\left(z\right) \cdot X_1\left(0\right) + G\left(z\right)^{-1} \cdot X_2\left(0\right)$, where *G(z)* is a field gain coefficient defined

by the particular process used to generate PSA. Suppose the variance of X_1 and X_2 are each equal to 1/2 so that the noise is uniformly distributed between the two quadratures (the coherent state from quantum optics). As indicated in Figure 3.1, after PSA the noise is re-distributed such that the uncertainty product is still satisfied but now $\Delta X_1 > 1/2$ and $\Delta X_2 < 1/2$, indicating the noise has been "squeezed" from one quadrature to the other. The noise in the de-amplified quadrature is said to lie below the standard quantum limit.

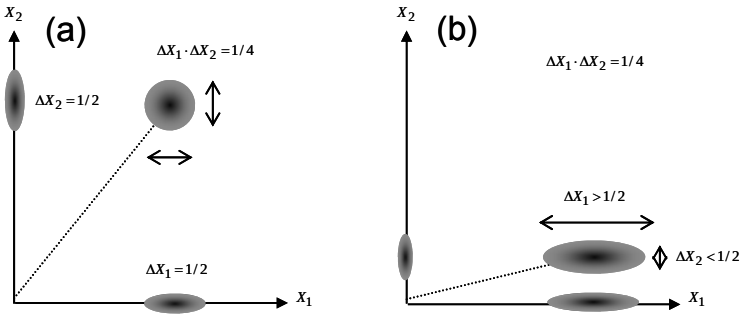

Figure 3.1: Effects of PSA on a coherent-state input. (a) Input field decomposed into orthogonal quadratures with equal noise variance. (b) "Squeezed" field after phase-sensitive amplification.

The operation of PSA from a classical point of view is analogous except in general ΔX >> ½ for both quadratures. The photon-number uncertainties are exchanged for classical noise variances that can be related to, for example, the peak amplitude and average phase of many pulses in a data stream. It is more appropriate to write the uncertainty relationship $\Delta a \cdot \Delta \phi \geq 1/2$ [106], where Δ*a* describes the fluctuations in photon number (translated to field amplitude). For the proper choice of pump and signal (mean) phases, the effects of PSA are as

illustrated in Figure 3.2. Compared to the input, the output phase fluctuations are reduced, while the amplitude fluctuation has increased.

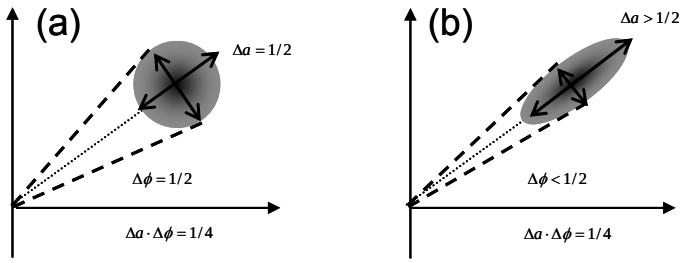

Figure 3.2: Effects of PSA visualized using a polar plot. (a) Polar plot of Input field showing amplitude and phase noise variance. (b) "Squeezed" field after phase-sensitive amplification.

The simplest implementation of PSA is the degenerate parametric down-conversion process, where a single pump photon at frequency 2ω is converted into two correlated signal photons at frequency ω in a second order nonlinear interaction. Both degenerate and non-degenerate parametric down-conversion have been studied extensively in nonlinear optics [108]. Degenerate parametric down-conversion (DPDC) was discussed at length theoretically for its potential to produce amplitude-squeezed states see, for example, [109] and references therein, however this was not observed until a 1986 experiment utilizing Lithium-Niobate with pump and signal wavelengths of 1060 and 530 nanometers [110]. The DPDC process has since been the most successfully utilized method for producing amplitude-squeezing, normally with the input signal in the vacuum state. Numerous other processes provide squeezing and therefore PSA. Particular interest has been paid to four-wave mixing (FWM) in both degenerate and non-degenerate architectures, which occur in $\chi^{(3)}$ media. In these processes,

squeezing exists as correlations between coupled modes. Non-degenerate FWM in Sodium atoms was used to observe amplitude squeezing in 1985 [111]. In that experiment the fields involved propagated in different directions, including backwards. Forward degenerate FWM was later proposed as a method for observing squeezing [112], avoiding some of the limitations imposed by the counter-propagating geometry of earlier experiments.

3.3. Phase-Sensitive Amplification for Optical Communications

Three wave mixing processes such as DPA do not occur directly in fiber. An important advance for optical communications was the realization that a 3rd-order nonlinear interferometer could produce squeezed states of light in a manner similar to FWM processes [113-115]. The advent of a fiber-based PSA enabled applications at wavelengths suitable for fiber communications. It was widely realized from the first analyses of PSAs that such amplifiers did not suffer the same quantum noise figure limit of phase-insensitive amplifiers (PIAs), which degrade the signal to noise ratio by at least 3-dB [116]. After the first experiments realizing PSA in fiber interferometers, it was quickly pointed out such devices could be used as amplifiers in communications links to replace erbium-doped fiber amplifiers (EDFAs). This reduces the accumulated amplitude noise power by at least a factor of four while simultaneously suppressing the Gordon-Haus soliton timing jitter [117]. The first demonstration of optical amplification with a noise figure less than the 3-dB quantum limit was achieved in 1999, when a PSA with a noise figure of 1.8 dB was used to produce 16 dB of signal gain [118].

Further experiments revealed the ability of a PSA to act as a limiting amplifier [119]. Before the advent of cost-effective dispersion compensating fibers, both parametric amplifiers and PSA's were proposed for dispersion compensation [120]. More recently the interest in providing low-noise amplification or distributed amplification of signals has led to the development of novel PSA architectures that operate directly in fiber, without the need for interferometric structures. These schemes are based on non-degenerate four-wave mixing and require multiple pump waves [121], or excitation of both signal and idler modes at the input [122, 123]. In 1992, it was pointed out that phase-sensitive parametric amplifiers could suppress accumulated phase noise [124] in PSK systems. However interest in the subject, and therefore thorough analysis and experiments, waned due to the success of OOK systems based on WDM. The topic resurfaced in 2004 [101], after a resurgence of interest in DPSK systems brought on by numerous system demonstrations that showed their superiority to OOK systems [79].

Many previous PSA experiments used CW signals or optical pulses without phase modulation [118, 119, 125]. In such cases, straightforward techniques employing phase-locked loops [126, 127] or optical injection locking [128] allow synchronization between the pump and signal carrier phase. However PSK systems do not exhibit a strong carrier, due to the data phase modulation. An optical carrier must be derived from the incoming signal through alternate means, such as a decision-directed phase-locked loop [129]. Figure 3.3 shows a schematic for a practical PSA, including the clock recovery (CR), carrier phase

and polarization recovery (CPPR) and injection-locking to a local laser (IL) functionalities. Phase stabilization is also required at injection to the PSA.

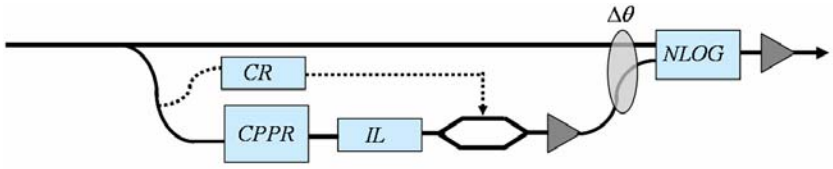

Figure 3.3: Schematic of practical PSA.

Recently a novel method based on a phase-sensitive oscillator, using a PSA as a gain block, has been demonstrated [130, 131]. The latter technique has the advantage that it can simultaneously recover the carrier phase and polarization, as well as the optical clock (for RZ-DPSK data). Because these techniques are considerably complex, the experiments described in this dissertation relating to PSA derive the pumps and signal from the same source.

CHAPTER FOUR: DPSK REGENERATION WITH A NONLINEAR INTERFEROMETER-BASED PSA

4.1. Theory

Phase-sensitive amplification can be obtained using nonlinear interferometers constructed of Kerr media such as fibers [113]. The phase-sensitivity of the gain arises from interference of the waves at the input, combined with nonlinear phase shifts (through SPM or CPM) that imbalance the interferometer. The operation of a Sagnac or Mach-Zehnder based PSA has also been interpreted as phase-matched, degenerate FWM [114].

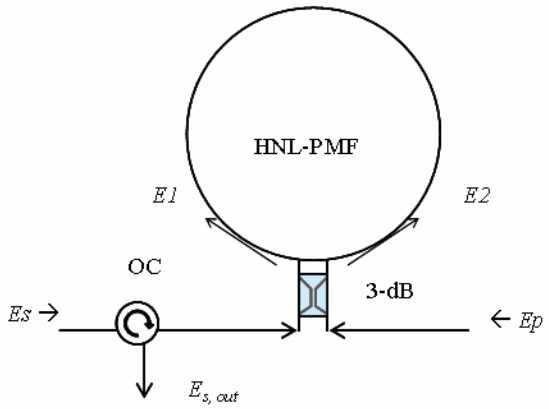

Figure 4.1: Schematic of a PSA based on a nonlinear Sagnac interferometer. HNL-PMF: highly nonlinear, polarization maintaining fiber. OC: Optical circulator.

A Sagnac PSA is depicted in Figure 4.1. Let the pump and signal fields (*Ep(z)* and *Es(z)*) be defined in terms of real amplitudes A_p and A_s as $E_{p,s}(z) = A_{p,s}(z) \cdot e^{i \cdot \phi_{p,s}}$. Plane waves are considered; however the conclusions are applicable to square pulses with duration shorter than the fiber length. Dispersive effects are neglected as well since a typical fiber PSA is less than a few

kilometers in length. The pump and signal are combined in a 3-dB coupler and launched into a highly nonlinear fiber (HNLF) loop. For only one input the Sagnac interferometer operates as a NOLM, reflecting the pump or signal to the respective input port. The output signal is thus extracted by an optical circulator. Inside the HNLF the pump and signal combine to form the counter-propagating clockwise (E_1) and counter-clockwise (E_2) fields

$$E_1 = \frac{1}{\sqrt{2}} \cdot \left(Ep(0) + i \cdot Es(0)\right), \qquad E_2 = \frac{1}{\sqrt{2}} \cdot \left(i \cdot Ep(0) + Es(0)\right) \tag{4.1}$$

When the pump and signal frequencies are degenerate and the two beams are co-polarized the combined fields E_1 and E_2 evolve as

$$\frac{dE_{1,2}}{dz} = i \cdot \gamma \cdot \left|E_{1,2}(0)\right|^2 \cdot E_{1,2}(z) - \frac{\alpha}{2} \cdot E_{1,2}(z) \tag{4.2}$$

where α is fiber loss in m^{-1}, γ is the effective fiber nonlinearity in $W^{-1}km^{-1}$ and the quantity $|E_{1,2}(0)|^2$ is the optical power in each of the counter propagating waves,

$$P_{1,2} = \frac{1}{2} \cdot \left[Pp(0) + Ps(0) \pm 2 \cdot \sqrt{Pp(0) \cdot Ps(0)} \cdot \sin(\varphi_{po} - \varphi_{so})\right] \tag{4.3}$$

The fields $E_{1,2}$ accumulate nonlinear phase terms that may be separated into two parts. The first is independent of the pump-signal input phase difference:

$$\phi_o = \frac{\gamma \cdot z}{2} \cdot \left(Pp(0) + Ps(0) \right) \tag{4.4}$$

while the second term is phase-sensitive:

$$\phi_{nl} = \gamma \cdot z \cdot \sqrt{Pp(0) \cdot Ps(0)} \cdot \sin\left(\phi_{po} - \phi_{so} \right) \tag{4.5}$$

This term is referred to as the nonlinear phase shift (NLPS). The field at the output signal port is

$$E_{s,out} = \frac{1}{\sqrt{2}} \cdot \left(E1(L) + i \cdot E2(L) \right) \tag{4.6}$$

where L is the total loop length. For a fiber with (power) loss coefficient α (m^{-1}), nonlinear effects are scaled appropriately by replacing L with the effective fiber length $Leff = \left(1 - e^{-\alpha \cdot L}\right) / \alpha$. The exact solutions for the output signal field and power are

$$E_{s,out} = e^{i \cdot \phi_o} \cdot i \cdot \left[Ap(0) \cdot e^{i \cdot \phi_{po}} \cdot \sin\left(\phi_{nl} \right) + As(0) \cdot e^{i \cdot \phi_{so}} \cdot \cos\left(\phi_{nl} \right) \right] \cdot e^{\frac{\alpha}{2} \cdot L}, \tag{4.7}$$

$$P_{s,out} = \left\{ \begin{matrix} Pp(0) \cdot \sin\left(\phi_{nl} \right)^2 + Ps(0) \cdot \cos\left(\phi_{nl} \right)^2 \ldots \\ \sqrt{Pp(0) \cdot Ps(0)} \cdot \sin\left(2 \cdot \phi_{nl} \right) \cdot \cos\left(\phi_{po} - \phi_{so} \right) \end{matrix} \right\} \cdot e^{-\alpha \cdot L} \tag{4.8}$$

Equations (4.7) and (4.8) reveal the phase-sensitive nature of the interaction. When δ = 0 or π the NLPS vanishes and no interaction takes place. Physically, the optical powers $P_{1,2}$ are matched and the interferometer is balanced. Amplification takes place for the orthogonal quadrature (δ = π/2 or 3π/2), and when the coefficient $\gamma \cdot z \cdot \sqrt{Pp(0) \cdot Ps(0)} \equiv |\phi_{nl}| = \pi/2$ equation (4.7) states the output signal is derived entirely from the pump, with an added nonlinear phase. This indicates it is possible to transfer the entire input pump light to the output signal port. Further analysis shows that for a DPSK signal input the output phase shifts by π whenever the input *signal* phase shifts by π, allowing the NOLM-PSA to preserve the phase characteristics of the input signal even when the gain is large. However the output phase remains the same when the pump phase shifts by π, allowing use of a binary phase modulated pump.

In the un-depleted pump regime $\phi_{nl} << 1$ and the output signal can be written in the form

$$E_{s,out} = \mu(z) \cdot Es(0) + \nu(z) \cdot Es^{*}(0) \tag{4.9}$$

where *Es(0)* and *Es*(0)* are the complex signal amplitude and its conjugate, the functions $\mu(z) = i \cdot \sqrt{1 + \phi'^{2}_{nl}} \cdot e^{i \cdot (\phi'_{nl} + ArcTan(\phi'_{nl}))}$ and $\nu(z) = i \cdot \phi'_{nl} \cdot e^{i \cdot (\phi'_{nl} + 2 \cdot \phi_{po} - \pi/2)}$, and $\phi'_{nl} = \gamma \cdot L_{eff}/2 \cdot Pp(0)$. This equation has the general form of a (single-mode)

squeezing transformation [106]. The amplified quadrature *Es* reaches maximum gain for the input phase relationship

$$\delta_{\max G} = ArcTan(\phi'_{nl})/2 + \pi \cdot (m + 1/4), \qquad g_{\max} = \phi'_{nl} + \sqrt{1 + \phi'^{2}_{nl}} \,. \tag{4.10}$$

whereas the orthogonal quadrature $i \cdot Es^{*}$ is maximally attenuated for a phase difference of

$$\delta_{\min G} = ArcTan(\phi'_{nl})/2 + \pi \cdot (m + 1/4) + \pi/2, \quad g_{\min} = \sqrt{1 + \phi'^{2}_{nl}} - \phi'_{nl} \,. \tag{4.11}$$

The corresponding maximal and minimal power gain is given by $G_{\max,\min} = 1 + 2\phi'^{2}_{nl} \pm 2 \cdot \phi'_{nl} \sqrt{1 + \phi'^{2}_{nl}}$.

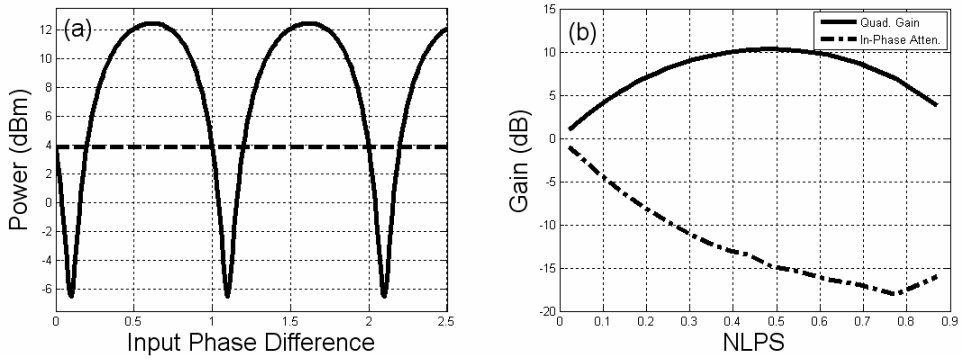

Figure 4.2: NOLM-PSA phase response and gain. (a) Signal output power vs. relative input phase for NLPS = π/4. Dashed line: transmitted signal power in absence of pump. (b) Quadrature gain (solid line) and in-phase attenuation (dashed line) for increasing NLPS, for an input power ratio Γ = 10 dB. Both plots have phase units normalized to π.

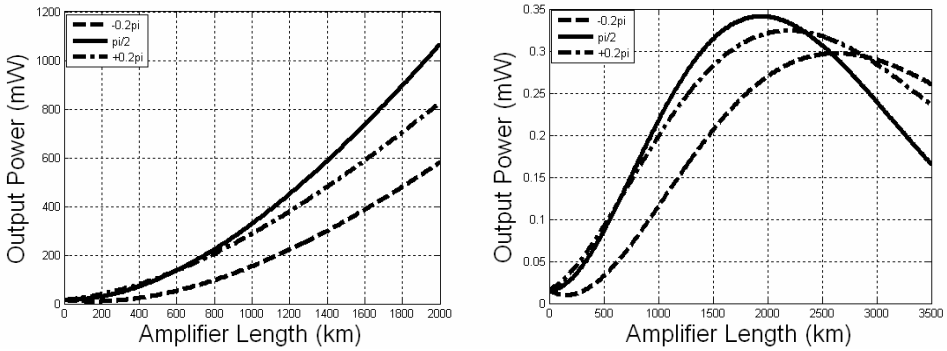

Figure 4.3: Signal power plotted for increasing amplifier length. Phase deviations shown are relative to δ = π/2. (a) Un-depleted pump calculation assuming *Pp(0)* = 500 mW. (b) Depleted pump calculation.

Figure 4.2(a) shows the variation of signal output power with input phase difference for NLPS ~ π/4. Maximum and minimum output powers are obtained the phase differences given by equations 4.10 and 4.11. The differential gain can be inferred from Figure 4.2(b). At small NLPS the gain and attenuation of orthogonal quadratures are approximately equal. At NLPS = π/2 the gain saturates to the value Γ = *Pp(0)/Ps(0),* however the in-phase attenuation continues to increase. The resulting differential gain is as high as 25 dB in the figure, for Γ = 10 dB.

Figure 4.3(a) and Figure 4.3(b) show evolution of the signal power for un-depleted and depleted pump PSA's, respectively, for varying values of input phase difference. The input pump and signal powers were 500 mW and 16 mW respectively. The un-depleted pump calculation is based on equation (4.9), assuming a fiber loss of 0.8 dB/km. In contrast to other PSA schemes based on parametric amplification, which achieve exponential growth in the small-signal

approximation, the NOLM-PSA achieves only quadratic growth. This fact reflects the different physical mechanism behind the gain.

The phase-regenerative property of the PSA is observed directly by calculating the signal input-output phase response. Figure 4.4 shows the result for increasing values of NLPS up to π/2. At sufficient NLPS two distinct phases emerge at the output, separated by π. If a noisy DPSK signal with mean phases of π/2 and 3π/2 is the input then the output will exhibit significantly reduced phase fluctuations above NLPS ~ 0.2π.

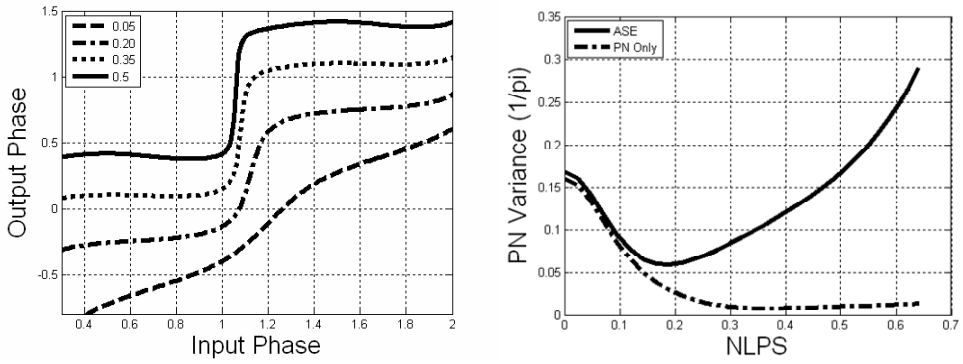

Figure 4.4: Input-output phase and growth of phase noise variance in the NOLM-PSA.. (a) Phase regeneration graphs for different values of NLPS (legend). (b) Calculated PN variance for increasing NLPS for two cases: Dotted line, input exhibits PN only. Solid line, input exhibits both AN and PN.

In the limit of NLPS = π/2 the output at the signal port is just a phase shifted, spectrally broadened version of the input pump light. From equation (4.7),

$$E_{s,out} \approx i \cdot e^{i \cdot \phi o} \cdot \left[Ap(0) \cdot e^{i \cdot \phi_p} \cdot \sin(\phi_{nl}) \right] \cdot e^{-\frac{\alpha \cdot L}{2}}, \qquad (4.12)$$

$$\phi_{s,out} \approx \frac{\gamma \cdot z}{2} \cdot \left(Pp(0) + Ps(0) \right) + \phi_p + \frac{\pi}{2} \cdot \sin(\phi_p - \phi_s) \tag{4.13}$$

Equation (4.13) shows the PSA process is phase-difference preserving since the output phase will change by π whenever the input signal phase changes by π. On the other hand a shift of the pump phase by π does not affect the output signal phase. This fact is exploited in experiments for suppression of stimulated Brillouin scattering (SBS) by binary phase modulation of the pump. It is important to note the nonlinear phase term in equation (4.12): $\phi o = \gamma \cdot z / 2 \cdot \left(Pp(0) + Ps(0) \right)$ and its implications. This produces a rotation of the output phase proportional to both the pump and signal powers at the input, providing a mechanism for amplitude-to-phase noise (AN → PN) conversion. In Figure 4.4(b) the output phase noise variance is calculated for increasing values of NLPS for two cases, first with (solid line) then without (dotted line) input signal AN. A strong increase is observed above NLPS = 0.2π when input AN is accounted for.

When the signal gain saturates (NLPS = π/2) the PSA may operate as a limiting amplifier. Figure 4.5(a) shows evolution of the signal power for three different input powers. Taking the fiber length as a variable for increasing NLPS it is straightforward to calculate the saturation length at which the output power is equal to the input pump power: $L_{sat} = \pi / \left(2 \cdot \gamma \cdot Ap(0) \cdot As(0) \cdot \sin(\delta) \right)$. When the fiber length is selected properly the output power becomes inversely proportional

to the input power, resulting in limiting amplification. In Figure 4.5(b) the output power is plotted against input signal power, assuming constant pump power. The amplifier length is the saturation length for the mean input signal power, which is 15 dBm, and the pump power is 27 dBm. Significant noise reductions are predicted when phase noise is not considered, however the inevitable presence of input PN will limit the efficiency of amplitude regeneration.

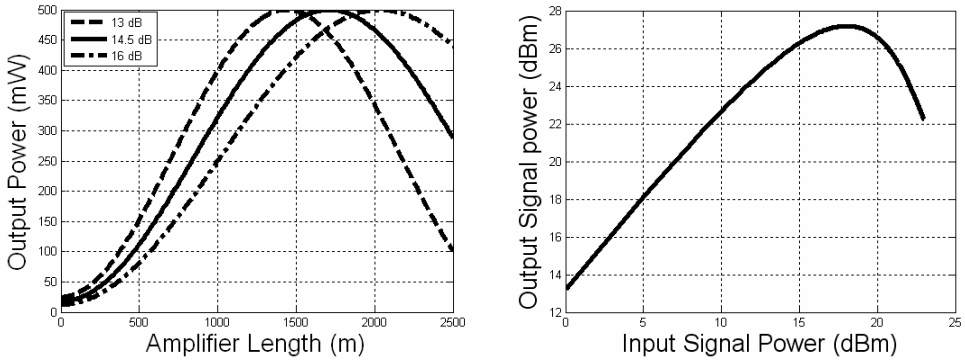

Figure 4.5: Signal power plotted for increasing amplifier length for different input powers assuming (a) un-depleted pump and (b) depleted pump, with no fiber loss. Input relative phase δ = π/2. Pump power is 500 mW and the input power ratio is specified in dB on the graphs.

4.2. Experiments

4.2.1. Experimental Setup

The setup for the DPSK regeneration experiment is shown in Figure 4.6. 10 Gb/s RZ-DPSK data with 33% duty cycle and pattern length of at least 211-1 was generated using a phase modulator and Mach-Zehnder intensity modulator. The data was amplified by an EDFA and separated into a pump (for the PSA) and signal (to be regenerated) using a 90/10 splitter. As previously described the use

of a binary phase modulated pump eliminates excess noise due to Stimulated Brillouin Scattering. Different path lengths for the pump and signal ensure de-correlation of the PRBS data by > 50 bits. Phase and amplitude distortions were added to the signal using two additional modulators, which were driven sinusoidally. This allowed independent adjustment of the relative AN and PN levels. The driving frequencies were typically different, with f_{AN} > 6 GHz and f_{PN} determined by mixing the synthesizer output with the 10 GHz clock signal from the BERT: $f_{PN} = 10GHz - f_{AN} \leq 4GHz$. For constellation diagram measurements the noise frequencies were synchronized to integer multiples of the sampling frequency of the oscilloscope, which is 6.25 GHz. The addition of PN is quantified in terms of the maximum phase error, where $MPE = \max\left(\phi_{n-1} - \phi_n\right)$ is the maximum deviation of all detected differential phases from original encoded values. Note that logical errors are only produced for *MPE* > 90^o. An optical attenuator is used to adjust the pump to signal power ratio from 10 to ~20 dB at the input, limited by the available pumping power. A free-space delay line in the pump path allows temporal alignment of the pump and signal pulses at the PSA input as well as a method for manually scanning the input phase difference. Input phase drift was stabilized by monitoring the signal gain and driving a fiber stretcher. The PSA was comprised of a 3-dB coupler and 6058 meters of HNLF (not polarization maintaining) with a total insertion loss of 5 dB and effective nonlinear coefficient of 9.75 $W^{-1}km^{-1}$. An intra-loop polarization controller was required to maximize reflection of the pump and transmission of the regenerated

signal, which was extracted by the optical circulator, tapped for feedback, and sent to a DPSK demodulator and BER tester or oscilloscope for detection.

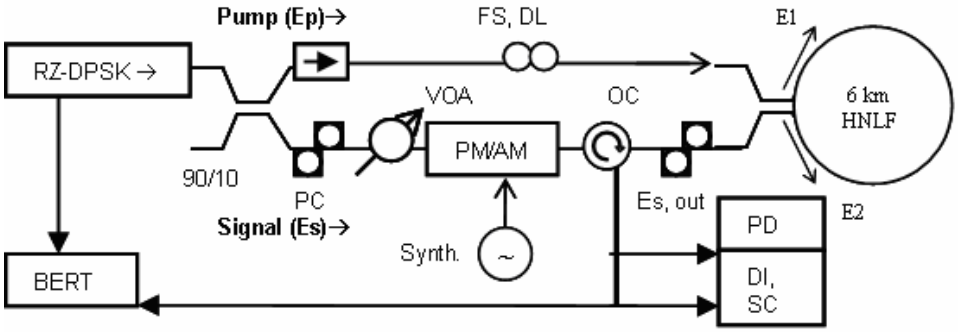

Figure 4.6. Experimental setup. FS, DL: fiber stretcher, delay line; VOA: optical attenuator; OC: optical circulator; PC: polarization controller; PD: photodiode; DI, SC: delay interferometer + sampling oscilloscope; Synth: synthesizer; BERT: bit-error-ratio tester; PM/AM: noise adding phase and amplitude modulators.

Calculations show phase regeneration may be accomplished with values of NLPS of the order of 0.2π, regardless of the input AN level. Combining phase and amplitude regeneration requires NLPS ~ 0.5π. Experimentally the value of NLPS can be estimated by observing the characteristics of the phase-sensitive gain. Figure 4.7 shows the measured (a-d) and calculated (e-h) signal power (versus input phase δ) for different values of NLPS. For experiments, the input phase difference is deterministically varied by rotating the free space delay line. The amplified signal is then recorded as a function of time on an optical spectrum analyzer operating in zero-span mode. The time axis may be correlated to relative phase for each case, although the phase-scanning rate varies slightly between cases. The dashed line represents the background signal power (in absence of pump) while solid lines show the amplified signal with pump leakage

subtracted. The condition of NLPS = 0.5π is held for all regeneration experiments by obtaining a flattened gain peak as shown in Figure 4.7 (c) and (g). Simultaneous regeneration is optimized by varying the input pump-to-signal power ratio Γ = $P_p(0)/P_s(0)$, which also determines the maximum signal gain.

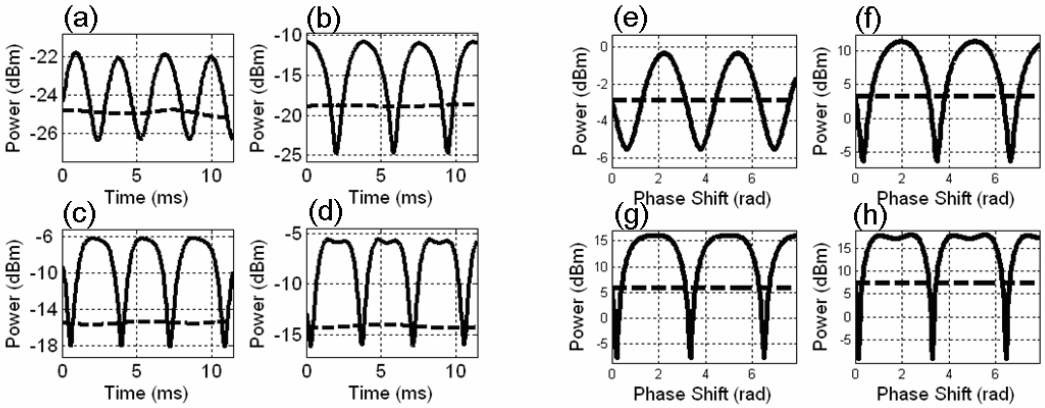

Figure 4.7. Measured (a-d) and calculated (e-h) signal output power versus relative input phase for the PSA for NLPS of 0.1π, 0.25π, 0.5π and 0.55π. Solid lines: amplified signal, dotted lines: transmitted signal power in the absence of the pump.

4.2.2. Amplitude Regeneration

The addition of amplitude noise, as well as amplitude regeneration, was monitored by observing the intensity waveform and eye diagram since as shown below the demodulated eye is not sensitive to high frequency AN. Figure 4.8(a) shows the back-to-back intensity eye when AN was added at a random frequency near 6 GHz. The electrical SNR, defined as average of all peak powers divided by the standard deviation of this distribution, is degraded to approximately 5.8 dB at a received power of 1 dBm. The degraded signal waveform is visualized in Figure 4.8(c) by adding similar AN at the sampling

frequency of the scope (6.25 GHz). Large bit-to-bit amplitude shifts are generated similar to those acquired by a realistic DPSK signal after transmission. The corresponding PN source adds maximum phase errors slightly greater than 80^{o}, and in all results reported herein the input suffers from both PN and AN. The PSA was operated with an average pump power of 93 mW (peak power just over 200 mW) and a pump to signal power ratio of almost 12 dB. Without the pump present the transmitted signal power was 300 μW, and the pump leakage detected through the signal port was around 30 μW. The amplified signal power was 4.25 mW corresponding to 11.5 dB of gain, although under stable phase-locking the output power was reduced somewhat to 3.95 mW (11.2 dB gain). The net gain and observed phase-sensitive gain profile (Figure 4.7) agree with generation of NLPS = 0.5π.

Figure 4.8(b) shows a typical intensity eye diagram of the phase-and-amplitude regenerated DPSK signal, at the same received power of 1 dBm as in Figure 4.8(a). The improvement in AN statistics is clearly evident. The output SNR reaches nearly 11 dB, corresponding to 5 dB of improvement. Figure 4.8(d) shows considerably smaller amplitude fluctuations for the regenerated signal, proving the amplitude regeneration property of the PSA to be robust with respect to the presence of phase noise. A short sample of the waveform is shown for clarity; however similar results are obtained regardless of which time interval is chosen. This is reflected in the SNR improvement of 5 dB, which accounts for many repetitions of the entire PRBS pattern.

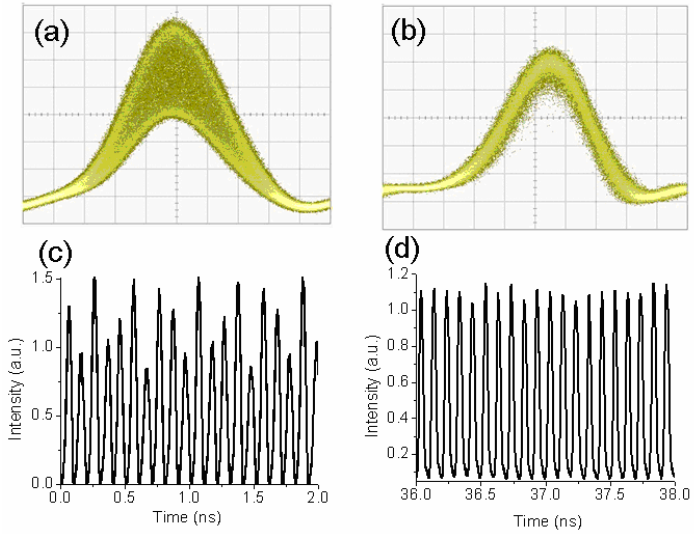

Figure 4.8. Intensity eye diagram (a) back to back with SNR of 5.75 dB, and (b) after regeneration for the same received power with an improved SNR of 11 dB. Signal waveform (c) back to back with added PN and AN and (d) after regeneration. AN is added at the sampling frequency of the oscilloscope (6.25 GHz).

4.2.3. Phase Regeneration and Bit-Error-Ratio Measurements

In Figure 4.9 the demodulated eye diagram of the DPSK signal is visualized before and after combined phase-and-amplitude regeneration. The back-to-back eye is shown without any added noise in Figure 4.9(a), with added AN in Figure 4.9(b) and with both PN and AN added in Figure 4.9(c). The addition of PN in Figure 4.9(c) at a frequency near 4 GHz leads to a severely reduced eye opening. The fact that the eye is nearly closed proves the added PN produces differential phase errors approaching 90^{o} (the threshold for producing a logical error). After regeneration the eye, shown on the same scale and for the same received power in Figure 4.9(d), was clearly open indicating highly effective removal of phase noise. From the obvious improvement in demodulated eye Q-

factor one expects a strong improvement in the differential phase statistics, with a related improvement in BER performance. The slight residual eye closure indicates the presence of phase noise after regeneration, resulting primarily from signal AN to PN conversion. Some small, additional fluctuations in both amplitude and phase result from the transfer of pump fluctuations.

BER performance was measured for back-to-back degraded signals with AN only and with PN and AN, and after regeneration for the cases described above. The received power is measured at the input to the delayed interferometer, without pre-amplification by an additional EDFA. Thus the results in Figure 4.10 are useful for comparing BER performance of the signals but do not suggest the actual receiver sensitivity that would be obtained. Without regeneration, the back-to-back signal reaches an error floor approaching 10^{-9} at a received power of 0 dBm when both PN and AN are added, indicating the presence of logical errors. The regenerated signal must exhibit the same error floor since the PSA (or any other regeneration scheme) may not remove phase errors that have already accumulated. However a negative power penalty of nearly 6 dB is clearly demonstrated, and for the same received power the BER was reduced by up to 7 orders of magnitude. This indicates the removal of signal phase noise despite the presence of large amplitude noise at the input. For reference the BER of the back-to-back signal with only added AN is shown as well, indicating that even though the SNR was highly degraded by adding AN, the BER performance is not strongly affected.

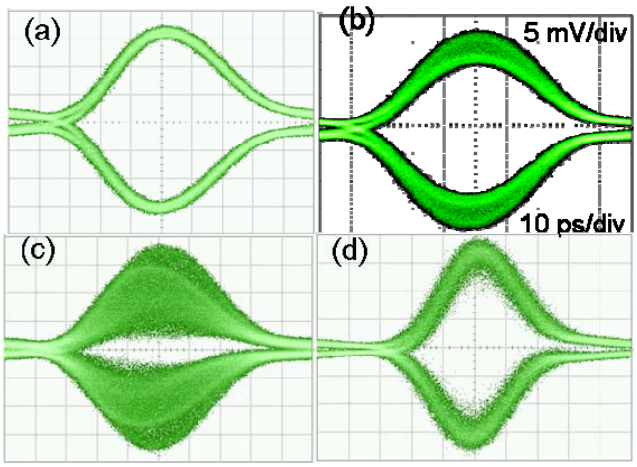

Figure 4.9. Demodulated eye diagrams. Back to back with (a) no added noise; (b) with added AN only and (c) with PN and AN added. Note the lack of eye closure for the AN-only case. (d) Demodulated eye after phase-amplitude regeneration.

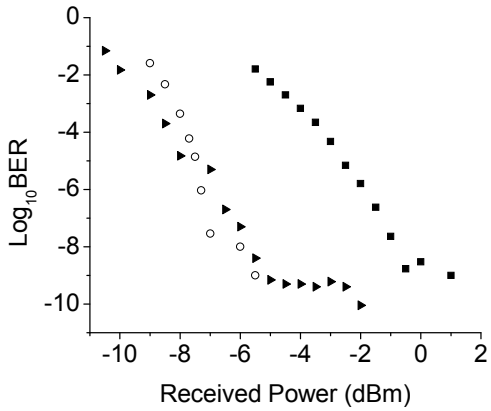

Figure 4.10. BER curves for back-to-back degraded data (squares) and regenerated data (triangles). Negative power penalty is 5 dB. Empty circles represent back-to-back data with only amplitude noise added.

4.2.4. Characterization of Results using Coherent Detection

The signal was fully characterized by measurements of the complex field. From this the differential phase statistics are calculated in a straightforward manner.

Experimentally, the technique of linear optical sampling can be used to measure signal amplitude and phase [132-134]. Normally the technique when applied to high speed signals requires a sophisticated pulsed local oscillator. However in the present case, a simple CW local oscillator derived from the same source as the pump and signal has been used. This is sufficient for measuring highly periodic signals, requiring only that PN and AN be added at multiples of the same frequency. In Figure 4.11 the directly measured constellation diagram, amplitude histogram and calculated differential phase (with distribution superimposed) are shown for three cases. All data were obtained by sampling periodically at the bit rate, so each data point represents the peak amplitude and phase of a single bit near the bit center.

The back-to-back signal reveals phase noise present on both the pump and signal from modulation. The data of Figure 4.11(a) indicate the angular width of the encoded 0, π phase states each to be around 10^{o}. Differential phase noise of the same order is present and visible in the graph at the bottom of Figure 4.11(a). This phase noise contribution was quite small compared to the PN added to the signal intentionally. It is the fact that it exists on the pump wave as well that has repercussions for the operation of the PSA. Residual amplitude noise shown in the histogram reflects small signal intensity pattern effects generated by the pulse carver. Without noise addition, the SNR was 17.6 dB and the calculated differential phase Q-factor was 14.3 dB.

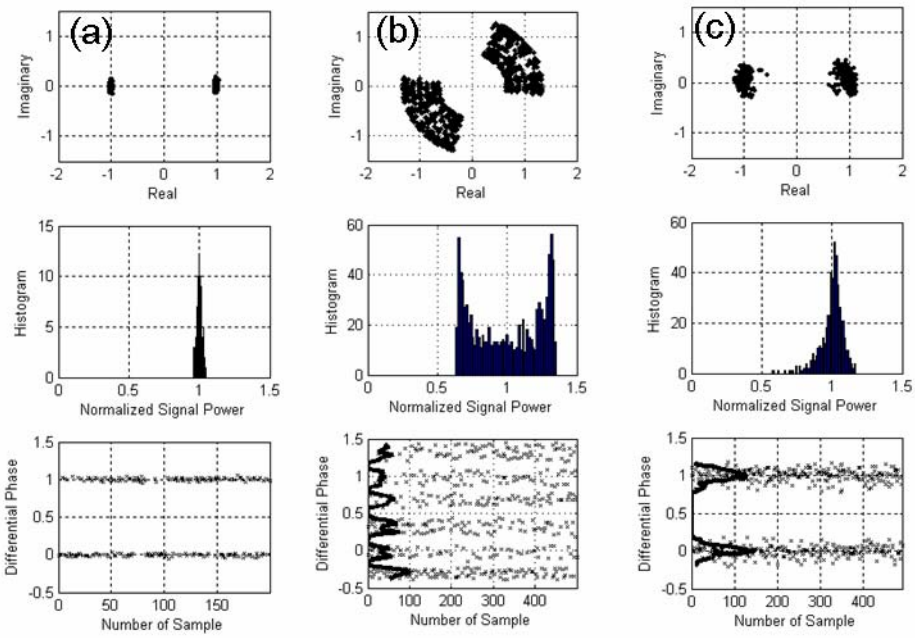

Figure 4.11: Signal constellation measured through linear optical sampling. From top to bottom: directly measured constellation diagram, histogram of signal power sampled at bit center and calculated differential phase (crosses) with distribution super-imposed (solid line). Back to back signal (a) with no added noise and (b) with added PN and AN. (c) Signal after phase-and-amplitude regeneration.

Figure 4.11(b) shows the back-to-back signal with phase and amplitude noise added for a series of 400 consecutive bits. The constellation diagram shows nearly uniformly distributed noise for the case of AN added at 6.25 GHz and PN added at 3.125 GHz, representing all relevant combinations of input amplitude and phase. The degraded SNR was 5.75 dB, and calculated differential phase Q-factor was only 2.64 dB. The maximum measured differential phase error from the lower plot was 82^{o}. The data after regeneration are shown in Figure 4.11(c). The SNR and differential phase-Q were both improved by 6 dB, to 11 dB and 8.2 dB respectively, and the maximum phase error was reduced

from 82^{o} to 41^{o}. It was observed that much better PN reduction could be obtained by increasing Γ (e.g. MPE reduced to 25^{o}), but this inevitably resulted in a lower output SNR. The degradation in output SNR at larger Γ is a consequence of the pump fluctuations. This seems to suggest a trade-off between optimizing either phase or amplitude regeneration when pump fluctuations are taken into account.

CHAPTER FIVE: DPSK REGENERATION IN TRAVELING-WAVE PHASE-SENSITIVE AMPLIFIERS

5.1. Theory

PSA can be produced directly in fiber using either single-stage or cascaded FWM processes [121]. The single-stage process involves two pumps and a signal that is at the center frequency: $\omega_s = (\omega_1 + \omega_2)/2$. It is referred to as a symmetric-pump phase-sensitive amplifier (SP-PSA). This scheme is the 3rd order analog of the degenerate parametric amplification processes occur ring in 2nd order materials. Because the signal undergoes continuous PSA as it propagates in fiber, the conversion between amplitude and phase noise (prominent in the NI-based PSA) is strongly suppressed.

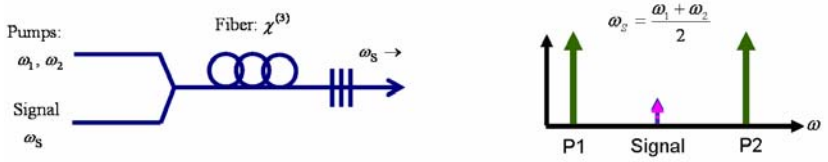

Figure 5.1: Simplified schematic and frequency arrangement of SP-PSA.

Figure 5.1 shows a schematic diagram and the optical frequency arrangement for a PSA based on degenerate PC. Light from two pumps is combined with a weak signal at the center frequency in an optical fiber. This is similar to the two-pump PC process where normally a signal is placed at an arbitrary frequency between the pumps, producing a frequency shifted phase-conjugate idler. In the degenerate process the signal is at the center frequency, therefore the PC wave would be produced at the same frequency as the signal

itself. This leads to the phase-sensitivity of signal gain with characteristics that are required for DPSK phase regeneration. The coupled mode equations for co-polarized pumps and signal are

$$\partial_z A_S = i\gamma\left(\left|A_S\right|^2 + 2\left|A_1\right|^2 + 2\left|A_2\right|^2\right)A_S + i2\gamma A_1 A_2 A_S^{*} e^{-i\beta z} \tag{5.1a}$$

$$\partial_z A_{1,2} = i\gamma\left(2\left|A_S\right|^2 + 2\left|A_{2,1}\right|^2 + \left|A_{1,2}\right|^2\right)A_{1,2} + i\gamma A^{*}_{2,1} A_S^{\,2} e^{i\beta z} \tag{5.1b,c}$$

where $\beta = 2k_s - k_1 - k_2$, and $k_{1,2}$ are the linear wave-vectors for pumps 1 and 2 respectively. The propagation equation for signal intensity can be written in the form as $\partial_z I_s = -2\gamma\sqrt{I_s^{\,2} I_1 I_2}\cdot\sin(\theta)$ where $\theta = \phi_1 + \phi_2 - 2\phi_s - \beta(z)$: if the pump phases are treated as reference phases, the condition for maximum signal gain (θ = -π/2) is satisfied for inputs of π/4 and π/4+π. In general equations 5.1 are solved numerically to study effects of pump depletion. In the UDP regime equation 5.1(a) and its PC are solved by assuming P_1=P_2=constant and neglecting effects of signal SPM, and CPM of the pumps by the signal. The solution has the form of a squeezing transformation [106]:

$$B_s(z) = \mu(z)\cdot B_s(0) + \nu(z)\cdot B_s^{*}(0) \tag{5.2}$$

with the amplitude $A_s(z) = B_s(z) \cdot \exp(-i\beta z/2 + i3\gamma(P_1 + P_2)z/2)$, and the auxiliary functions

$$\mu(z) = \cosh(\kappa z) + \frac{i\delta}{\kappa}\sinh(\kappa z) \tag{5.3}$$

$$\nu(z) = i\frac{\Gamma}{\kappa}\sinh(\kappa z) \tag{5.4}$$

The gain coefficient $\kappa = \sqrt{|\Gamma|^2 - \delta^2}$ where the parameter $\Gamma = 2\gamma A_1 A_2$ and $\delta = \beta/2 + \gamma(P_1 + P_2)/2$. The maximum available gain depends on the net phase-matching parameter δ. Under normal dispersion the interaction can be phase-matched. In that case the maximal and minimal small-signal gain

$$G_{\substack{\max(+)\\ \min(-)}} = \cosh^2(\kappa z) + \frac{|\Gamma|^2}{\kappa^2}\sinh^2(\kappa z) \pm 2\frac{|\Gamma|}{\kappa}\sinh(\kappa z)\cosh(\kappa z) \tag{5.5}$$

Numerical solutions to Equations 5.1 allow analysis of the AN→PN conversion processes that occurs through SPM during regeneration. Figure 5.2(a) shows the numerically calculated input-output phase relationships for several different input signal powers, ranging from -20 to 17 dBm. Pump powers were set to 30 dBm each, the fiber length, nonlinearity and distributed loss were 50 meters, $12W^{-1}km^{-1}$ and 0.7 dB/km respectively, and perfect linear phase

matching was assumed. Although all SPM and CPM processes were taken into account, the output phases for radically differing input powers were remarkably similar. The inset shows a detailed view for a restricted input phase range. Figure 5.2(b) shows the calculated output phase for one given input phase, for a range of input power from -20 to 20 dBm. The input-output power transfer function is also shown. The fiber length was increased to 150 meters to allow the highest signal powers (>15 dBm) to saturate the available gain. The initial phase was chosen so that, in the small-signal limit, maximum amplification would occur. The output phase variation over the entire range of input powers is as small as 13 degrees. Near the gain saturation point, the variation of output phase with power vanishes, suggesting excellent performance for the PSA when used to regenerate both phase and amplitude of degraded signals.

In this PSA implementation, noise conversion between AN and PN is suppressed strongly. This results from the growth of quadrature attenuation, which counteracts the nonlinear phase shifts continuously due to the traveling-wave geometry. This feature allows advanced regeneration performance of the SP-PSA compared to the NOLM-PSA. For the same conditions, regeneration behavior is visualized in Figure 5.3 through Monte-Carlo simulations.

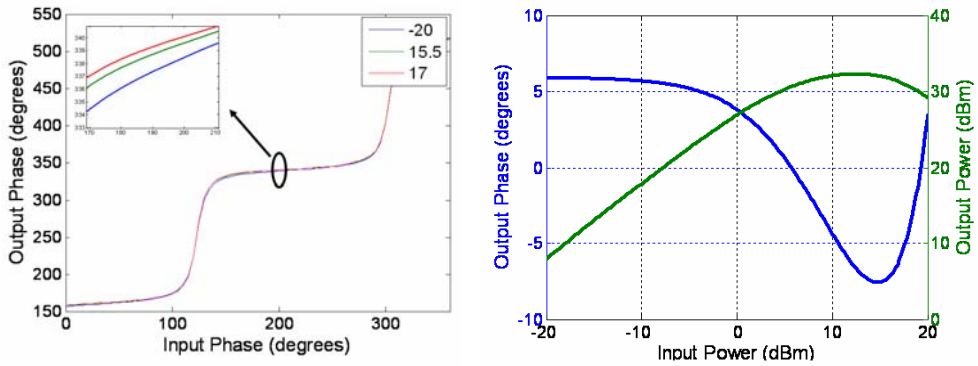

Figure 5.2. (a) Numerically calculated input-output phase relationships for the SP-PSA for three input powers. Inset shows splitting of output phase levels. (b) Output phase and power for a single input phase value over the entire range of input power.

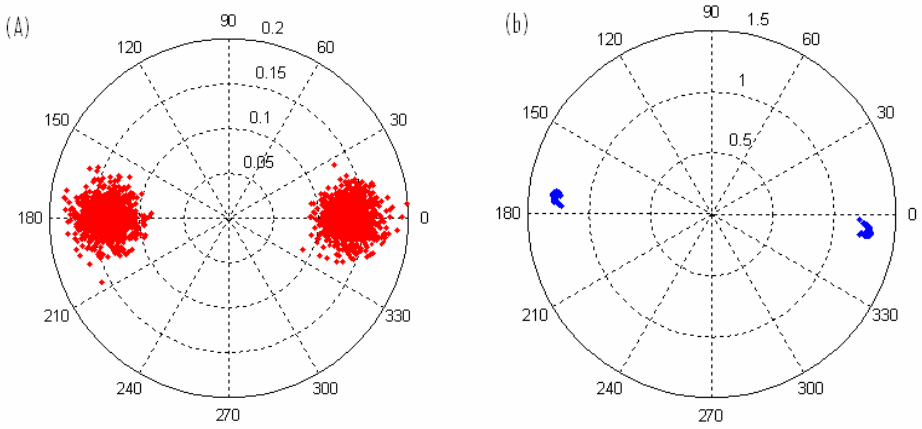

Figure 5.3. Polar plots of an ASE-degraded signal before (left) and after (right) regeneration.

Efficient PSA requires phase matching of the pumps and signal, which in general depends on the fiber dispersion profile, pump power, fiber nonlinearity and loss. Fibers of interest for inline PSA and regeneration are dispersion-flattened high-confinement fibers (HCFs) and dispersion shifted fibers (DSFs), which have effective nonlinear coefficients of (11-17) /W/km and (~6-7) /W/km,

respectively. Dispersion compensating fibers (DCFs) exhibit higher nonlinear coefficients (~16/W/km) but are not typically used because of their large dispersion coefficients. Recently Bismuth-Oxide HCFs have been developed with effective nonlinear coefficients of 1000/W/km or greater. This radical increase in nonlinearity is tempered by excessive losses (0.8-3 dB/m) and high dispersion (D ~200-300 ps/nm/km); however several recent experiments have demonstrated a variety of efficient nonlinear effects. The high nonlinearity allows use of fibers less than 10 meters in length for most experiments (the fiber length can potentially be shorter than 1 m), partially alleviating the effects of high dispersion. Experiments described below were conducted using Bismuth-Oxide fibers.

For arbitrary values of dispersion and pumping power the maximum and minimum small signal gain, and the phases for which these occur, are modified. The maximum gain occurs when the two terms in equation (5.3) add in-phase:

$$\phi_1 + \phi_2 - 2\phi_s = a\tan\left(\frac{\delta \cdot \sinh(\kappa z)}{\kappa \cdot \cosh(\kappa z)}\right) - \frac{\pi}{2} \tag{5.6}$$

For δ = 0 and pump phases of zero, the required signal phase is π/4. As the magnitude of δ increases towards $|\Gamma|$ the required phase reaches limiting values of 0 (for $\beta = 2\gamma(P_1 + P_2)$) and π/2 (for $\beta = -2\gamma(P_1 + P_2)$). These values for β establish limits on for example the spacing of pumps, or on deviations of the signal from the fiber ZDF; higher values lead to imaginary values of $\kappa = \sqrt{|\Gamma|^2 - \delta^2}$

that do not produce signal gain. The modified expression for small-signal gain allowing for non-optimal phase matching is

$$G = \cosh^2(\kappa z) + \left(\frac{\delta^2 + |\Gamma|^2}{\kappa^2} \right) \sinh^2(\kappa z) - 2\frac{|\Gamma|}{\kappa} \sinh(\kappa z)\cosh(\kappa z)\sin(\theta)... \\ +2\delta\frac{|\Gamma|}{\kappa^2}\sinh^2(\kappa z)\cos(\theta) \tag{5.7}$$

where θ is the relative phase between the signal and pumps and the net phase-mismatch δ can be either positive or negative depending on which type of fiber is chosen. For comparison with experiments Bismuth-Oxide fibers are analyzed with parameters γ = 1100/W/km and D = -300 ps/nm/km. The fiber loss of 1.4 dB/m also modifies the phase-matching condition due to the non-constant pump power even in the small signal regime; this was taken into account in calculations. The linear wave-number mismatch $\beta = 2k_s - k_1 - k_2$ is calculated using the Taylor expansion for the propagation constants with the signal frequency as the reference: $\beta(\omega) = \beta(\omega_o) + \beta_2(\omega - \omega_o)^2/2 + ...$ Due to the large GVD coefficient higher order dispersive effects can be ignored. The total phase-matching condition becomes $\beta_T(\Delta\omega) = \gamma(P_1 + P_2) - \beta_2\Delta\omega^2$ where $\Delta\omega$ is the frequency separation between the signal and each pump. The frequency separation that maximizes signal gain $(\beta_T = 0)$ Is $\Delta\omega = \sqrt{\gamma/\beta_2(P_1 + P_2)}$, which decreases with higher dispersion. In Figure 5.4(a) an example of the small-signal

gain obtained from equation (5.7) is plotted as a function of the total pump frequency separation using the previous values of fiber nonlinearity, loss and dispersion (for Bismuth Oxide fibers) and a length of 5.64 meters. The total pump power was 28 dBm (25 dBm for each pump) and the input signal power was set 40 dB below the total pump power. For wavelengths near 1550 nm a frequency spacing of 300 GHz (nearly maximal gain) is approximately 2.4 nm. The lower plot shows the required signal phase to maximize the gain at each value of pump separation. Figure 5.4(b) is the normalized small-signal gain for increasing values of total pump power ranging from 24.5 to 28.5 dBm. Variation of the gain with pump spacing increases at higher powers making precise placement of the pumps more critical. However the frequency separations suggested in Figure 5.4(b) are difficult to obtain experimentally: pumps are generally produced by modulating light at the signal frequency and filtering symmetric sidebands. For ~40 GHz modulation sidebands greater than 160 GHz apart are generally too weak to be filtered and used as pumps for the PSA. Alternate means of generating pumps based on cascaded FWM are also being explored. For comparison, Figure 5.4(c,d) show similar graphs for a fiber with a large anomalous dispersion (D = 300 ps/nm/km), illustrating the degenerate PC process is perfectly phase-matched for non-zero pump spacing only in the normal dispersion regime.

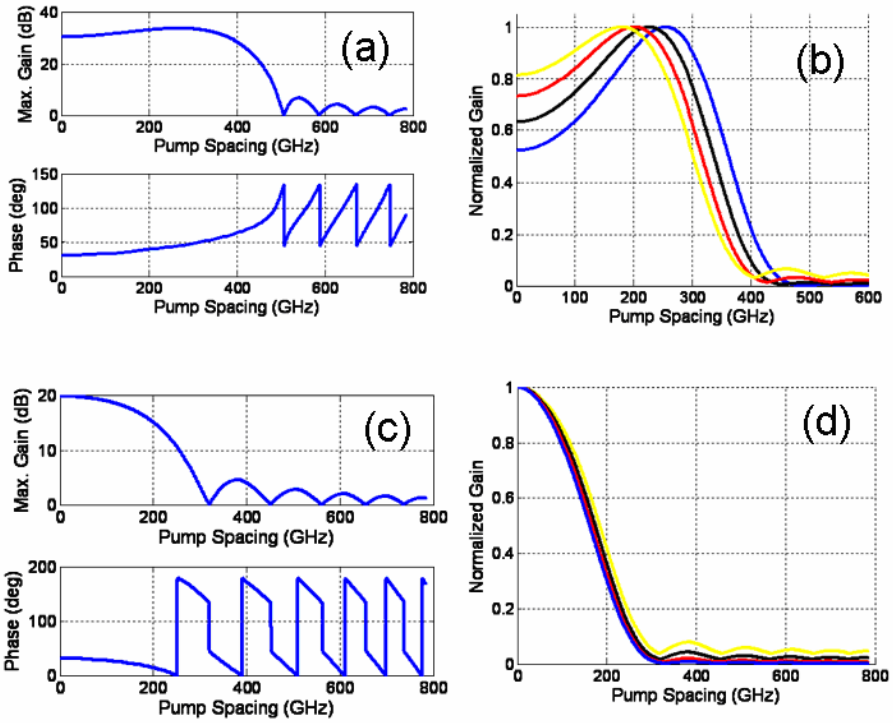

Figure 5.4: Phase-matching calculations for SP-PSA.. Top (a): small-signal PSA gain for D = -300 ps/nm/km, L = 5.64 m, γ = 1100/W/km and total pumping power of 28 dBm. Distributed losses of 1.4 dB/m were taken into account. Bottom (a): signal input phase required to produce maximum gain at each pump separation, for constant parameters otherwise. (b) Normalized small-signal gain for increasing pump spacing at four pumping powers: 24.5 dBm (total, yellow), 25.5 dBm (red), 26.5 dBm (black) and 27 dBm (blue). (c) and (d) are corresponding graphs, for the same parameters but positive dispersion coefficient D = 300 ps/nm/km.

5.2. Phase Regeneration Experiments

5.2.1. Experimental Setup

The experimental setup is shown in Figure 5.5. Light from a single tunable laser was divided into two paths for generation of pumps and a degraded signal to be regenerated. The signal was modulated with 10 Gb/s NRZ-DPSK data with pattern length at least 2^{15}-1 using a phase modulator. For regeneration

experiments nonlinear phase noise was simulated by driving a second phase modulator with a high-frequency sinusoidal tone to produce large differential phase errors. For characterization measurements, data modulation was not necessarily applied. The signal was amplified, filtered and attenuated before being coupled into a high-power amplifier with the pumps. Pump waves symmetric around the signal frequency were generated using carrier-suppressed return-to-zero (CSRZ) modulation by driving a zero-biased amplitude modulator with a sinusoidal tone. Experiments were conducted with driving frequencies of both 20 and 40 GHz. The sideband separation is twice the driving frequency of the modulator, while power at the carrier frequency is typically reduced ~23 dB below that of either sideband. An example of the pump spectrum is shown in Figure 5.5. A fiber-Bragg grating (FBG) was used to further suppress light at the carrier frequency in the pump path down to -38 dB, to minimize interference with the DPSK signal when the waves are recombined. The pumps and signal were amplified together using a high-power EDFA and launched into a Bismuth Oxide-based optical fiber. This fiber had an effective nonlinear coefficient of 1100/W/km, length of 5.6 meters, distributed loss of 1.4 dB/m, splicing losses totaling 3.1 dB and dispersion of -290 ps/nm/km. Total launch powers (combined pumps/signal) exceeding 32.5 dBm were possible without phase-modulating the pumps to suppress SBS. The output signal is filtered, and divided for feedback control, direct and differential detection. The input pump-signal relative phase is maintained by monitoring the signal output power and driving a fiber stretcher to counteract environmental fluctuations.

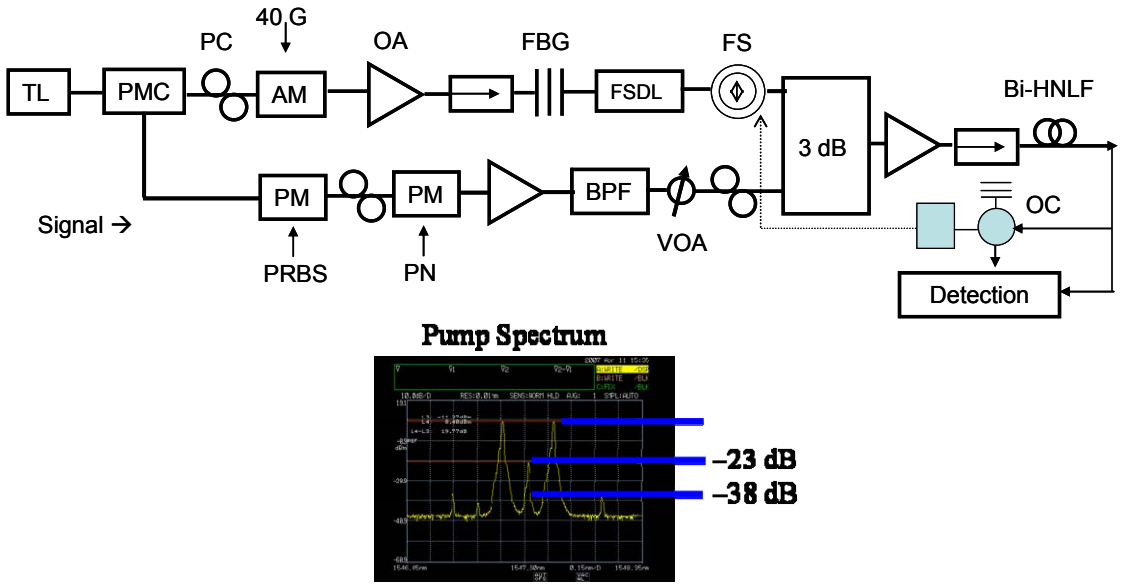

Figure 5.5: Experimental setup for NRZ-DPSK phase regeneration. TL: tunable laser; PMC: polarization maintaining coupler; PC: polarization controller; OA: optical amplifier (EDFA); FSDL: free-space delay line; FS: fiber stretcher; AM: amplitude modulator; PM: phase modulator; BPF: bandpass filter; VOA: variable optical attenuator; Bi-HNLF: bismuth-oxide highly nonlinear fiber; FBG: fiber Bragg grating; OC: optical circulator. A typical spectrum of CSRZ modulation is also shown.

5.2.2. PSA Characterization

The PSA was initially operated with a pump spacing of 40 GHz. Signal light was filtered at the output using a fiber-Bragg grating with approximately 15 GHz bandwidth. The grating bandwidth was slightly too narrow given the 10G data modulation rate, but was required to sufficiently reject light from the nearby pumps. Figure 5.6(a) shows an example of the input and output spectrum for 40G spaced pumps without filtering of the output signal. In this case a phase-modulated signal was amplified. The signal power was reduced ~12 dB below the total pump power at the input to Bi-NLF and the total launched power was 32.5 dBm. The minimum signal power level was restricted by the presence of

residual carrier light from generation of the pumps. Figure 5.6(b) shows the output spectrum before and after filtering using the narrowband FBG. The full output spectrum after PSA is shown in Figure 5.6(c). At high launch powers the signal and pump waves initiate a phase-sensitive FWM cascade that produces symmetric pairs of new signals and pumps [135], increasing signal noise and modifying pump depletion characteristics. This frequency cascade can be avoided by using orthogonal pumps when the inputs are near the fiber ZDF [136]. The cascade is driven primarily by the single-pump MI interaction (although several processes participate in generation of even the first few signals and new pumps). The MI process is not phase-matched in normally dispersive fiber; therefore it becomes less efficient as the pump spacing is increased.

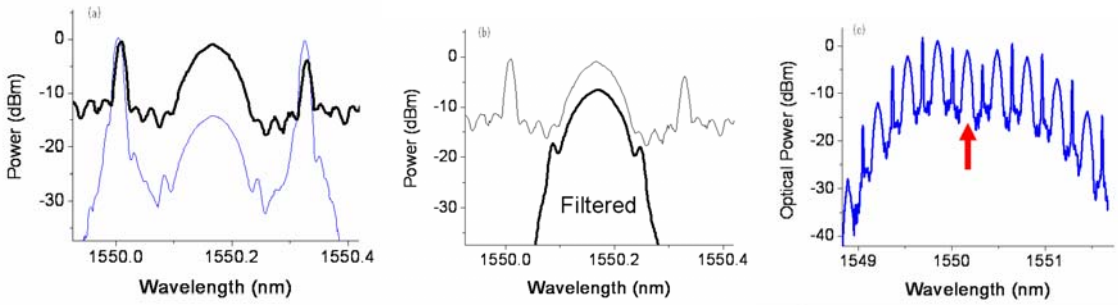

Figure 5.6: Spectra for SP-PSA with 40 GHz spaced pumps. (a) Spectrum after EDFA (blue) and after PSA (black) for pump spacing of 40 GHz. (b) Output spectrum after PSA before and after filtering with the FBG. (c) Full output spectrum; red arrow indicates location of the input signal. Total launch power: 32.5 dBm.

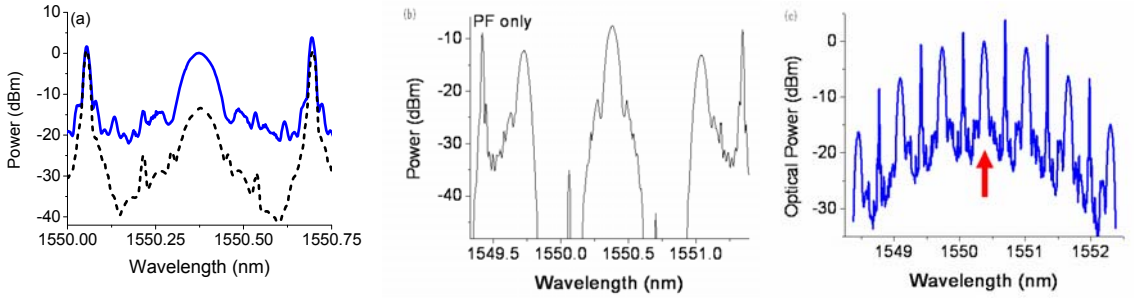

Figure 5.7: Spectra for SP-PSA with 80 GHz spaced pumps. (a) Spectrum after EDFA (black) and after PSA (blue). (b) Output spectrum after filtering with 25 GHz bandwidth periodic filter (interleaver). (c) Full output spectrum; red arrow indicates location of the input signal. Total launch power: 32.5 dBm.

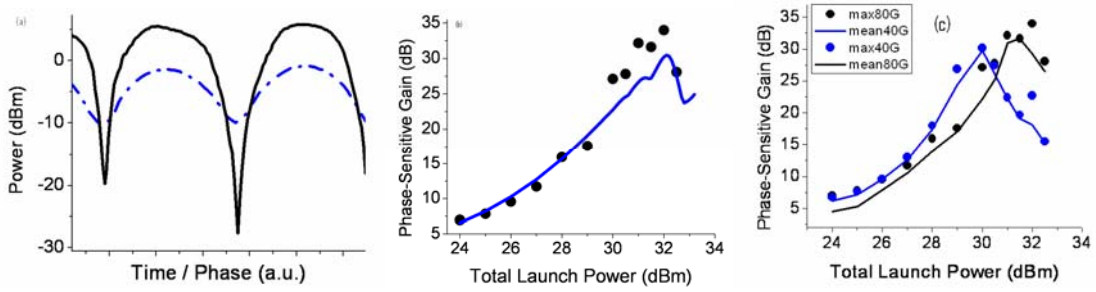

Figure 5.8. (a) Signal power-phase response for launch powers of 26.5 dBm (blue) and 31.5 dBm (black). (b) Evolution of phase-sensitive gain with increasing total launch power. Blue line: solution to Equation 5.2. (c) Comparison of phase-sensitive gain for 40G and 80G spaced pumps. Circles (lines) are maximum (average) values.

Corresponding spectra for pumps spaced 80GHz apart are shown in Figure 5.7. A 25GHz (FWHM) periodic filter used to obtain the spectrum in Figure 5.7(b) is better matched to the signal bandwidth but allows higher order light to be detected along with the signal. The presence of these additional waves leads to heterodyne beating, visible as deterministic modulation after both direct and differential detection. In agreement with theory, cascaded FWM is reduced for the broader pump spacing.

Figure 5.8(a) shows the response of signal power to phase variations for two launch powers of 26 and 31.5 dBm at a constant input pump-to-signal power ratio of 10.5 dB. The response obtained at the highest power is similar to results for other PSAs and implies limiting amplification with respect to phase, which normally coincides with amplitude limiting. PSG is characterized for increasing total power while maintaining the same input power ratio of 10.5 dB. The results in Figure 5.8(b) show the signal reaches a maximum PSG of 35 dB for a launch power of around 31.5 dBm, before reducing at higher launch powers. The solid line is calculated numerically based on only three interacting waves, neglecting the effects of cascaded FWM. The theoretical results do include the effects of residual carrier interference at the input, by assumption of a launched signal of the form $E_{s,total} = E_s(t) + \rho E_{rc}$ where $E_s(t)$ is the actual signal and E_{rc} is the residual carrier, which in experiments has the same phase as the pumps. Remarkable agreement is obtained despite the large actual number of interacting waves (Figure 5.6c). Figure 5.8(c) compares maximum and average measured PSG for the two different pump separations of 40 and 80 gigahertz. The gain for 80 GHz spacing slightly exceeds that at 40 GHz due to better phase-matching.

5.2.3. Phase Regeneration Results

The phase-regenerative properties of the PSA were tested using phase-noise (PN) degraded 10 Gb/s NRZ-DPSK signals. Phase noise was simulated by driving a phase modulator with a 3.3 GHz sinusoidal tone. Figure 5.9 shows an example of regeneration results obtained using pumps spaced 40 GHz apart.

The back-to-back eye diagram after differential detection is widely open but distorted due to filtering. Figure 5.9(b) shows the eye with phase noise added before regeneration. The amount of eye closure suggests differential phase errors approaching the threshold of 90 degrees are imposed on the signal. However the regenerated result in Figure 5.9(c) is similar to the noiseless case. For this measurement the pump power entering the high-power EDFA was 9.6 dBm and the signal power was -0.8 dBm for a ratio of 10.4 dB. The total power launched into the Bismuth fiber was adjusted to 32.5 dBm, the maximum that was used, which produced depletion of the pumps by the signal (aided by cascaded FWM). In the depleted pump regime, the conversion of severe input phase noise to output amplitude noise is clearly suppressed. Residual amplitude noise is visible in the outer edges of the eye; however a portion of this arises from excess ASE noise added by the high-power EDFA and is not related to PSA.

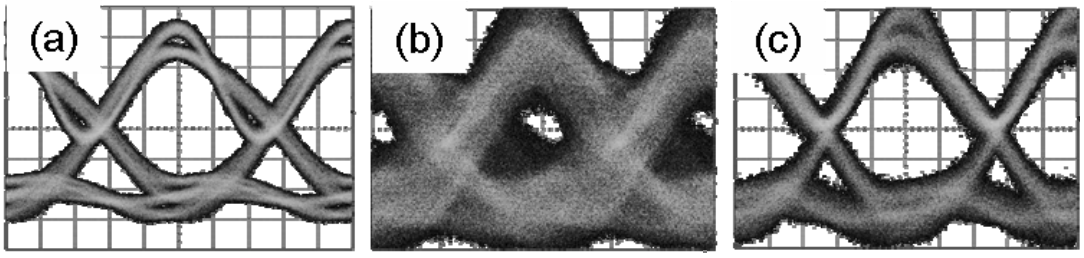

Figure 5.9: DPSK eye diagrams after differential detection for 40G spaced pumps. (a) Back-to-back without phase noise added. With added phase noise (b) before and (c) after regeneration.

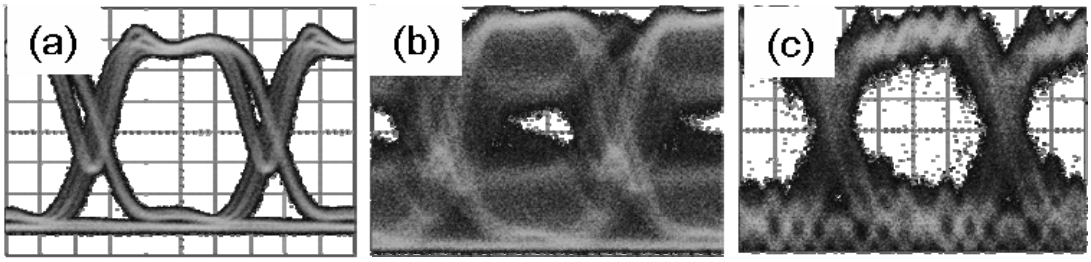

Figure 5.10: DPSK eye diagrams after differential detection for 80G spaced pumps. (a) Back-to-back without phase noise added. With added phase noise (b) before and (c) after regeneration.

Figure 5.10 shows the results of phase regeneration with pumps separated by 80 GHz (0.64 nm). Both the added phase noise and the amount of phase noise reduction are similar to that obtained with the narrower pump spacing. The high-frequency heterodyne beating results from detection of higher order FWM products along with the signal, and can be removed through better optical filtering.

5.3. Phase-and-Amplitude Regeneration Experiments

To verify performance for arbitrary inputs the SP-PSA was characterized using an input signal suffering both phase and amplitude distortions. The experimental setup was the same as that in Figure 5.5 except for the addition of an amplitude modulator to produce the amplitude distortions. This modulator was driven with a swept frequency synthesizer (9 kHz – 1.5 GHz continuous sweep), at different power outputs to adjust the relative amount of phase and amplitude noise. Coherent detection facilitated by digital signal processing was used to give a clearer picture of regeneration performance.

The schematic for coherent detection is given in Figure 5.11. Data output from the PSA is combined with a strong local oscillator in a 90 degree optical hybrid. Use of two outputs from the interferometer gives information about the real and imaginary components of the data electric field. The two channel outputs are sampled with a high-speed oscilloscope at a rate of 40 Gsamp/sec (providing 4 samples per symbol for 10 Gb/s data) and a series of up to 500,000 samples is stored. The data are processed offline using commercially available software that eliminates the need for phase-locking between the data and local oscillator through carrier phase estimation. After phase estimation, the software provides the complex BPSK data stream for use in plotting eye diagrams, time-domain waveforms and constellation diagrams. An additional routine was written to convert the data from BPSK into DPSK, since experiments were designed to test DPSK regeneration specifically. Typically a sequence of between 15,000 and 50,000 symbols is represented in the final output (e.g. on a constellation).

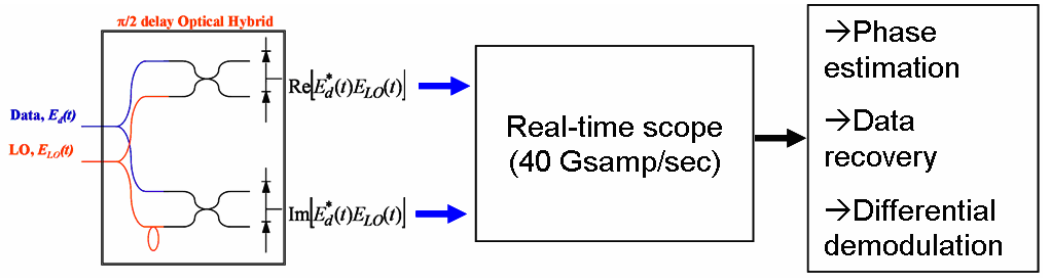

Figure 5.11: Schematic for coherent detection and offline processing

The coherent detection system was characterized to see the difference between a recovered BPSK and DPSK data stream. In all regeneration measurements, the recovered signal is extracted from the PSA using the FBG

filter and therefore suffers distortions; these manifest after coherent detection as well as direct detection. Figure 5.12 shows a constellation histogram, BPSK eye and the calculated DPSK eye. The constellation histogram is calculated by dividing the data series (one sample per symbol) into bins in the complex plane. The resolution was set to produce 40,000 bins, and the color axis corresponding to the frequency count per bin was calculated on a logarithmic scale. Each eye diagram is characterized by a decision-threshold Q-factor on a linear scale to give an estimate of the signal quality.

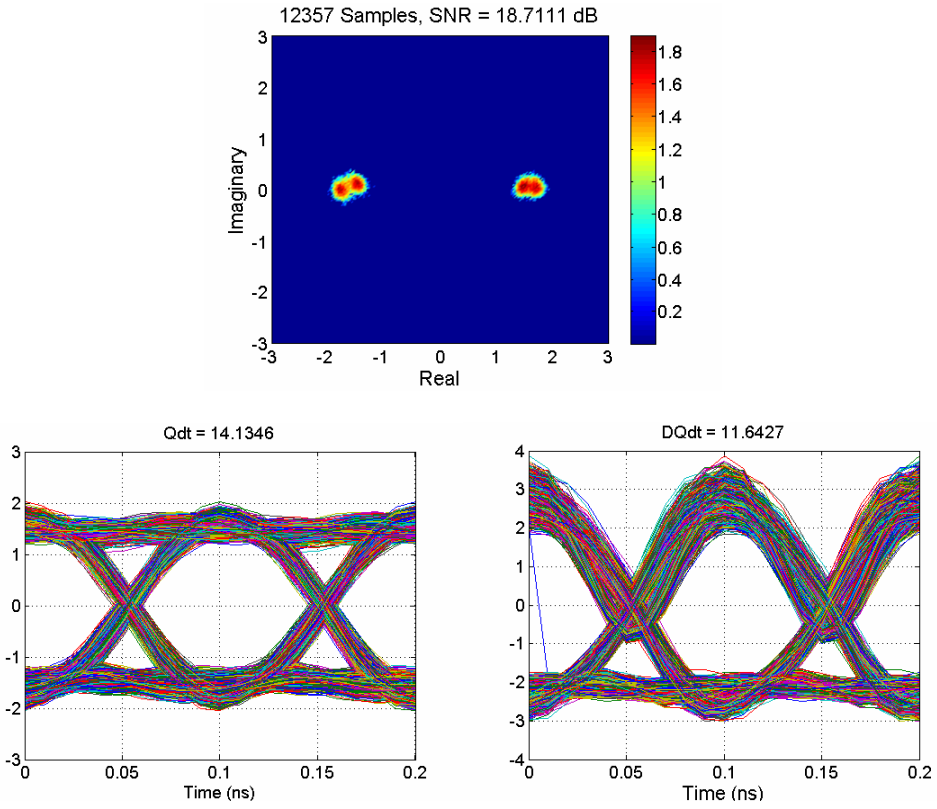

Figure 5.12: Constellation histogram (top), BPSK eye and DPSK eye (bottom, left to right) of a clean phase-modulated signal.

Examination of the histogram reveals four, rather than two, distinct phase and amplitude centers. This is attributed to the combination of imperfect DPSK modulation (in this case, a phase modulator was used to produce the data) with polarization modulation, and imperfect alignment of the signal and LO polarizations at detection. The polarization modulation results from misalignment of the signal polarization with the modulator crystal axis. Even for perfect phase information (i.e. generated by driving an amplitude modulator instead of a phase modulator), a similar effect was observed that allowed the signal polarization fluctuations to show up as amplitude and phase fluctuations after coherent detection. This constellation is shown as an example because this effect frequently inhibited clean measurement of experimental results. Subsequent constellations with similar distributions suffer from this effect, which is present even in the back-to-back case.

Figure 5.13 directly compares the coherent detection of BPSK data with and without narrowband filtering (a-b). The typical eye closure penalty due to introduced waveform distortions was < 0.5 dB. In (c-d), DPSK data demodulated in the software domain is compared. Compared to the BPSK case, the eye Q-factor degraded 0.8 – 1.23 dB, while the penalty for narrowband filtering of BPSK was typically 0.4 dB.

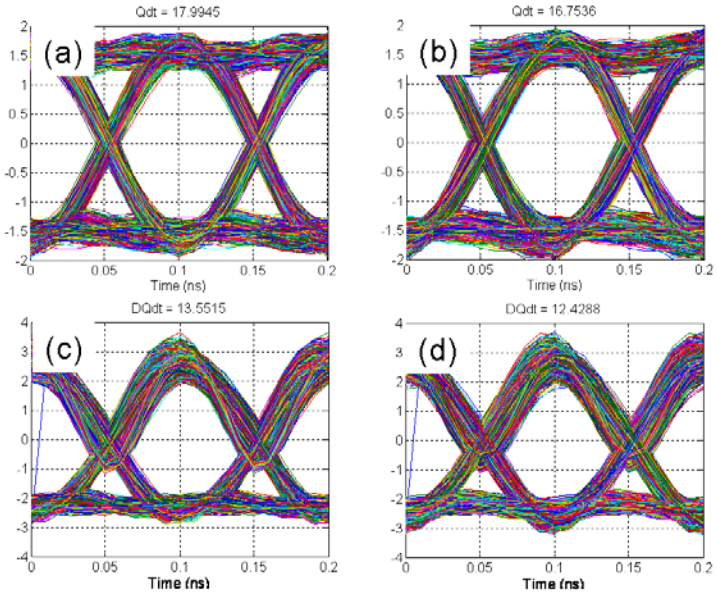

Figure 5.13: Eye diagrams for BPSK (top) and DPSK (bottom) before (left) and after (right) narrowband optical filtering.

To verify the PSA can simultaneously suppress amplitude and phase fluctuations, deterministic (emulating dispersion-induced pattern effects, FWM, SPM and XPM) distortions were imposed on the input signal. The signal was attenuated ~11 to 15 dB below the total pump power before all three waves were amplified together. Larger power ratios (pump/signal) produce better regeneration results in theory; here the maximum ratio is limited by available pumping power and the level of residual carrier after generation of the symmetric pumps. The output signal was characterized at different operating points corresponding to progressively larger total launch powers. This allowed observation of phase-only regeneration (in the small-signal regime) and the transition to complete signal regeneration.

Constellation histograms shown in Figure 5.14 characterize the signal (a) without PSA with distortions imposed, and (b-f) at total launch powers of ranging from 140 to 922 mW. The degraded signal in Figure 5.14(a) exhibits large phase variations, with standard deviation 29 degrees and a maximum differential phase error of 65 degrees. The calculated SNR was around 7.3 dB. Figure 5.14(d) was recorded for a total pump power of 337 mW and signal launch power of 11.4 mW (15 dB ratio), and represents the output with minimal phase noise. In this regime amplitude noise is still present, however the maximum differential phase error and phase noise standard deviation reduced to 38 and 6.45 degrees, respectively. The total power was then increased to observe removal of amplitude noise and see the effects on the phase distribution. At the maximum launch power, the maximum error and standard deviation measured were 39 and 9.2 degrees, respectively. The slight increase of phase noise for increasing launch power is commensurate with theory. It may be exaggerated in this experiment due to a number of factors, including excess ASE from the booster amplifier and strong FWM between the pumps. A strong SNR improvement from 7.3 to 15.7 dB is demonstrated for operation in the depleted-pump regime.

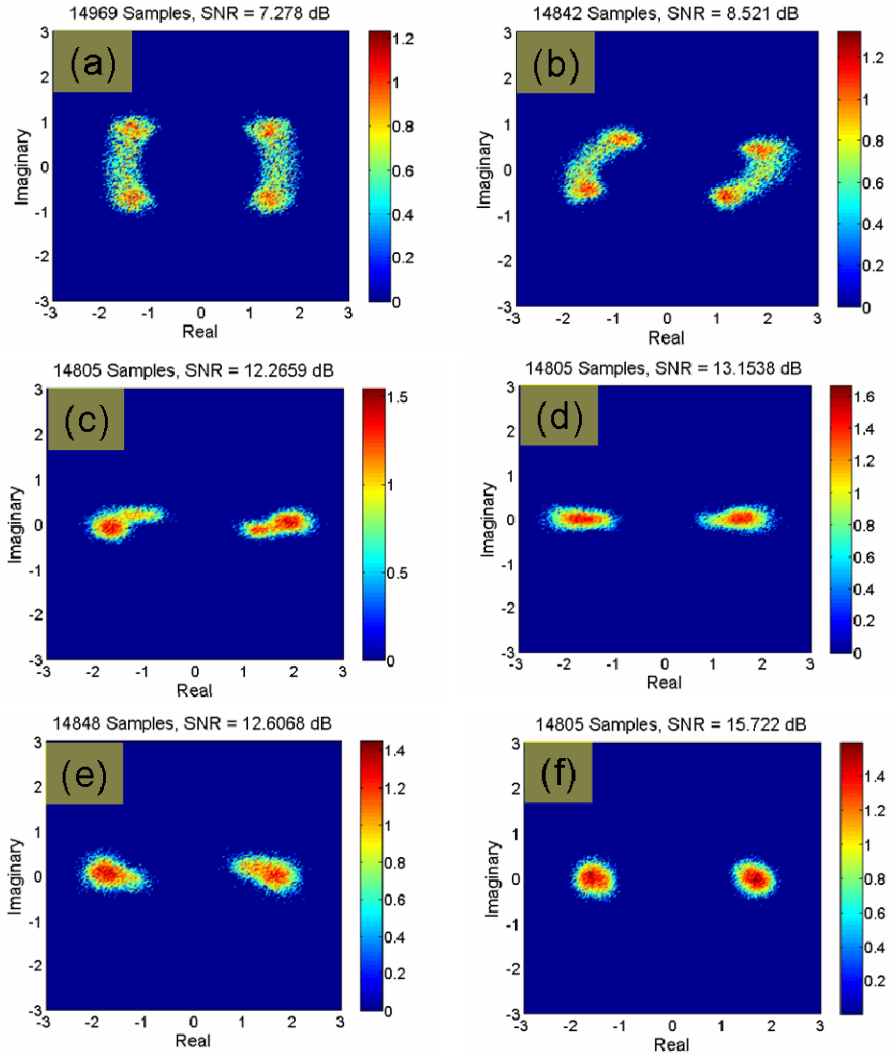

Figure 5.14: Evolution of signal constellation during PSA with input phase and amplitude distortions.

Figure 5.15 shows eye diagrams obtained from differential detection for four cases. Clean (filtered through FBG) and degraded eyes are shown in (a-b). Figure 5.15(c) shows the eye corresponding to Figure 5.14(d) with minimal phase noise, where strong amplitude noise is introduced by the PSA process. The final eye corresponds to Figure 5.14(f), which exhibits the most improvement in terms of signal to noise ratio. The Q-factor improvement (from 4.9 to 6.63 on a linear

scale) obtained was about 2.6 dB. Further improvement would be obtained under the same conditions with use of a suitable output filter, since the FBG produced significant amplitude distortions even for clean signals. The regenerated output was obtained for 922 mW total pumping power and 65 mW signal power (11.5 dB ratio, the signal power was large to increase depletion of the pumps).

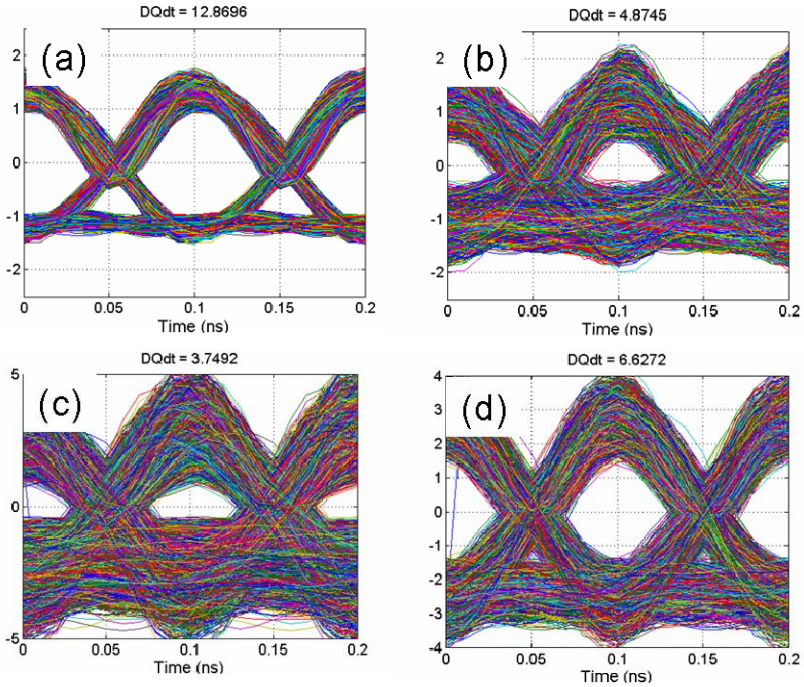

Figure 5.15: Eye diagrams for (a) clean signal, (b) distorted signal before PSA, (c) with phase-only regeneration and (d) after simultaneous phase and amplitude regeneration.

5.4. Summary

The results of this and the preceding chapter show effectiveness of two PSA techniques for improving DPSK signal quality. Both allow removal of amplitude and phase distortions commensurate with signals that have undergone

significant dispersion, FWM, SPM and CPM. Each implementation has relative advantages and technical challenges.

The NOLM-PSA was hindered by the requirement to phase-modulate the pump for SBS suppression. The imperfections in pump phase modulation produced signal gain fluctuations, while pump amplitude noise contributes to both phase and amplitude noise of the signal. With use of suitable materials (e.g. Bismuth-oxide fibers with lower insertion loss) this requirement can be removed, which would allow significantly higher pump-to-signal power ratios and consequently better performance. One advantage of the NOLM is that once carrier phase and polarization recovery are complete, no additional modulation is required to produce symmetric pumps. However compared to the SP-PSA, a NOLM-PSA requires more optical components (e.g. circulators), and it is ultimately limited by its intrinsic amplitude-to-phase noise conversion.

The SP-PSA offers improved performance over the NOLM-PSA because it suppresses AN to PN conversion. The gain of a SP-PSA is also exponential with distance, whereas for the NOLM-PSA growth of the signal is quadratic. The major challenge to implementing a SP-PSA practically is generation of suitable pumps. These require modulation of the recovered carrier, combined with efficient filtering of ASE noise after amplification and strong suppression of any residual carrier. In the current experiments a single FBG was sufficient to reduce the residual carrier > 33 dB below the level of each pump; however the signal could only be reduced ~15 dB below the pumps before effects associated with residual carrier interference became significant. Higher reflectivity gratings can

further suppress the carrier, but the requirement for tight ASE filtering will introduce further complexity. Finally, the pumps should potentially be spaced further apart. In the experiments described above, doubling the pump spacing would in principle allow phase-matching while discriminating against cascaded FWM.

Both PSAs are currently limited to single-channel operation; however OEO regeneration also requires parallel operation on all individual channels. The other advantages of all-optical networking remain, including elimination of expensive and power-consuming high-speed RF electronics, and transparency to bit-rate (with a suitable pumping scheme).

CHAPTER SIX: PHASE-REGENERATIVE WAVELENGTH CONVERSION

6.1. Introduction: Regenerative Wavelength Conversion

Wavelength conversion can be accomplished using a wide variety of nonlinear optical devices. In PSK systems it is necessary to preserve both the amplitude and phase of the signal during conversion to the new wavelength. This renders FWM-based devices suitable [137-139], with the majority of these relying on the single-pump phase-conjugation process studied in Chapter 2. PC produces a wavelength-converted idler from optical noise which is amplified along with the signal; consequently this process decreases the optical signal-to-noise ratio by ~3 dB [140].

An alternate FWM process called Bragg-Scattering (BS) provides wavelength translation without amplification: signal light is converted to the idler wavelength, but the total sideband power is constant [141]. BS has a theoretical noise figure of 0 dB [140] which is not reached due to the same complications associated with PC. Experiments have shown the noise performance of BS to exceed that of PC [142].

These NF limits are valid for input signals processed with high gain, linear amplifiers: those that do not deplete the pumps during the respective FWM process. Within the context of FWM, regeneration occurs in nonlinear amplifiers where the gain is depleted. In the nonlinear regime one or more of the signal noise statistics (amplitude or phase variance, or the quadrature amplitude variances) can be improved. For example, during PC the output signal (or idler)

can exhibit reduced amplitude fluctuations even if the input signal does not suffer excess noise [54, 55, 143]. This regenerative property was exploited in Chapter 2, but the wavelength-converted output was not chosen because of the inherent degradation of the idler phase. If this penalty can be tolerated, amplitude-regenerative wavelength conversion can be provided for PSK signals by PC.

Phase-regenerative wavelength conversion (PR-WC) requires more intensive study. Some techniques suggested for DPSK regeneration, namely those that seek to regenerate phase by first equalizing amplitudes and then re-coding the phase information in an all-optical fashion, could potentially provide PR-WC ([92], for example). These face challenges in all-optical phase re-coding. A recent SOA-based device has shown promise in providing WC with small penalties [144-146], although thus far the amount of phase regeneration obtained has been limited. Additionally, SOA-based devices retain bit-rate limitations when processing OOK-type signals. Phase-sensitive amplification remains the most convincing technique for phase noise suppression and thus a likely source for PR-WC solutions. The most straightforward way to accomplish PR-WC using PSA is to implement a serial, two-stage process: for example the existing SP-PSA architecture, followed by PC or BS.

6.1.1. Two-Stage Phase-Regenerative Wavelength Conversion

In a recent paper cascaded FWM was studied [121] and shown to provide PSA at the input signal wavelength as well as at the new (idler) wavelength [147]. The conditions for obtaining phase regeneration at the idler wavelength were not

clearly defined, and practical issues were not discussed. Both are therefore reviewed below. Ultimately this two stage process is impractical, but provides a basis for the single-stage implementation derived in this research.

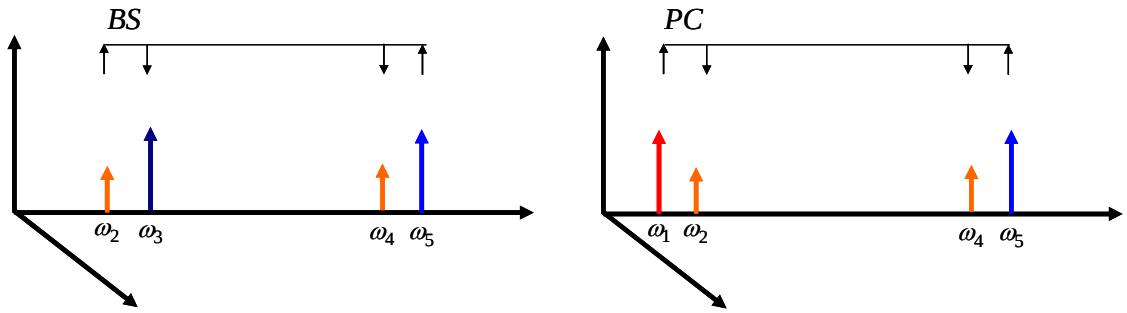

Figure 6.1: Frequency arrangement for cascaded Bragg-scattering and phase-conjugation. Arrows indicate direction of energy flow between the waves.

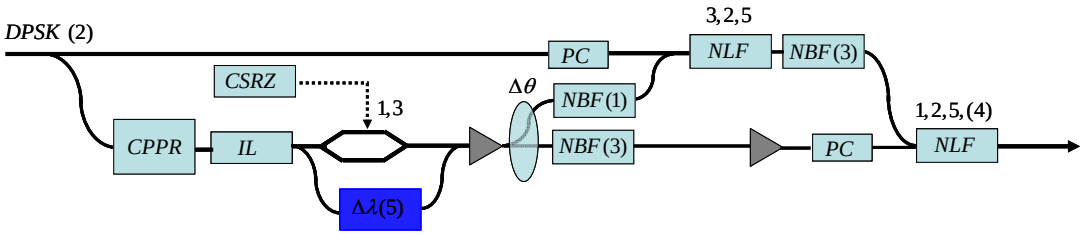

Figure 6.2: Schematic for 2-stage PSA (BS followed by PC). Numbers denote interacting waves.

Frequency arrangements for the cascaded processes are given in Figure 6.1. Alternative implementations may also be used, and the order of implementation can be reversed. The schematic in Figure 6.2 shows a possible experimental configuration. Modulation, such as CSRZ, should be used to derive pumps 1 and 3, which are near in frequency to the signal and must be symmetric around it. This allows free placement of the third pump (denoted 5), in contrast to the configuration of [121] where none of the required frequency spacings were

satisfied automatically. Pump 5 should share the same carrier phase as the signal and other pumps; therefore it must be a wavelength shifted image of the recovered carrier. This suggests use of a nonlinear frequency conversion process is required to generate this pump, although this has not been thoroughly investigated. Note the presence of three narrow-band filters (NBF), which are required for rejection of waves entering each stage and between stages (*NBF*(x) denotes *rejection* of wave "x").

Referring to the originally proposed frequency arrangement [121], the idler output after cascaded BS→PC interactions takes the form

$$B_4(z') = \overline{\mu}^*(L)\cdot\nu(z')\cdot B_2^*(0) - \overline{\nu}^*(L)\cdot\mu(z')\cdot B_2(0). \tag{6.1}$$

The auxiliary functions

$$\begin{aligned}
&\overline{\mu}^*(L) = \cos(kL) - i\frac{\delta}{k}\sin(kL)\\
&\nu(z') = i\frac{\gamma'}{k'}\sinh(k'z')\\
&\overline{\nu}^*(L) = -i\frac{\gamma}{k}\sin(kL)\\
&\mu(z') = \cosh(k'z') + i\frac{\delta'}{k'}\sinh(k'z')
\end{aligned} \tag{6.2}$$

The length of the first stage is L, propagation distance in the PC stage is denoted by *z'*, and the gain coefficients are $k = \sqrt{|\gamma|^2 + \delta^2}$ and $k' = \sqrt{|\gamma'|^2 - \delta'^2}$ for BS and PC. The (complex) pumping parameters are $\gamma = \overline{\gamma}\varepsilon B_1 B_3^*$ and $\gamma' = \overline{\gamma}\varepsilon B_1 B_5$ for the BS and PC processes, respectively, and net phase-mismatch parameters $\delta = \Delta\beta/2 + \overline{\gamma}/2\cdot(P_1 - P_3)$ and $\delta' = \Delta\beta'/2 + \overline{\gamma}/2\cdot(P_1 + P_5)$. Finally, the linear phase-

mismatch parameters are defined $\Delta\beta = \beta_2 + \beta_3 - \beta_1 - \beta_4$ and $\Delta\beta' = \beta_2 + \beta_4 - \beta_1 - \beta_5$. The idler is subject to CPM from the pumps; after including the amplitude transformations that lead to Equation 6.1, the idler field can be written $A_4(z') = \bar{\mu}^*(L)\cdot\nu(z')\cdot A_2^*(0)\cdot e^{i\phi_1} - \bar{\nu}^*(L)\cdot\mu(z')\cdot A_2(0)\cdot e^{i\phi_2}$ with phase terms

$$\theta_1 = \frac{(\Delta\beta L - \Delta\beta' z')}{2} + \bar{\gamma}P_1\cdot\left[\frac{(2\varepsilon-1)z'}{2} - \frac{3L}{2}\right] - \bar{\gamma}P_3(\varepsilon+1/2)L + \bar{\gamma}P_5\frac{3z'}{2} \tag{6.3}$$

$$\theta_2 = \frac{(\Delta\beta L - \Delta\beta' z')}{2} + \bar{\gamma}P_1\cdot\left[\frac{(2\varepsilon-1)z'}{2} + \frac{(\varepsilon+1/2)}{2}\right] + \bar{\gamma}P_3\frac{3L}{2} + \bar{\gamma}P_5\frac{3z'}{2} \tag{6.4}$$

From Equation 6.1 with the phase terms (6.3-6.4), the output idler power reads

$$P_4 = |A_2(0)|^2\left\{\begin{array}{l}\left|\bar{\mu}(L)\right|^2\left|\nu(z')\right|^2 + \left|\bar{\nu}(L)\right|^2\left|\mu(z')\right|^2 + \ldots \\ 4\left|\bar{\mu}(L)\right|\left|\mu(z')\right|\left|\bar{\nu}(L)\right|\left|\nu(z')\right|\cos\left[2\phi_1 - \phi_3 + \phi_5 - 2\phi_2 + \theta_1 - \theta_2\right]\end{array}\right\} \tag{6.5}$$

A critical feature of this PSA architecture is the dependence of idler power on all the pump phases. For practical implementation, these must have well-defined relationships, which is difficult if pumps 3 and 5 are placed far from the signal (if the configuration in Figure 6.1 is used then only synchronization of pump 5 is difficult).

Equation 6.1 describes a squeezing transformation with input amplitudes $\overline{\mu}^{*}(L)\cdot B_2^{*}(0)$ and $\overline{\nu}^{*}(L)\cdot B_2(0)$. Phase regeneration in the second stage depends on the power transfer from signal to idler in the first stage, resulting in three regimes of operation with different characteristics. These are summarized in Figure 6.3, which shows growth of the signal and idler amplitudes during each stage, and second-stage input-output idler phase at various points (bold black lines indicate the phase at or near the end of stage 2).

Ideally the stage-two input amplitudes are equal (half the signal power is transferred to the idler), in which case $\overline{\mu}^{*}(L)\cdot B_2^{*}(0)=\overline{\nu}^{*}(L)\cdot B_2(0)$. As the signal and idler are amplified by PC in the second stage, phase regeneration improves in the same manner as for the SP-PSA. This is the first situation shown in Figure 6.3; it has the advantage that, to optimize phase-regeneration, one need only increase the length (or pumping power) during stage 2.

If power transfer in the first stage is incomplete, $\overline{\mu}^{*}(L)\cdot B_2^{*}(0)>\overline{\nu}^{*}(L)\cdot B_2(0)$ and the idler is initially smaller than the signal. Because in stage 2 the non-conjugate term growth is $\propto \cosh(k'z')$, the two contributions equalize at a single propagation length, where ideal PR is obtained. Performance is reduced for both shorter and longer interaction lengths. For excess power transfer $\overline{\mu}^{*}(L)\cdot B_2^{*}(0)<\overline{\nu}^{*}(L)\cdot B_2(0)$ and the contributions can not equalize; consequently this regime will not produce ideal PR.

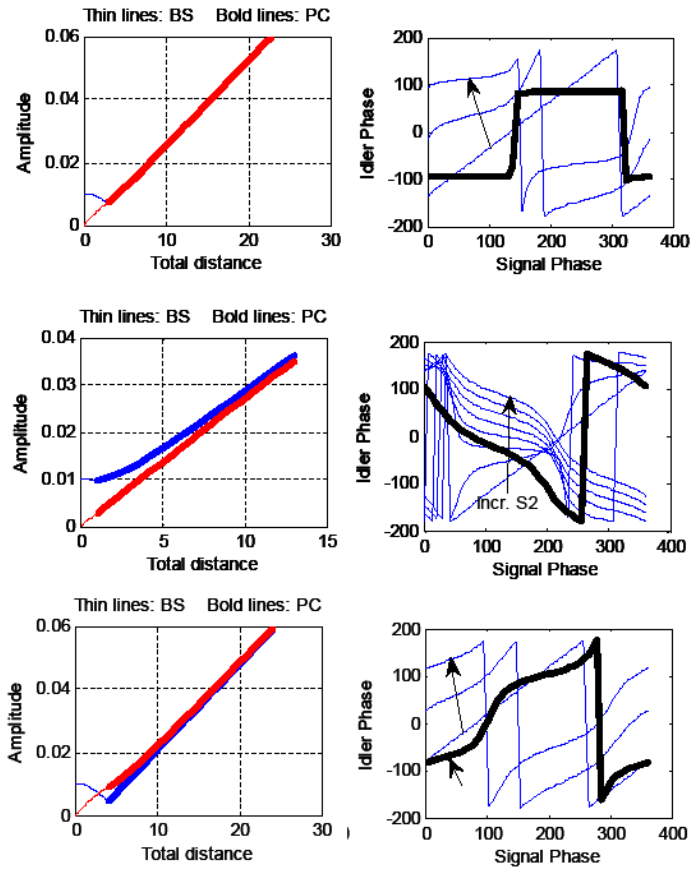

Figure 6.3: Phase regeneration through cascaded BS→PC, three different regimes of operation. Cases 1, 2 and 3 from the text are represented from top to bottom, respectively.

6.1.2. Single-Stage Regenerative Wavelength Conversion

As an alternative to cascaded BS→PC a parallel process has been proposed, analyzed and demonstrated experimentally. Conceptually, two FWM processes can occur simultaneously with each contributing to a new wave at the same frequency. Two source terms drive the material nonlinear polarization at the new frequency, with differing phases. A simple analysis shows the phases are anti-

correlated with respect to signal phase shifts, resulting in stabilization of the new idler phase.

Figure 6.4: Frequency allocations for parallel BS-PS providing PR-WC. Input waves 1-3, 5 produce new waves 4 and 6 through parallel FWM processes.

Single-stage PR-WC results when the BS and PC processes occur simultaneously in a single fiber. In this parallel implementation, the waves of Figure 6.1 are arranged as shown in Figure 6.4. Inputs are waves 1-3 and 5 as in the cascaded process with waves 1, 3 and 5 acting as pumps. Pumps 1 and 3 are positioned at frequency spacing $\pm\delta\omega$ relative to the signal frequency. The placement of pump 5 is then arbitrary, providing tunable wavelength conversion. In the scalar process, all inputs are co-polarized. Two new waves, 4 and 6, are generated simultaneously and in principle provide PR-WC. Each has an associated PC and BS contribution as outlined in Figure 6.5. A schematic for implementation is shown in Figure 6.6; this should be compared with Figure 6.2.

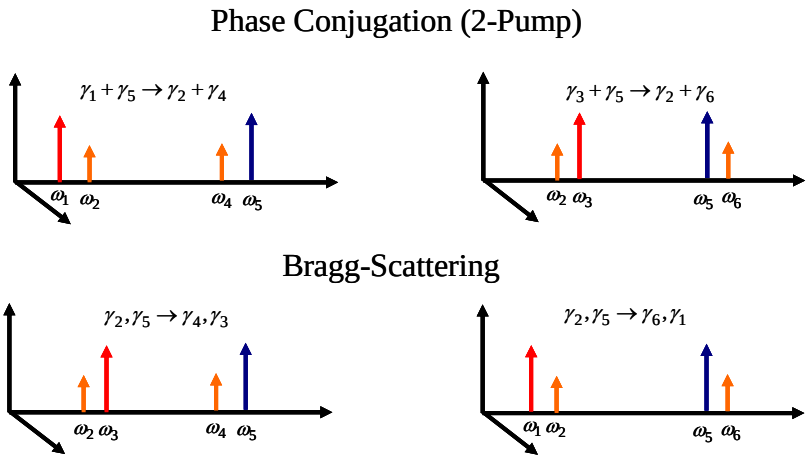

Figure 6.5: Parallel FWM processes contributing to idlers 4 (left) and 6 (right).

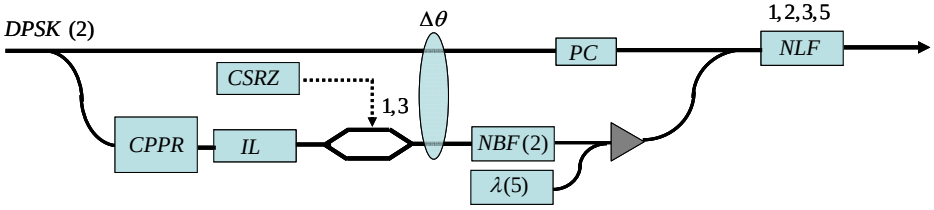

Figure 6.6: Schematic for single-stage (parallel) BS-PC.

The parallel BS-PC process provides PSA similar to, but distinct from, the cascaded BS-PC process. Neglecting the effects of SPM and CPM, the CMEs for new waves 4 and 6 in the scalar case read

$$\partial_z A_4 = i2\gamma A_1 A_5 A^*_2 e^{-i\Delta\beta_{pc4}z} + i2\gamma A_2 A_5 A^*_3 e^{-i\Delta\beta_{BS4}z}$$

$$\partial_z A_6 = i2\gamma A_2 A_5 A^*_1 e^{-i\Delta\beta_{BS6}z} + i2\gamma A_3 A_5 A^*_2 e^{-i\Delta\beta_{pc6}z} \qquad (6.6a,b)$$

In Equation 6.6a the first term results from the dual-pump PC process $\omega_1+\omega_5=\omega_4+\omega_2$, while the second term results from the Bragg-Scattering

process $\omega_2 + \omega_5 = \omega_3 + \omega_4$. The associated linear wave-number mismatches $\Delta\beta_{pc4} = \beta_2 + \beta_4 - \beta_1 - \beta_5$ and $\Delta\beta_{BS4} = \beta_3 + \beta_4 - \beta_2 - \beta_5$. Similar relationships hold for Equation 6.6b. It is useful to graph the two contributions on a phasor diagram as shown in Figure 6.7, where wave 4 is considered as the output. From Equation 6.6a, the BS process produces an idler at ω_4 with initial phase $\phi_{4,BS} = \pi/2 - \phi_3 + \phi_2 + \phi_5$. Similarly the PC process contributes an idler with initial phase $\phi_{4,pc} = \pi/2 + \phi_1 - \phi_2 + \phi_5$. These vectors are plotted in Figure 6.7 under the assumption $\phi_3 = \phi_1$. An exemplary value of $\phi_2 \sim \pi/4$ is used for illustration. Both contributions exhibit the same dependence on the phase of wave 5, allowing this to serve as a reference phase (therefore set to 0). The output exhibits the phase $\phi_4 = \pi/2$ when the signal (wave 2) phase lies in the interval $[-\pi/2,\ \pi/2]$. On the other hand if the signal phase is in the interval $[\pi/2,\ -\pi/2]$ relative to pumps 1 and 3, the output phase $\phi_4 = -\pi/2$.

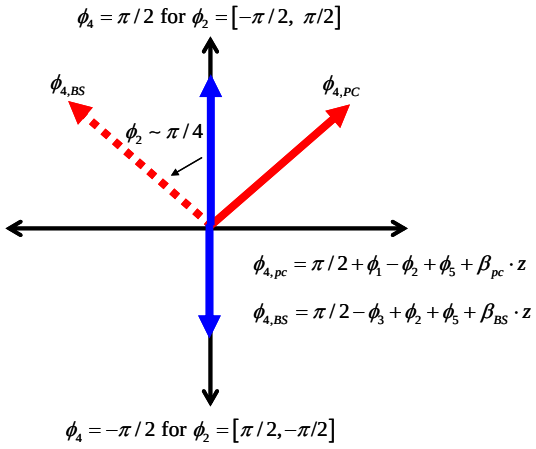

Figure 6.7: Phasor diagram for initial generation of idler 4.

The description above suggests some important features for the new waves 4 and 6. First, these are generated initially with perfectly regenerated phases, in contrast to other phase-sensitive processes where phase-regeneration performance increases with signal gain. The relative contributions from BS and PC as distance increases will either preserve or perturb the initial phase characteristics. Second, the phase of wave 5 can be completely arbitrary since it serves only as a reference phase: phase-locking of this wave is not required. Because the output phase of idler 4 rotates freely with that of pump 5, its linewidth must be limited. However this limitation is the same as for any DPSK transmitter laser. As for the SP-PSA, the signal phase must be stabilized relative to the phases of pumps 1 and 3. This is easily achieved because these pumps are derived from a source that shares the signal carrier phase.

6.2. Small-Signal Analysis

6.2.1. Approximate Solution to Coupled-Mode Equations

An approximate analytical expression was derived for waves 4 and 6 under the following assumptions: (1) All pumps are assumed to be un-depleted; (2) waves 4 and 6 do not experience coupled propagation (only first order FWM interactions are considered); (3) the signal is a constant: it does not evolve with distance. The first assumption is familiar in nonlinear optics for small interaction lengths. Assumption 2 ignores the single-pump PC process in which $2\omega_5 = \omega_4 + \omega_6$, which does not occur until waves 4 and 6 are generated by parallel BS-PC. A simple analysis reveals the initial relative phase between waves 4, 5 and 6 is $\mp\pi$, which

inhibits the single-pump PC interaction (it requires a relative phase of $-\pi/2$). Assumption 3 is more controversial, and in fact the effects of wave 5 (and newly generated waves 4 and 6) on the input signal evolution are of significant physical interest. Further analysis reveals (1) the signal does not evolve in the initial stages, due to its phase relative to pumps 1 and 3, and (2) the subsequent evolution of the signal is largely independent of waves 4, 5 and 6.

Pumps 1, 3 and 5 experience both SPM and CPM: $\Phi_{nl,j} = \gamma \cdot z \cdot \left(\sum 2P_{k \neq j} + P_j \right)$ for j = 1, 3, and 5. Signal 2 and idler 4 undergo cross-phase shifts $\Phi_{nl2,4} = \gamma \cdot z \cdot \sum 2P_j$ that, along with the pump phase shifts, contribute the nonlinear component of the net phase-mismatch. For simplicity it is assumed that $P_1 = P_3 = P_p$ and the phases of pumps 1 and 3 are equalized to zero (these pumps are synchronized to the signal carrier phase). Using amplitude transformations $B(z) = A(z) \cdot e^{-i \cdot \Phi_{nl}}$ for each wave leads to the following CME for idler 4:

$$\partial_z B_4 = i2\gamma \sqrt{P_p P_5 P_2} \cdot \left(e^{i\left(\phi_p - \phi_2 + \Delta_{pc} \cdot z\right)} + e^{-i\left(\phi_p - \phi_2 - \Delta_{BS} \cdot z\right)} \right) \cdot e^{i\phi_5} \tag{6.7}$$

The net wave-number mismatch parameters are $\Delta_{BS} = \Delta\beta_{BS} - \gamma\left(P_3 - P_5\right)$ and $\Delta_{pc} = \Delta\beta_{pc} + \gamma\left(P_1 + P_5\right)$. Equation 6.7 can be re-written

$$\partial_z B_4 = i2\gamma \sqrt{P_p P_5 P_2} \cdot \left(e^{i\delta\phi} e^{i\Delta_{pc} \cdot z} + e^{-i\delta\phi} e^{i\Delta_{BS} \cdot z} \right) \cdot e^{i\phi_5} \tag{6.8}$$

The phase difference $\delta\phi = \phi_p - \phi_2$. The solution to Equation 6.8 is easily obtained. The resulting field and output power are

$$B_4(z) = i2\gamma\sqrt{P_p P_5 P_2}\cdot e^{i\phi_5}\cdot\left(e^{i\delta\phi}\cdot\operatorname{sinc}\left(\frac{\Delta_{pc}\cdot z}{2}\right)\cdot e^{i\Delta_{pc}\cdot z/2} + e^{-i\delta\phi}\cdot\operatorname{sinc}\left(\frac{\Delta_{BS}\cdot z}{2}\right)\cdot e^{i\Delta_{BS}\cdot z/2}\right)\cdot z$$

(6.9)

$$P_4(z) = 4\gamma^2 P_p P_5 P_2\cdot z^2\cdot\begin{pmatrix}\operatorname{sinc}\left(\frac{\Delta_{pc}\cdot z}{2}\right)^2 + \operatorname{sinc}\left(\frac{\Delta_{BS}\cdot z}{2}\right)^2 + \ldots \\ 2\cdot\operatorname{sinc}\left(\frac{\Delta_{pc}\cdot z}{2}\right)\operatorname{sinc}\left(\frac{\Delta_{BS}\cdot z}{2}\right)\cos(\theta(z))\end{pmatrix} \qquad (6.10)$$

Identical equations hold for idler 6, with subscripts 4→6. Equation 6.9 suggests idler 4 is initially perfectly phase-regenerated (see Figure 6.8). Phase shifts that accumulate due to CPM and non-zero linear phase-mismatch detune idler growth and disrupt phase regeneration (it remains ideal as long as the two "sinc" arguments remain equalized). In Equation 6.10, $\theta(z) = 2\delta\phi + (\Delta_{PC} - \Delta_{BS})\cdot z/2$ contributes the phase-sensitive part of idler generation. When the signal is taken to be constant, the maximum power growth is quadratic (for small values of Δ_{BS} and Δ_{pc}) with distance. Otherwise, the idler power should increase linearly with either pump or signal input power. These equations also show the conditions for maximum idler generation occur for (at z =

0) $\delta\phi = 0$, which suggests if $\phi_1 = \phi_3 = 0$ the signal phase should be $0, \pi$. This is in contrast to $\phi_S = \pi/4, 5\pi/4$ for maximization of signal PSA. In fact, if pumps 1 and 3 and the signal are phased for maximum idler growth, the theory outlined in Chapter 5 states the signal will propagate with unity gain (unaffected). In the general solution the signal will experience slow growth: the same PC processes amplifying the idlers also amplify the signal, but BS continuously transfers signal power to the new idlers. Finally, the solutions make clear that the phase of pump 5 need not be synchronized to the phases of other waves. Pump 5 provides a new carrier phase for the PR-WC idlers.

6.2.2. Limitations due to Phase-Matching

The material dispersive properties play a prominent role in determining both the conversion efficiency and the degree of phase regeneration. The absolute magnitudes of the phase-mismatch parameters affect the idler growth rate, while their relative magnitudes determine the interaction length over which phase-regeneration is retained. It is possible to obtain ideal phase-regenerative behavior when the wave-number mismatches are large, provided the interaction length is small. However since the arguments $\mathrm{sinc}\left(\Delta_{pc,BS} \cdot z/2\right)$ depend on the product of $\Delta_{pc,BS}$ and distance, the phase-regenerative behavior will degrade more rapidly as the values of Δ_{BS} and Δ_{PC} increase. If Δ_{BS} and Δ_{PC} are equalized, Equations 6.9 and 6.10 predict phase-regenerative behavior is retained over any interaction length, even if the idler power is vanishingly small.

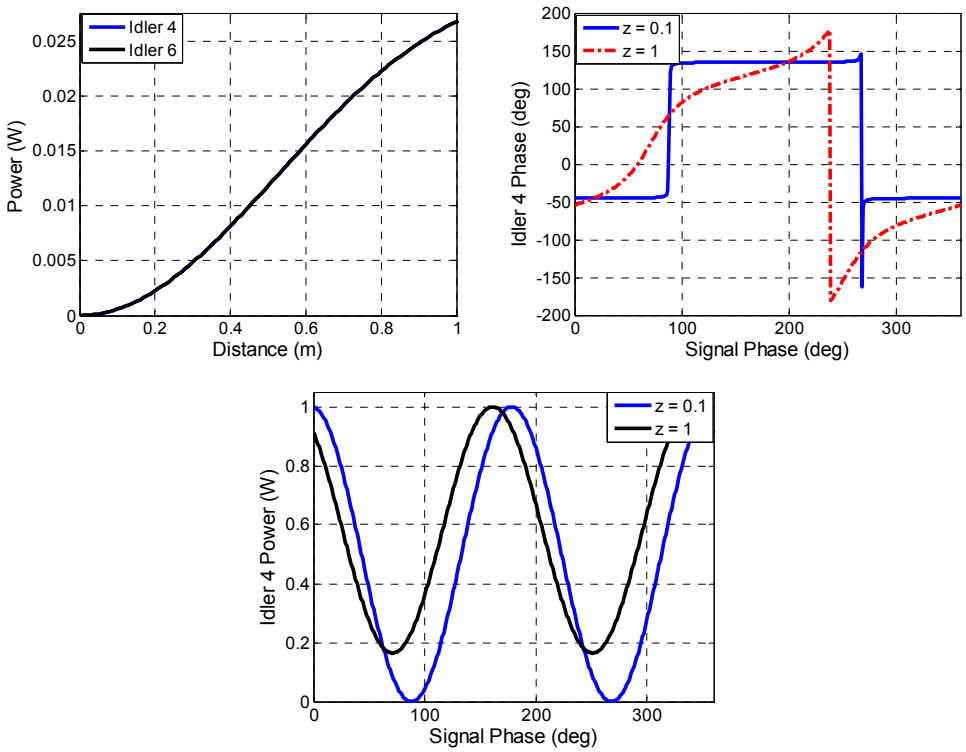

Figure 6.8: Idler propagation, input-output phase, and normalized power versus phase response at two distances.

To illustrate the effects of detuning between Δ_{BS} and Δ_{PC}, Equations 6.9 and 6.10 were used to generate graphs for the idler growth, input-output phase and power versus phase response under the assumption that the linear parts of Δ_{BS} and Δ_{PC} were zero (leaving only nonlinear detuning). The results are shown in Figure 6.8. Calculations were made assuming parameters for the Bismuth-Oxide HNLF used for experiments in Chapter 5, with pumping powers of 600 mW each and a signal power of ~8 mW. Fiber loss was neglected in analytical solutions.

When the linear contributions to phase mismatch are zero (and $P_1 = P_3$), idlers 4 and 6 evolve identically. Figure 6.8(b) indicates initially perfect phase

regeneration, which is degraded for longer distances. When pumps 1 and 3 are taken to be equal, the nonlinear contributions to phase-matching for BS and PC differ by $\left|\Delta_{BS}-\Delta_{pc}\right|=2\gamma P_p$. This reduces the phase-sensitive gain, as observed in Figure 6.8(c). The quadrature attenuation, which can ideally be infinite, is strongly sensitive to changes in the relative values of Δ_{BS} and Δ_{PC}. In the simplified theory, a reduction of nonlinear detuning is predicted for simply reducing the PSA pumps (1 and 3) and increasing the WC pump (5) to compensate.

In practice the linear phase-mismatch will be non-zero and will not be equalized for the BS and PC processes. Their values depend on both the fiber dispersion profile and the frequency arrangement that is chosen. Because of the different BS and PC arrangements, idlers 4 and 6 have different linear phase-mismatches. Definitions of the linear contributions and the total wave-number mismatches are given in Equations 6.11(a-d) and 6.12(a-d) respectively:

$$\begin{aligned}
\Delta\beta_{pc4} &= \beta_2+\beta_4-\beta_1-\beta_5 \\
\Delta\beta_{BS4} &= \beta_3+\beta_4-\beta_2-\beta_5 \\
\Delta\beta_{pc6} &= \beta_2+\beta_6-\beta_3-\beta_5 \\
\Delta\beta_{BS6} &= \beta_1+\beta_6-\beta_2-\beta_5
\end{aligned} \qquad \text{(6.11a-d)}$$

$$\begin{aligned}
\Delta_{pc4} &= \Delta\beta_{pc4}+\gamma\left(P_1+P_5\right) \\
\Delta_{BS4} &= \Delta\beta_{BS4}-\gamma\left(P_3-P_5\right) \\
\Delta_{pc6} &= \Delta\beta_{pc6}+\gamma\left(P_3+P_5\right) \\
\Delta_{BS6} &= \Delta\beta_{BS6}-\gamma\left(P_1-P_5\right)
\end{aligned} \qquad \text{(6.12a-d)}$$

These apply to PC and BS processes under the un-depleted pump approximation, in which signal and idler SPM are neglected along with any CPM of the pumps by the weaker waves. The linear contributions can be calculated for a particular fiber dispersion profile by expanding the propagation constant $\beta(\omega)$

around a reference frequency at which the dispersion parameters are known (it may or may not be the fiber ZDF). In the experiments that follow Bismuth-Oxide HNLF is used; therefore calculations consider values for this type of fiber (D = -300 to -260 ps/nm/km, dispersion slope = 0.947 ps/nm^2/km). Note the large group-velocity dispersion coefficient makes inclusion of higher order terms largely un-necessary.

If the center frequency is chosen as a reference, simplified expressions can be derived for the PC wave-number differences. For idler 4: $\Delta\beta_{pc4} \approx \beta_2 \cdot \left(\Delta\omega_2^{\,2} - \Delta\omega_1^{\,2}\right)$ where $\Delta\omega_1 = \omega_1 - \omega_o$, $\Delta\omega_2 = \omega_2 - \omega_o$ and $\omega_o = (\omega_1 + \omega_5)/2$. For idler 6, $\Delta\beta_{pc6} \approx \beta_2 \cdot \left(\Delta\omega_2'^{\,2} - \Delta\omega_3'^{\,2}\right)$ where $\Delta\omega_3' = \omega_3 - \omega_o'$, $\Delta\omega_2' = \omega_2 - \omega_o'$ and $\omega_o' = (\omega_3 + \omega_5)/2$. In the normal dispersion regime $\beta_2 > 0$. The linear part is negative for idler 4 ($\omega_1 < \omega_2$, two-pump PC) and positive for idler 6 ($\omega_3 > \omega_2$, MI-type PC). According to Equations 6.12(a, c), the PC process for idler 4 can be phase matched while that for idler 6 can not. Similar arguments provide approximate expressions for the linear phase-mismatch for each BS process. For idler 4: $\Delta\beta_{BS4} \approx \beta_2 \cdot \left(\Delta\omega_3''^{2} - \Delta\omega_2''^{2}\right)$ where each $\Delta\omega'' = \omega - \omega_o''$ and $\omega_o'' = (\omega_2 + \omega_5)/2$. For idler 6: $\Delta\beta_{BS6} \approx \beta_2 \cdot \left(\Delta\omega_1''^{2} - \Delta\omega_2''^{2}\right)$ where each $\Delta\omega'' = \omega - \omega_o''$ and again $\omega_o'' = (\omega_2 + \omega_5)/2$. Since $\Delta\omega_1'' > \Delta\omega_2'' > \Delta\omega_3''$, the linear part is negative for idler 4 and positive for idler 6. According to Equations 6.12(b, d), if pump 5 is stronger than pumps 1 and 3, BS can be phase-matched for idler 4 but not for idler 6.

In the normal dispersion regime, the linear and nonlinear WNMM for idler 4 counteract one another, while for idler 6 they reinforce one another. Idler 4 can be expected to exhibit larger conversion efficiency. In the context of PR-WC, the differences between the net WNMM are of interest. For idler 4 and 6, the quantity $\delta_{PR} = \Delta_{BS} - \Delta_{pc}$ takes on the values $\delta_{PR4,6} = \beta_2\left(\omega_2{}^2 - \omega_3{}^2 \pm \omega_2(\omega_3 - \omega_1)\right) + 2\gamma P_{1,3}$. The linear term is larger (in magnitude) for idler 6. Consequently both its conversion efficiency and phase-regeneration are expected to be slightly inferior to that of idler 4 in normally dispersive fibers (this conclusion is reversed if the waves all lie in the anomalous dispersion regime). The fact that the two idlers behave differently allows one to choose a suitable output for a particular medium.

6.2.3. Improved Performance in Linear Regime

Use of three independent pumps offers the interesting possibility of judiciously tuning the total wave-number mismatch for each FWM process. In doing so it is possible to find solutions for a particular frequency arrangement for which phase-regenerative characteristics are maintained over any interaction length. This requires equalization of the two functions $\mathrm{sinc}\left(\Delta_{pc} \cdot z/2\right)$ and $\mathrm{sinc}\left(\Delta_{BS} \cdot z/2\right)$ independent of distance, for which there are two solutions: $\Delta_{pc} = \Delta_{BS}$ and $\Delta_{pc} = -\Delta_{BS}$. For the first case, $P_{psa} = \left(\Delta\beta_{BS} - \Delta\beta_{pc}\right)/2\gamma$ where P_{psa} is the individual power of pump 1 or 3 (assumed equalized). For reasonable values of the linear wave-number mismatches in Bismuth fibers, P_{psa} is small, of the order of a few milliwatts, because it is related to the difference between $\Delta\beta_{BS}$ and $\Delta\beta_{pc}$. This is

referred to as the “weak PSA” solution. Its dependence on large values of pump 5 to produce reasonable output idler powers limits its practicality. For the remaining solution $P_5(0) = \left(-(\Delta\beta_{pc} + \Delta\beta_{BS})\right)/2\gamma$. Pump 5 is chosen based on fiber dispersion parameters and the frequency arrangement, while the PSA pumps can be arbitrarily large or small. Consequently this is referred to as the “strong” or “arbitrary” PSA solution. For the strong-PSA solution, the output idler takes the form

$$B_4(z) = i2\gamma\sqrt{P_{psa}P_5P_2}\cdot e^{i\phi_5}\cdot \mathrm{sinc}\left(\Delta_4\cdot z/2\right)\left(e^{i\delta\phi}e^{i\Delta_4\cdot z/2} + e^{-i\delta\phi}e^{-i\Delta_4\cdot z/2}\right)\cdot z \qquad (6.13)$$

where Δ_4 describes the new, total WNMM. Equation 6.13 clearly retains perfect phase-regenerative characteristics for any interaction length. The strong-PSA solution can be used to optimize PR-WC for idler 4 under normal dispersion, or idler 6 under anomalous dispersion, for an arbitrary tuning range. In Bismuth fibers the quantity $-(\Delta\beta_{pc} + \Delta\beta_{BS})/2\gamma$ will take on values ranging from 50 to nearly 600 mW for wavelength differences between a signal and idler of 2 to 20 nm. Figure 6.9 illustrates use of this technique for equalization of BS and PC phase matching parameters for increased wavelength separation, for equalized PSA pumps of 600 mW. A similar illustration for the weak-PSA solution is shown in Figure 6.10. One feature of this technique is the weak dependence of the total WNMM on increased frequency separations. Substituting the solution for pump 5 power into, for example, Δ_{pc4} leads to $\Delta_4 = \pm\left[\gamma(P_1 + P_3)/2 + (\Delta\beta_{pc4} - \Delta\beta_{BS4})\right]$ (the

BS and PC parameters will have opposite signs). The last term is negative for normally dispersive fibers and weakly decreasing with increased signal-idler frequency separation. Consequently the total parameter Δ_4 is nearly constant over a broad wavelength range. Because the power of pump 5 is tuned nearly linear over increased wavelength separations (Figure 6.9), the power of the idler increases linearly as well. The weak-PSA solution produces much smaller idler output powers which are better equalized (Figure 6.10).

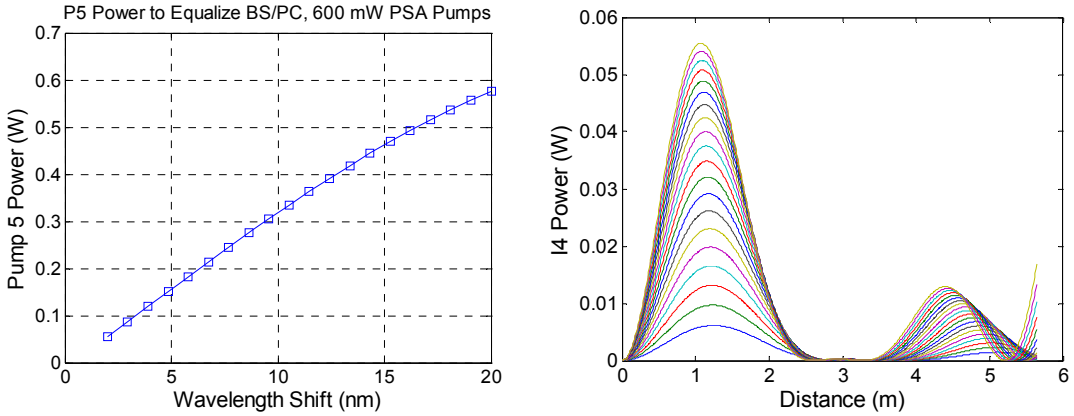

Figure 6.9: Power of the WC pump for equalization of BS and PC wave-number mismatches for increasing signal-idler wavelength separation (left). Right: Z-propagation of the idlers for wavelength spacings from 2 to 20 nm.

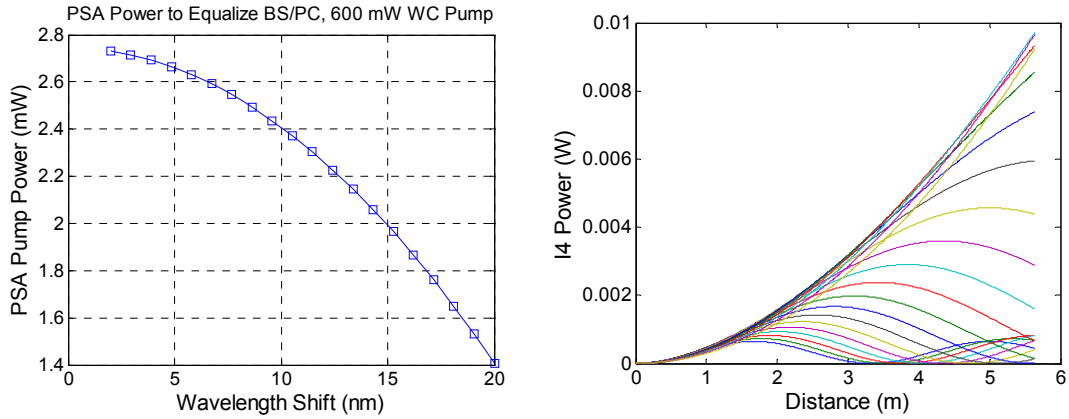

Figure 6.10 Power of each PSA pump for equalization of BS and PC wave-number mismatches for increasing signal-idler wavelength separation (left). Right: Z-propagation of the idlers for wavelength spacings from 2 to 20 nm.

More complex solutions exist for equalizing conversion efficiency and maintaining PR-WC performance in the general case, where the PSA pumps are not equalized. Additionally the frequency separation between the PSA pumps is a free parameter for a given signal-idler frequency separation; this can be tuned as well. The solutions above are restricted to small-signal inputs that do not produce pump depletion, and in which the signal and idlers remain small enough that their SPM (and CPM of other waves) can be neglected.

6.3. Coupled-Mode Analysis

6.3.1. Coupled-Mode Equation Model

Propagation of the signal and three pumps can be described approximately by a set of six coupled mode equations (CMEs). The frequency arrangement was given in Figure 6.4. These read

$$\partial_z A_1 = i\gamma\left(2\cdot\sum_{k\neq 1}\left|A_k\right|^2+\left|A_1\right|^2\right)\cdot A_1 + i2\gamma A_2 A_4 A_5^* e^{i\Delta\beta_{pc4}z} + i2\gamma A_2 A_5 A_6^* e^{i\Delta\beta_{BS6}z} + i\gamma A_2^2 A_3^* e^{i\Delta\beta_{psa}z}$$

(6.14)

$$\partial_z A_2 = i\gamma\left(2\cdot\sum_{k\neq 2}\left|A_k\right|^2+\left|A_2\right|^2\right)\cdot A_2 + i2\gamma A_1 A_5 A_4^* e^{-i\Delta\beta_{pc4}z} + i2\gamma A_1 A_6 A_5^* e^{-i\Delta\beta_{BS6}z} + \ldots$$
$$i2\gamma A_3 A_4 A_5^* e^{-i\Delta\beta_{BS4}z} + i2\gamma A_3 A_5 A_6^* e^{-i\Delta\beta_{pc6}z} + i2\gamma A_1 A_3 A_2^* e^{-i\Delta\beta_{psa}z} \quad (6.15)$$

$$\partial_z A_3 = i\gamma\left(2\cdot\sum_{k\neq 3}\left|A_k\right|^2+\left|A_3\right|^2\right)\cdot A_3 + i2\gamma A_2 A_5 A_4^* e^{i\Delta\beta_{BS4}z} + i2\gamma A_2 A_6 A_5^* e^{i\Delta\beta_{pc6}z} + i\gamma A_2^2 A_1^* e^{i\Delta\beta_{psa}z}$$

(6.16)

$$\partial_z A_4 = i\gamma\left(2\cdot\sum_{k\neq 4}\left|A_k\right|^2+\left|A_4\right|^2\right)\cdot A_4 + i2\gamma A_1 A_5 A_2^* e^{-i\Delta\beta_{pc4}z} + i2\gamma A_2 A_5 A_3^* e^{-i\Delta\beta_{BS4}z} + i\gamma A_5^2 A_6^* e^{-i\Delta\beta_{MI}z}$$

(6.17)

$$\partial_z A_5 = i\gamma\left(2\cdot\sum_{k\neq 5}\left|A_k\right|^2+\left|A_5\right|^2\right)\cdot A_5 + i2\gamma A_2 A_4 A_1^* e^{i\Delta\beta_{pc4}z} + i2\gamma A_1 A_6 A_2^* e^{i\Delta\beta_{BS6}z} + \ldots$$
$$i2\gamma A_3 A_4 A_2^* e^{i\Delta\beta_{BS4}z} + i2\gamma A_2 A_6 A_3^* e^{i\Delta\beta_{pc6}z} + i2\gamma A_4 A_6 A_5^* e^{i\Delta\beta_{MI}z}$$

(6.18)

$$\partial_z A_6 = i\gamma\left(2\cdot\sum_{k\neq 6}\left|A_k\right|^2+\left|A_6\right|^2\right)\cdot A_6 + i2\gamma A_2 A_5 A_1^* e^{-i\Delta\beta_{BS6}z} + i2\gamma A_3 A_5 A_2^* e^{-i\Delta\beta_{pc6}z} + i\gamma A_5^2 A_4^* e^{-i\Delta\beta_{MI}z}$$

(6.19)

In each equation, the first set of terms accounts for nonlinear phase modulation (SPM and CPM). In the general theory, all processes are accounted for. Pumps 1 and 3 are designated as PSA pumps and pump 5 provides wavelength conversion. FWM processes are identified by their associated linear WNMM that were defined in Equations 6.11 (for example, $\Delta\beta_{pc4}$ identifies the PC

process in which $\omega_1 + \omega_5 = \omega_2 + \omega_4$). The signal participates in five FWM processes: PSA, PC and BS. The second order MI interaction between waves 4, 5 and 6 is also included since this can participate for longer interaction lengths (it is initially suppressed as stated in the previous section). For PSA of the signal, $\Delta\beta_{psa} = 2\beta_2 - \beta_1 - \beta_3$ (in the un-depleted pump regime $\Delta_{psa} = \Delta\beta_{psa} + \gamma\left(P_1 + P_3\right)$); for the MI interaction $\Delta\beta_{MI} = \beta_4 + \beta_6 - 2\beta_5$ ($\Delta_{MI} = \Delta\beta_{MI} + 2\gamma P_5$ in the UDP regime).

The set of CMEs are solved numerically under different input conditions to evaluate the phase-regenerative behavior of the idlers compared to the signal. In the initial comparison of the numerical and analytical results (Section 6.3.2), calculations assume D = -300 ps/nm/km, Dslope = 0.947 ps/nm^2/km fourth-order dispersion of -6 x 10^{-51} s^4/m, nonlinearity parameter γ = 1.1/W/m, a fiber length of 5.64 meters and input and output splicing losses of 1.4 and 1.5 dB, respectively. The distributed loss of 1.4 dB/m is included in Monte-Carlo simulations that predict regeneration performance. Higher order dispersion was included to more accurately predict behaviors at larger wavelength spacings investigated in the numerical approach. Propagation constants are calculated from the expression

$$\beta\left(\omega_c\right) = \beta\left(\omega_o\right) + \beta_1\left(\omega_c - \omega_o\right) + \frac{\beta_2}{2}\left(\omega_c - \omega_o\right)^2 + \frac{\beta_3}{6}\left(\omega_c - \omega_o\right)^3 + \frac{\beta_4}{24}\left(\omega_c - \omega_o\right)^4$$

where ω_o is a reference frequency corresponding to a wavelength of 1550 nm. In the scalar theory, all waves share the same linear polarization.

6.3.2. Comparison to Analytical Results

Solutions to the CME model were compared with analytical results to validate that approach. Initially the powers of pumps 1, 3 and 5 were set to 150, 150 and 500 mW, respectively (pumps 1 and 3 were smaller to reduce the rate of nonlinear detuning). Signal power was 50 mW. Figure 6.11 compares the two approaches in the case of zero linear dispersion, in which idlers 4 and 6 propagate identically. In the initial stages of the interaction the analytical result accurately predicts idler growth. However the analytical approach predicts more rapid detuning of the interactions. Figure 6.11 reveals the most significant difference between the two approaches: in the analytical approach phase-regenerative behavior degrades at longer interaction lengths, whereas in the numerical solutions it is preserved.

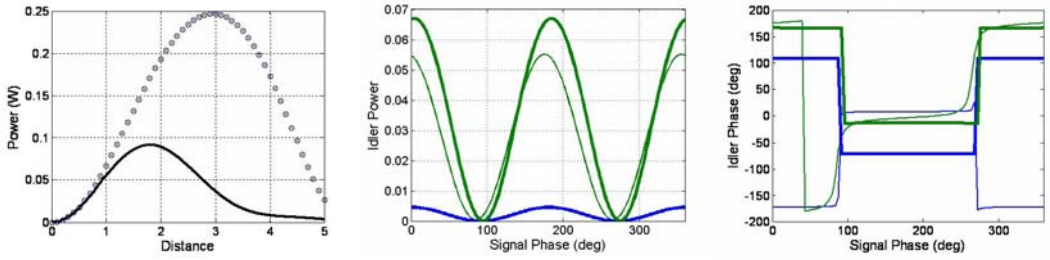

Figure 6.11: Comparison of CME model with analytical approach for zero dispersion. (a) Idler powers. Solid lines: analytical approach. Circles and crosses: numerical results for idler 4 and 6. (b) Idler power against signal phase at two distances: z = 0.25 (blue) and z = 1 (green). (c): Input-output phase at two distances, z = 0.25 (blue) and z = 1 (green). For b,c: bold (thin) lines represent numerical (analytical) results.

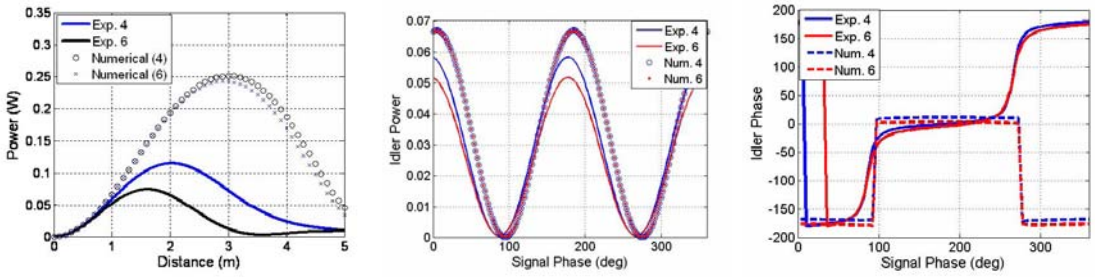

Figure 6.12: Comparison of CME model with analytical approach with dispersion included; 2 nm wavelength shift. Outputs are compared for the distance z = 1.

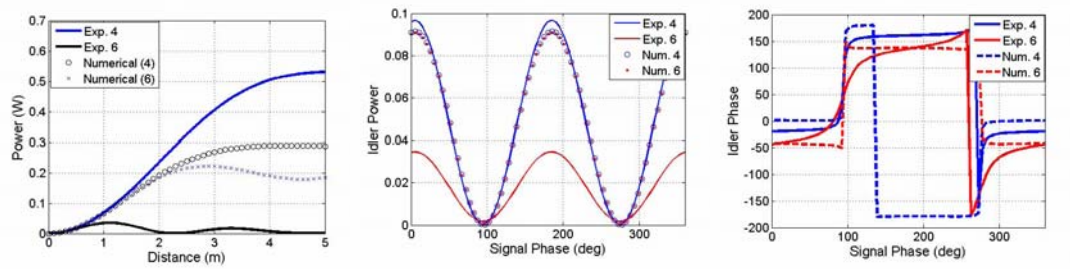

Figure 6.13: Comparison of CME model with analytical approach with dispersion included; 10 nm wavelength shift. Outputs are compared for the distance z = 1.

When dispersion is included idlers 4 and 6 evolve differently. Figure 6.12 shows behaviors of the two waves for a 2 nm wavelength shift when the effects of group-velocity dispersion are included (only β_2 is included for direct comparison between analytical and numerical results). Similar results for a 10 nm wavelength shift are shown in Figure 6.13. Both the power and phase properties of the new waves are more similar in the numerical solutions, compared to the analytical approach.

Analytical results neglect signal and idler SPM, CPM of other waves by these waves, and depletion of the pumps. When these processes are included idlers 4 and 6 behave more similarly. As an example consider the idler 4 PC

process in which $\partial_z A_4 = i\gamma\left(2\cdot\sum_{k\neq 4}\left|A_k\right|^2+\left|A_4\right|^2\right)\cdot A_4 + i2\gamma A_1 A_5 A_2^{*} e^{-i\Delta\beta_{pc4}z}$. The total WNMM $\Delta_{pc4}(z)=\Delta\beta_{pc4}-\Phi_{nl}(z)$ where $\Phi_{nl}(z)$ accounts for all related SPM and CPM processes. It takes the form $\Phi_{nl}(z)=\gamma\cdot\left[P_2(z)+P_4(z)-P_1(z)-P_5(z)\right]$. Its value can be calculated numerically as the waves exchange power along the fiber length. Inclusion of signal and idler SPM and CPM increases the nonlinear detuning of the mode 4 PC interaction. A similar argument shows the detuning rate for the mode 6 PC interaction is reduced, and that parallel results hold for the respective BS processes. Consequently the growth rate of idler 4 is reduced while that for idler 6 is enhanced.

The difference of the two parameters $\delta_{PR}=\Delta_{BS}-\Delta_{pc}$ affects the phase-regenerative behavior at a particular interaction length. For idler 4, $\delta_{PR4}=\beta_2\left(\omega_2{}^2-\omega_3{}^2+\omega_2(\omega_3-\omega_1)\right)+2P_2(z)-P_1(z)-P_3(z)$, which initially decreases in magnitude with distance (the signal is amplified while pumps 1 and 3 are depleted). Consequently Δ_{BS} approaches $-\Delta_{pc}$, at which point ideal phase-regeneration is obtained. Note this occurs for a specific interaction length. This can be seen in Figure 6.14, where the total wave-number mismatches for PC and BS and their difference is plotted against fiber length. PR-WC is expected to perform well even in the depleted pump regime because the BS and PC phase-mismatches become more similar as the signal and the idlers are amplified.

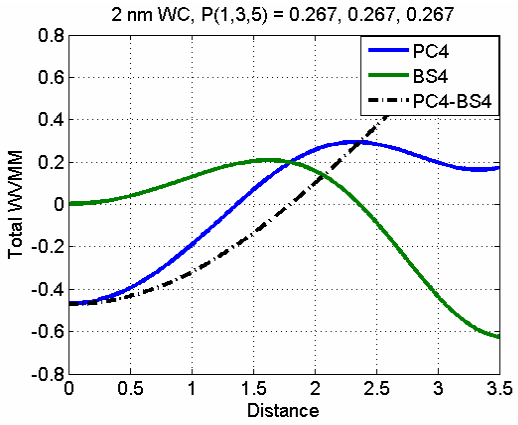

Figure 6.14: Total wave-number mismatches for idler 4 BS and PC processes and their difference plotted against distance.

6.3.3. Depleted-Pump Analysis

In general the exchange of energy between the six waves is complex to describe. PC amplifies the signal and idlers and depletes the pumps. Concurrently BS transfers energy from the signal to the idler wavelengths and from pump 5 to pumps 1 and 3. The continuous signal amplification facilitates continued energy transfer through BS; otherwise equalization of contributions to the idlers from the two FWM processes could not occur. The signal is also amplified through PSA, even though it is initially phased for minimal PSA interaction (this maximizes idler growth). This results in eventual signal regeneration, although theory clearly predicts this not to be required for obtaining phase-regenerated idlers. Despite the complex coupling of the six waves, a clear distinction arises with respect to depletion of the pumps and amplification of the signal and idlers.

The interaction was studied assuming the parameters for Bismuth-Oxide fiber quoted previously but without fiber loss. All pumps were set to 267 mW and

the signal was set to 50 mW. The CMEs were solved numerically to obtain the z-propagation of all waves for different input conditions. Figure 6.15(a) shows propagation of the 6 waves for 2 nm WC. Although dispersion is included in the calculations, idlers 4 and 6 evolve almost identically. Because both BS and PC are nearly phase-matched for the chosen powers and frequency arrangement, pump 5 is strongly depleted by growth of the idlers and transfer of energy to other pumps. The idlers grow until pump5, which participates in PC for each, is depleted by various processes. The signal experiences continued growth through PSA until pumps 1 and 3 are depleted.

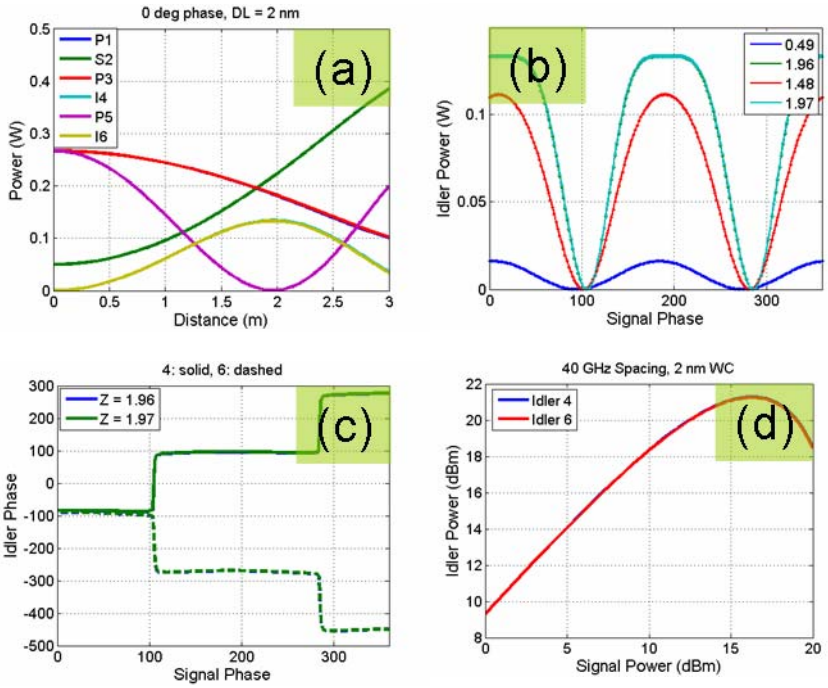

Figure 6.15: Behavior of PR-WC for no fiber loss, equalized pumps and a 2 nm wavelength shift.

Figure 6.15(b) shows the idler power response to changing signal phase for different propagation lengths, which is similar to previous results for PSAs.

The phase transfer function at maximum idler power is shown in Figure 6.15(c), revealing that nearly ideal phase regeneration is retained up to the point of pump depletion. Solid (dotted) lines indicate idler 4 (6) behavior. Finally, Figure 6.15(d) shows a calculation of the idler powers for a zero-phase input signal with continuously varying power. The propagation length was fixed at z = 1.97 meters, showing the expected result of limiting amplification at the idler wavelength coincident with depletion of pump 5.

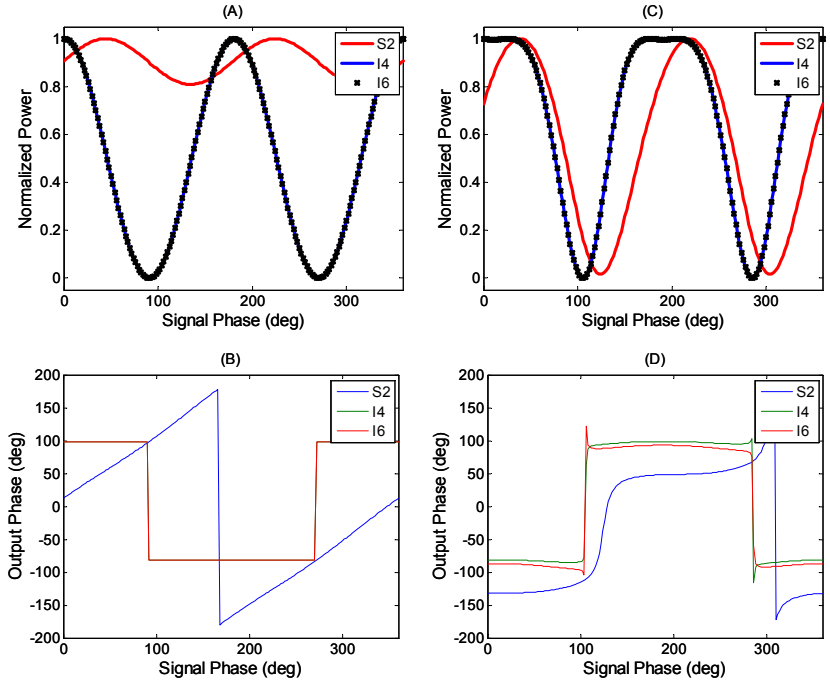

Figure 6.16: Comparison of signal and idler behavior in PR-WC with depleted pumps.

Figure 6.16 compares behavior of the signal with generated idlers for the same conditions. In (a, c) the normalized output powers are plotted as functions of signal phase for distances of Z = 0.1 and 2.0 meters, respectively. The idler gain is strongly phase-sensitive gain whereas phase-sensitivity of signal gain

requires considerably longer interaction lengths. The corresponding input-output phase is plotted for each wave in (b, d): at longer lengths the signal exhibits regeneration, although phase noise reduction is typically better for the idlers.

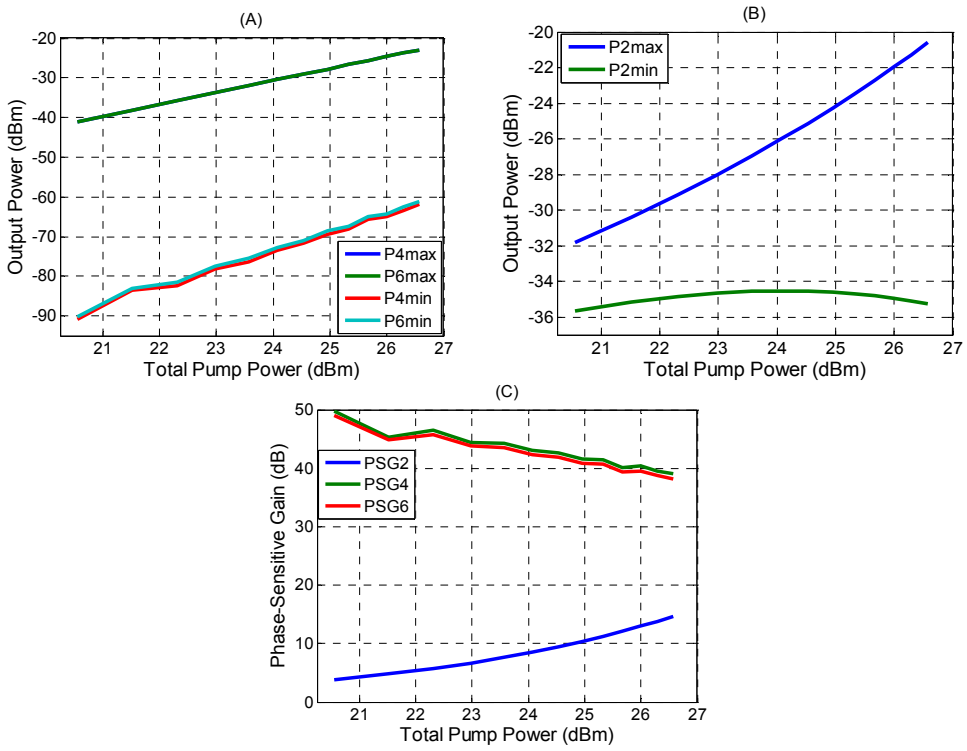

Figure 6.17: Maximum and minimum output powers (as functions of phase) for the idlers (a) and the signal (b). (c): Phase-sensitive gain calculated from output powers.

Figure 6.17 compares some properties of the signal and idlers that are measured experimentally. Numerical solutions to the CMEs were used to obtain the maximum and minimum output powers for each wave by solving for the complete range of signal phase. The fiber length is fixed at Z = 5.64 meters (corresponding to the length of the fiber used in experiments) and the propagation loss of 1.4 dB/m is taken into account. The launched signal power

and total pumping power are increased from 2.6 and 113.6 mW to 15 and 455 mW, respectively. The maximum power of the idlers is expected to increase with the pumps and signal, while the minimum power increases when the BS and PC phase-matching parameters are not equalized. Figure 6.17(a) clearly shows this increase of minimum power. Figure 6.17(c) compares the phase-sensitive gain for the three waves. PSG of the idlers decreases consistent with disruption of the phase-matching requirements.

6.3.4. Wavelength Tuning

The behavior of PR-WC was investigated for a signal and idler tuned from 2 to 20 nm apart. The same Bismuth-Oxide HNLF parameters were assumed. An input DPSK signal was generated with ASE-type noise and launched with the three pumps. The average (data) phases were aligned to ensure maximum idler growth. The CMEs were then solved to obtain the distributions of amplitude and phase at each distance for calculation of the SNR and differential phase Q-factor. Pumping powers of 420 mW each and a signal launch power of 12.5 mW were used. The simulation was repeated at each wavelength spacing with a different input distribution. In Figure 6.18 a signal with the average amplitude and phase is initially observed for reference for 2 nm WC. At each distance, the SNR and DPQ are calculated for three waves (the signal and both idlers, also shown in the Figure). Because a fixed fiber length is required in experiments, the fiber length is chosen as the value that maximizes the SNR of idler 4 for 2 nm WC.

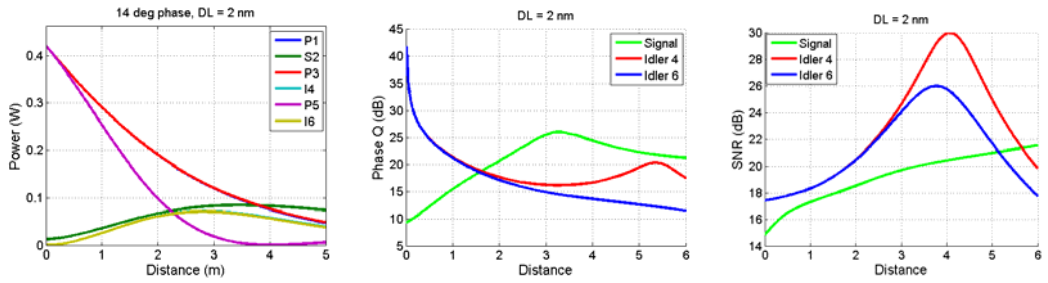

Figure 6.18: Optimization of fiber length for PR-WC.

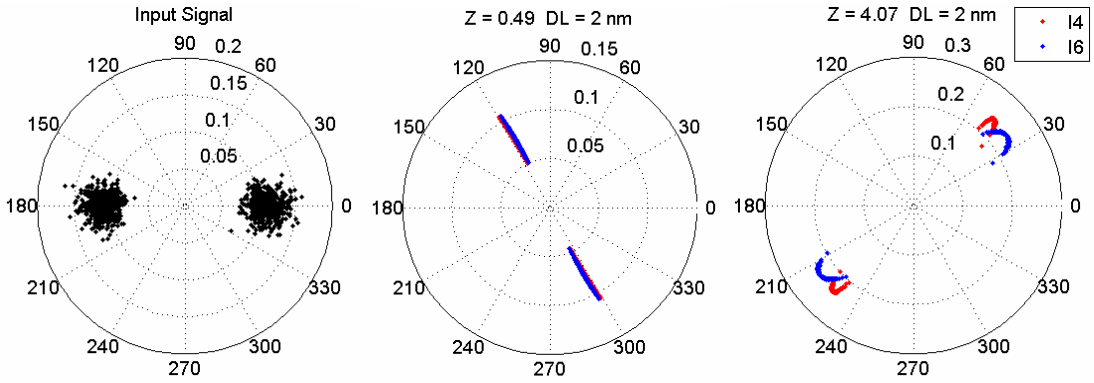

Figure 6.19: Constellation diagrams of input signal and the idler at two distances, for a 2 nm wavelength shift.

Figure 6.18(b, c) show evolution of the DPQ and SNR respectively. Phase regeneration is initially ideal and degrades continuously. The SNR improves with distance as amplitude fluctuations decrease in the depleted pump regime. From the figure it is evident the maximum SNR occurs slightly beyond the saturation length of idler 4, which is common when the phase-mismatch is finite and loss is taken into account: the maximum gain compression for the idlers coincides with the minimal power of the WC pump. Figure 6.19 shows polar plots of the input signal field and the idlers at z = 0.5 and z = 4.07 (“small z” and maximum SNR, respectively). Initially all signal phase noise is converted to idler amplitude noise.

The continuous decrease of phase-Q results from re-introduction of phase noise through idler SPM and CPM, which is incompletely suppressed in this case. This wraps the distribution at the output into the familiar form seen in Figure 6.19(c). In general the total SPM and CPM phase shifts exhibit inverse dependences on signal amplitude and phase. If the dependences are perfectly inverse, output phase noise reaches a minimal value.

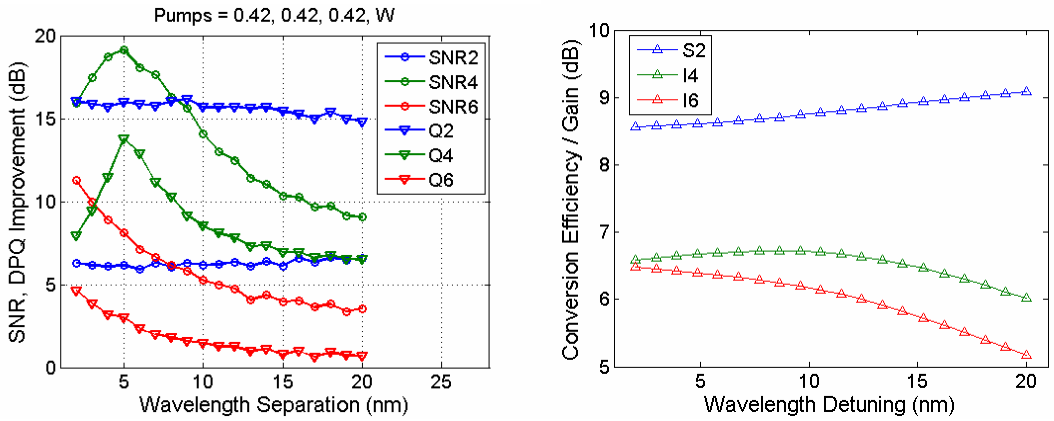

Figure 6.20: Behavior of the signal and idlers over 20 nm tuning range.

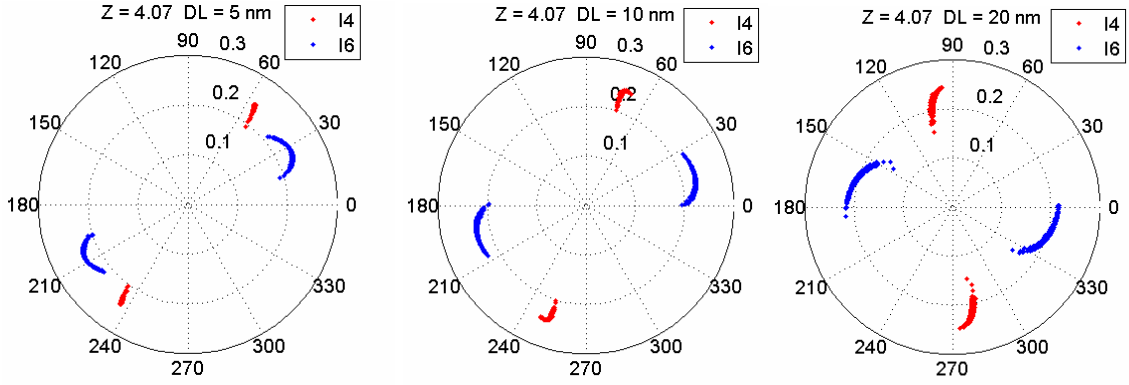

Figure 6.21: Idler constellations for three values of wavelength separation.

Figure 6.20 summarizes behavior of the signal and the idlers over 20 nm tuning range for fixed regenerator parameters by plotting the improvement of SNR and DPQ for each wave, and the signal gain and idler conversion efficiency. The input SNR and DPQ were 15 dB and 9.5 dB respectively. Signal performance is nearly constant, which confirms wave 2 evolves nearly independently of waves 4, 5 and 6. The performance of idler 6 degrades with wavelength separation because its contributing interactions are not phase-matched under normal dispersion. Idler 4 reaches an optimal SNR around a 5 nm wavelength separation, associated with an increase of the phase Q-factor. This result is not related to an increase of phase-sensitive gain at this wavelength separation, but to the aforementioned SPM and CPM noise contributions. For a particular set of launch powers and phase-matching parameters, these balance one another. Figure 6.21 shows idler outputs for 5 nm (best performance), and at 10 and 20 nm separation.

6.4. Experiments

6.4.1. Experimental Setup

The experimental setup for characterization of parallel BS/PC and demonstration of PR-WC is shown in Figure 6.22. An advantage of the technique is its similarity to the established PSA architecture depicted in Figure 5.5; the major difference being the addition of a second tunable laser and one additional polarization controller. In this case the WC pump (labeled 5 in discussions) was coupled in using the 10% output of a 90/10 combiner. All pumps and the signal are then

amplified together as in previous experiments. Coherent detection (described in Section 5.3) was used exclusively to see the effects of PR-WC on input signals degraded either by ASE noise or by imposition of phase and amplitude distortions. The data rate was maintained at 10 Gb/s, and NRZ-DPSK data was used. A typical input spectrum is shown in Figure 6.23. Note that in most experiments pump 5 was placed at a longer wavelength than the signal, in contrast to previous calculations. This was necessary to match the idler wavelength with available filter wavelengths. In the majority of experiments, only the characteristics of idler 4 were measured because this had better regenerative performance and higher conversion efficiency. The former was experimentally verified during the course of regeneration experiments.

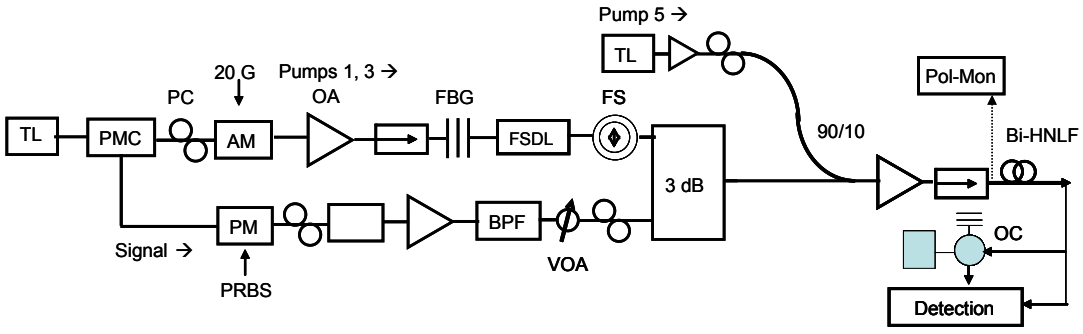

Figure 6.22: Experimental setup for phase-regenerative wavelength conversion (after Figure 5.5). Pol-Mon: polarization monitoring.

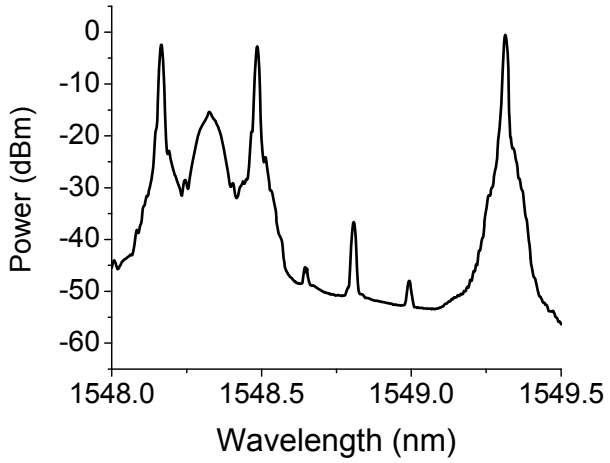

Figure 6.23: Typical PR-WC input spectrum after booster amplifier. The WC pump is near 1549.3 nm.

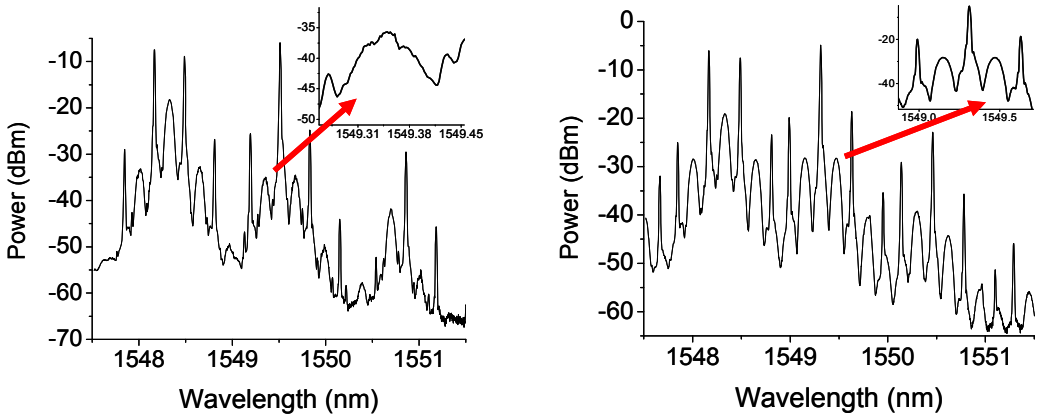

Figure 6.24: Output spectra from parallel BS/PC when the signal is used to drive phase stabilization (left) and when one of the output idlers is used (right). Arrows indicate idler wavelengths.

In order to maximize wavelength conversion it is necessary to launch good linear polarizations with all waves parallel. In practice this was difficult to achieve, and the monitoring method was insufficient to ensure LP states were always used. The normal technique for matching polarizations of the four launched

waves consisted of measuring their powers using an OSA, and then placing a polarizer before the OSA and measuring again. After accounting for insertion loss of the polarizer, the various polarization controllers were adjusted to maximize the power of each wave. Fine-tuning of polarization states could be accomplished by maximizing the PSA response of the signal or idler (this was observed on a real-time oscilloscope with 100 MHz bandwidth).

According to the results of Sections 6.2 and 6.3, the signal and idler gain do not share the same phase dependence. As a result, if the signal is used for feedback control the idler powers will fluctuate as the phases of pumps 1 and 3 (which are the actively adjusted parameters) are varied. It was therefore necessary to use one of the wavelength-converted idlers to stabilize the input phases of waves 1, 2 and 3. Figure 6.24 compares measured output spectra when the signal or an idler is used to drive the phase-stabilization circuitry. Fluctuations of the idlers are apparent when the signal is used for feedback. When an idler is used all output idlers are stabilized simultaneously.

6.4.2. Proof-of-Principle of Phase-Regenerative Wavelength Conversion

Phase-regenerative wavelength conversion is predicted to occur instantaneously when the new idlers are generated. One manifestation of this phenomenon is the removal of large phase distortions for very small interaction lengths (explicitly, the PN should immediately convert to AN). The signal should not exhibit regenerative behavior if the interaction length is kept small.

As an initial proof of the theory of Sections 6.2 and 6.3, an NRZ-DPSK signal was degraded by imposing strong phase distortions, similar to previous PSA experiments, and launched with weak pumps into the HNLF. The total pumping power of 181 mW was evenly distributed between the PSA and WC pumps; the signal power was 2.3 mW (the PSA pump-to-signal power ratio was 17.2 dB). The powers chosen generated idlers that could be detected without excess degradation (~-18 dBm after filtering). The output spectrum shown in Figure 6.25 shows relatively weak pump-pump FWM, although the new tones (around 1550.1 and 1550.7 nm) are ~15 dB stronger than the PR-WC idlers.

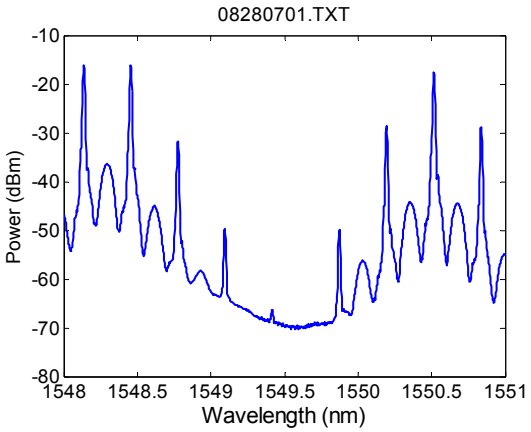

Figure 6.25: Optical spectrum for low-power PR-WC.

To see the phase regenerative behavior, the complex field was measured using coherent detection with digital signal processing in four cases. These are summarized in Figure 6.26. The back-to-back signal exhibited effects of polarization modulation that were previously discussed. Phase distortions were imposed by driving a modulator at ~1.9 GHz with sufficient amplitude to produce closure of the signal eye after differential detection; the amount of absolute

phase variation shown in Figure 6.26(b) is roughly half of the differential phase variation. The wavelength-converted idler exhibits strong amplitude fluctuations that result from conversion between PN and AN; the phase fluctuations themselves are entirely suppressed. This is consistent with the theory developed earlier. The output signal is shown as well, revealing only small changes of its noise distributions. For reference, Figure 6.27 shows distributions of the differential phase before and after PR-WC.

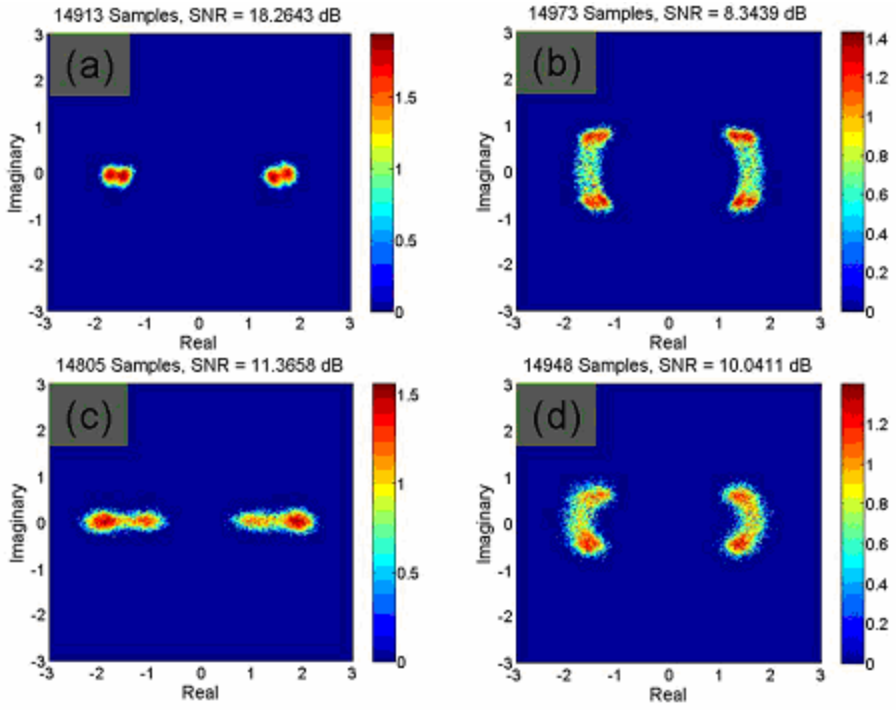

Figure 6.26: Constellations for back-to-back signal (a) clean and (b) with phase distortions added; idler 4 after regenerative wavelength conversion (c); signal output (d).

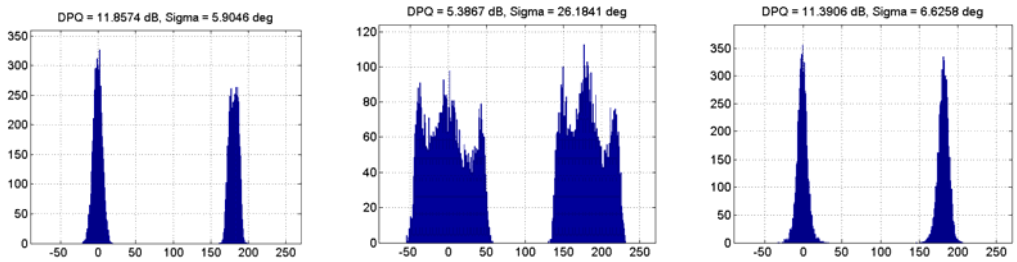

Figure 6.27: Differential phase distributions. From left to right: signal B2B, with phase distortions, and idler after PR-WC.

To verify the linewidth requirements of the WC pump are not more stringent than for a typical DPSK transmitter laser, the beating linewidth with a local oscillator was measured for different cases. The measurement entails mixing the LO with the signal under test (either the back-to-back DPSK signal or the PR-WC idler) and observing the RF spectrum after detection. Phase and frequency noise modulate the beating frequency; its deviation can be recorded using the "max hold" feature of the RFSA. For the LO mixed with the signal, the beating linewidth was 40.75 MHz, while for the LO mixed with a PR-WC idler the result was 43.88 MHz. These beating linewidths are similar and would be much narrower without data modulation of the signals under test.

6.4.3. Phase-Sensitive Gain and Conversion Efficiency

To characterize phase-sensitive gain ($G_{PS} = 10 \cdot \log\left(P(\phi)_{\max} / P(\phi)_{\min}\right)$), the maximal and minimal output powers were measured for the idlers as well as the input signal. The measurement technique was the same as used for previous PSA experiments. The powers were measured against increasing total pump power. This measurement is highly sensitive to polarization alignment between

the input waves, which is a critical issue when the launching power is changed. Heating of both the EDFA (due to pumping) and the Bismuth fiber altered the relative polarization states and inhibited precise measurements of maximal and minimal powers. However a clear trend can be observed and used to verify behavior of the PR-WC process.

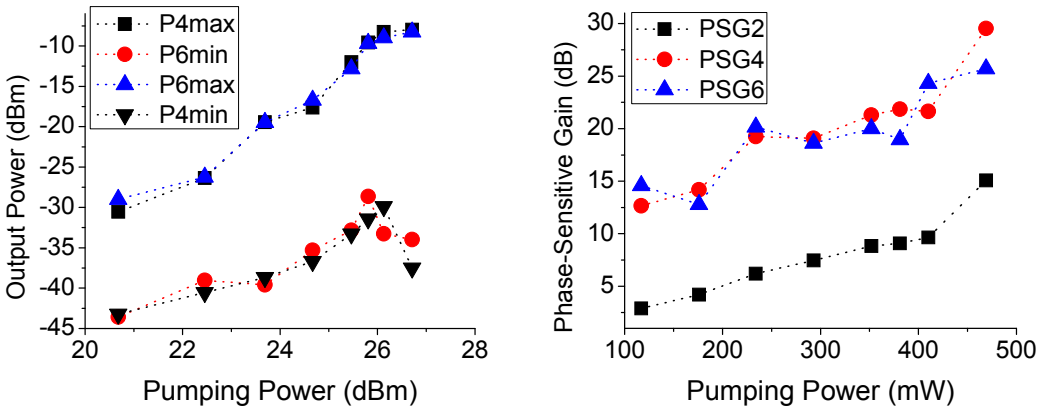

Figure 6.28: Measured maximum and minimum powers and phase-sensitive gain for the signal and both idlers.

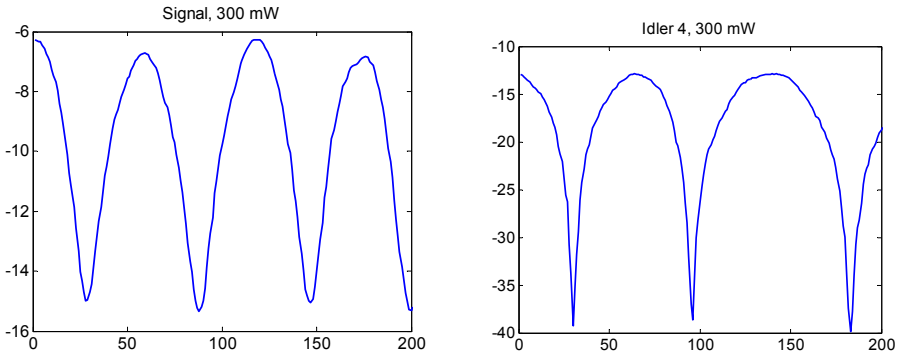

Figure 6.29: Signal (left) and idler 4 (right) output power for constant input phase rotation. Total launched pump power was ~300 mW.

Figure 6.28(a) shows that for increasing pumping power, both the maximal and minimal idler powers increase. Equation 6.10 predicts the minimal power depends on the relative values of the BS and PC phase-matching parameters: if these are not equalized the quadrature attenuation will decrease as observed in experiments. The growth of minimal power with increased pumping power results from the difference $\left|\Delta_{BS} - \Delta_{pc}\right| = 2\gamma P_p$ (the linear parts are constant for fixed frequencies). Overall, the phase-sensitive gain continuously increases as indicated in Figure 6.28(b) due to the growth of maximal idler power with pumping rate. This occurs despite considerable difficulty in maintaining polarization alignment at the higher launch powers (significant short-term instability was observed for total powers > ~350 mW). The phase-sensitive gain of the idlers exceeds that of the signal by 10 dB or greater over the entire measurement range. Example traces of the output power measurements are given in Figure 6.29.

For a practical wavelength converter an important parameter is the conversion efficiency, which is typically defined as $\eta = 10 \cdot \log\left(P(L)_{\lambda-out} / P(0)_{\lambda-in}\right)$, with $P(L)_{\lambda-out}$ measured at the idler wavelength and $P(0)_{\lambda-in}$ measured at the signal wavelength just before the HNLF. The conversion efficiency was measured in the small-signal regime for wavelength separations of 2 and 5 nm, limited by available narrowband filters. Signal launch power is calculated by recording the total EDFA output power, and the input powers for pumps 1, 3 and 5 and the signal, and correcting for input losses to the HNLF (splicing, due to

polarization monitoring, etc.). The idler power was measured after filtering; the actual output power is therefore calculated from known loss of components that follow the HNLF (couplers and the filter itself). Figure 6.30 and Figure 6.31 show the conversion efficiencies for 2 and 5 nm wavelength shifts (from the signal to idler 4), respectively.

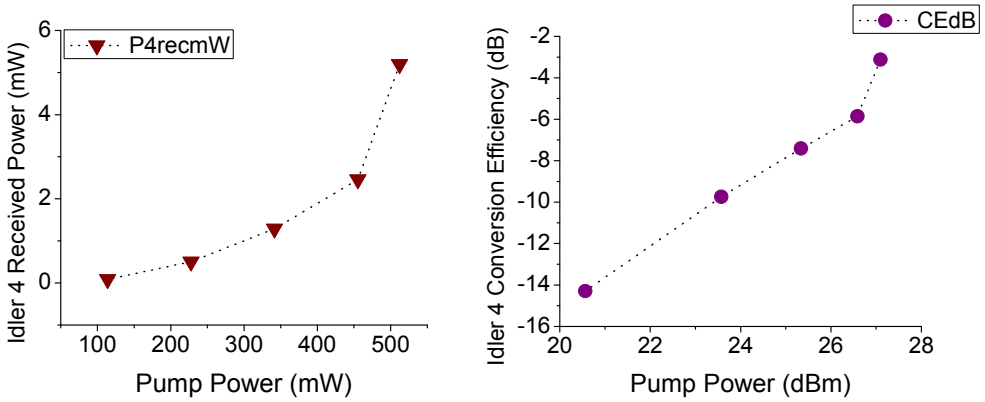

Figure 6.30: Idler 4 output power and conversion efficiency for 2 nm wavelength shift (NRZ-DPSK input without added noise).

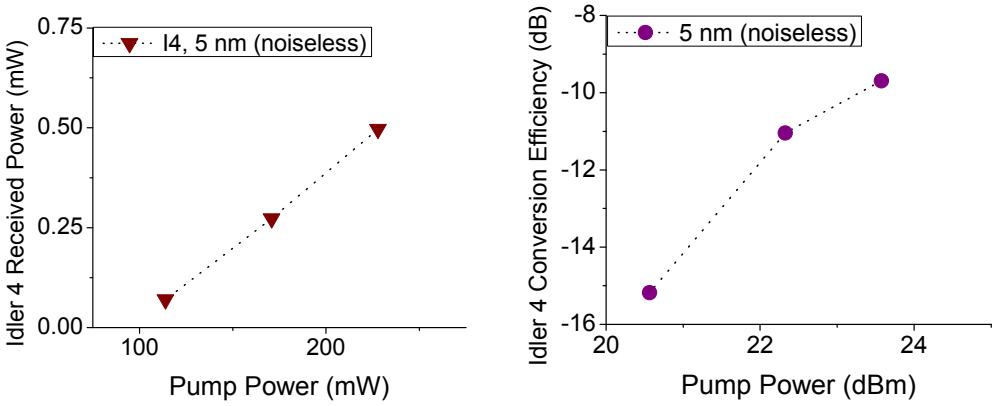

Figure 6.31: Idler 4 output power and conversion efficiency for a 5 nm wavelength shift (NRZ-DPSK input without added noise).

For small pumping powers the idler power increases linearly. In the case where all pumps share similar powers and are increased together, Equation 6.10 predicts stronger idler growth. However the finite values of the BS and PC wave-number mismatches can reduce the idler growth rate. For the 2 nm wavelength shift, stronger idler growth and conversion efficiency are achieved at higher pumping powers (measurements at 5 nm wavelength shift were limited to the small-signal regime).

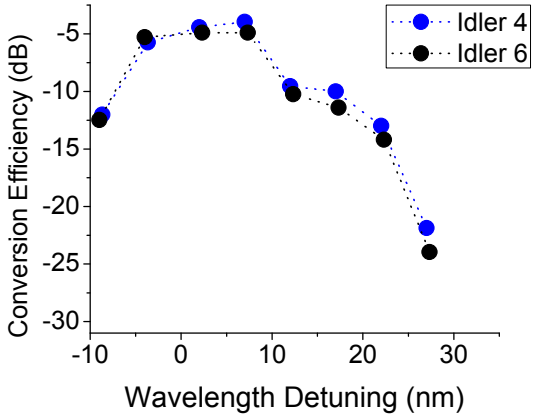

Figure 6.32: Conversion efficiency (defined in terms of maximal signal output power) measured against wavelength detuning (λ5-λ2) for both idlers.

Conversion efficiency was also characterized for an idler tuned across the available EDFA bandwidth. Because filters were not available, measurements could not be taken under stable phase-locking. In this case the optical powers were maintained, the signal wavelength was maintained and pump 5 was tuned from -10 to +30 nm relative to the signal, which was located at 1548.34 nm. A different conversion efficiency was defined as $\eta' = 10 \cdot \log\left(P(L)_{\lambda 4-out} / P(L)_{\lambda 2-in}\right)$.

Total pumping power was 522 mW. The results in Figure 6.32 indicate conversion efficiency first optimizes, and then rapidly decreases once pump 5 is tuned more than ~15 nm away from the signal (a similar drop on the short wavelength side is obscured by EDFA bandwidth limits). The optimal efficiency occurs for a wavelength detuning of ~8 nm; however an abrupt drop-off occurred between 8 and 10 nm detuning. It is likely other factors, such as polarization misalignment, produced this reduction in conversion efficiency.

6.4.4. Wavelength Conversion of Noiseless Signals

Wavelength conversion of a minimally degraded input signal was characterized for increasing conversion efficiency at wavelength shifts of 2 and 5 nm, limited by availability of tunable optical filters to select the idler wavelength for phase-locking. Results for the 2 nm case are given in Figure 6.33, which shows the measured SNR and differential phase Q-factor for increased nonlinear phase shift (total pumping power is progressively increased from 115 to 516 mW). Definitions $Q_{d\phi} = 10 \cdot \log\left(\pi / (\sigma_0 + \sigma_\pi)\right)$ and $SNR = 10 \cdot \log\left(\langle E_{nd} \rangle / \mathrm{var}(E_{nd})\right)$ were used, where E_{nd} is the complex electric field after elimination of data in the software domain, which centers both 0 and π (data phase) distributions on the positive real axis.

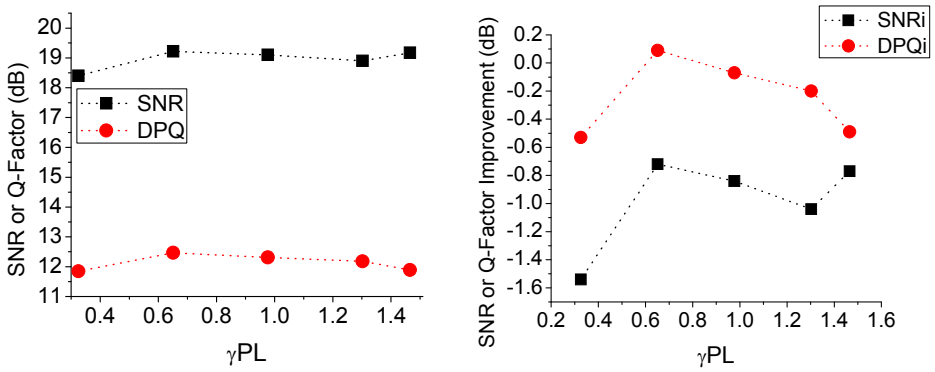

Figure 6.33: SNR and differential phase Q-factor and their improvement against increased nonlinear phase shift for a 2 nm wavelength shift.

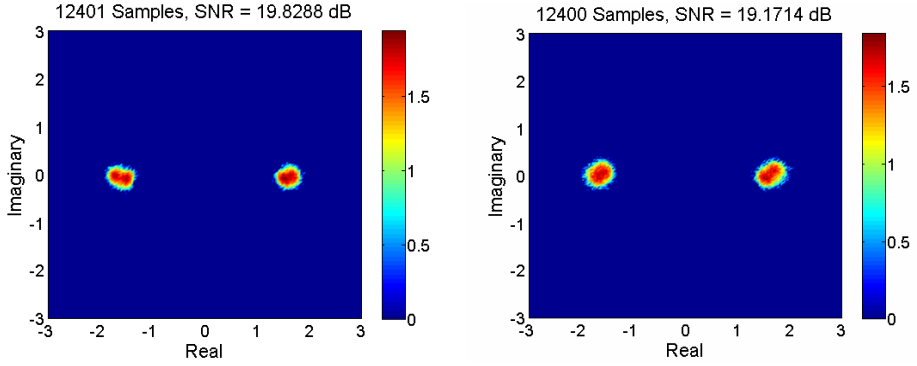

Figure 6.34: Input signal (left) and the output idler (right) constellation histogram for highest measured conversion efficiency.

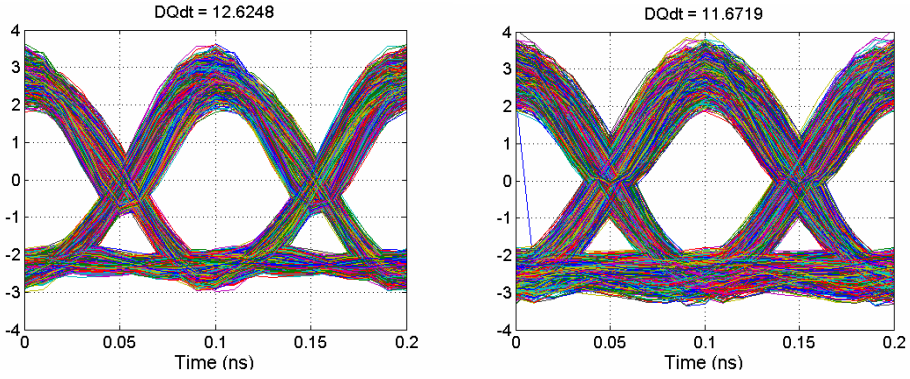

Figure 6.35: Input signal (left) and output idler (right) eye diagrams after differential demodulation in software domain.

In Figure 6.33 the measured SNR and phase Q-factor were nearly constant over the observed range of pumping power. Slow degradation of the phase statistics is predicted by theory because pump powers were not adjusted to maintain phase-matching of BS and PC simultaneously. The results indicate an initial improvement of the phase from the input to the output, despite the fact that input phase noise was not intentionally increased. This results from the strong phase-regenerative behavior of the process at initial formation of the idlers. The overall signal quality (SNR) is expected to degrade due to excessive ASE beating noise. In particular, ASE surrounds pump 5 (including the idler wavelengths) due to lack of optical filters. Figure 6.34 and Figure 6.35 compare constellations and eye diagrams (after differential demodulation) for the signal and idler at the maximum conversion efficiency (about –2 dB). The parameter "DQdt" is the decision threshold Q-factor calculated for differential detection (this is distinct from the differential phase Q-factor measured in Figure 6.33), which accounts for both amplitude and phase noise through calculation of the BER. The SNR and decision-threshold Q-factor degradations were similar (about 0.65 dB).

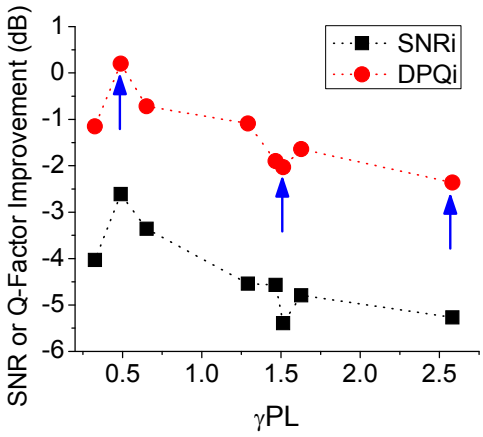

Figure 6.36: SNR and differential phase Q-factor improvement against increased nonlinear phase shift for a 5 nm wavelength shift.

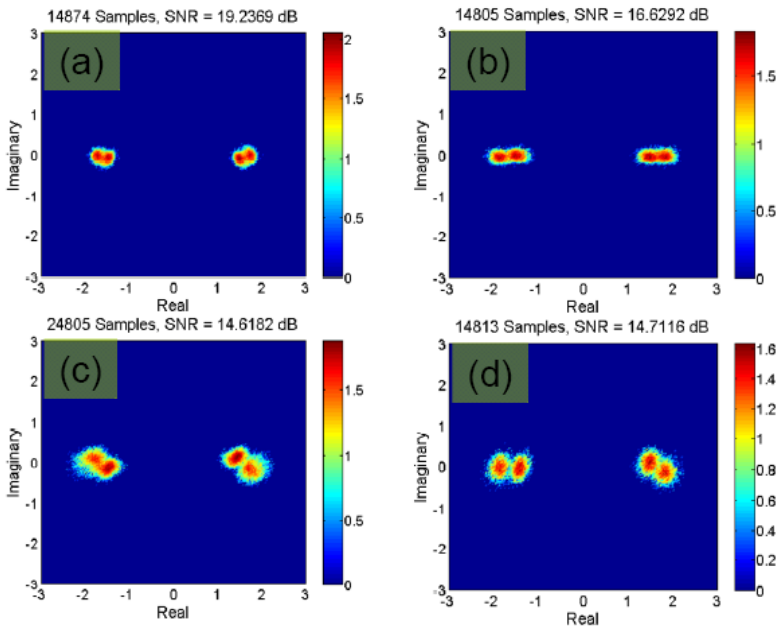

Figure 6.37: Constellations for (a) input signal and (b-c) wavelength-converted idler for 5 nm wavelength shift. Arrows in Figure 6.36 correspond to (b-c) respectively.

Stronger signal degradation was observed for the 5 nm wavelength shift because of polarization modulation of the original signal, which was not detected

during the experiments. Figure 6.36 compares the input and output SNR and phase Q-factors for increasing pumping power (from 115 to 918 mW) for the larger wavelength shift; constellations are shown in Figure 6.37. In this case the total pumping power ranged from 115 to 918 mW (evenly distributed). Inspection of the input signal reveals four localized distributions (two for each phase state) similar to what was observed in Section 5.3, which results from polarization modulation of the signal combined with improper signal-LO polarization alignment at detection. The same features are represented on the output idlers (Figure 6.37(b-c)). Taken independently, each distribution suffers degradation similar to that observed for 2 nm WC experiments. The combination of different distributions leads to an SNR degradation of 4.77 dB. The decision threshold Q-factor calculated from the eye after differential demodulation reduced by a similar amount (4.75 dB).

6.4.5. Regenerative Wavelength Conversion of Degraded Signals

To evaluate regenerative behavior, the back-to-back SNR was adjusted by imposing phase and amplitude distortions using the same technique applied in Section 5.3. Results were measured against increased pumping power for two wavelength shifts (2 and 5 nm to compare with processing of low-noise inputs). The input PSA pump-to-signal power ratio varied between 12 and 15 dB due to instabilities of the signal input to the booster amplifier, which was eventually traced to a variable optical attenuator. Total pumping power ranged from 116 mW to 952 mW (for 2 nm WC) and 116 mW to 896 mW for 5 nm WC.

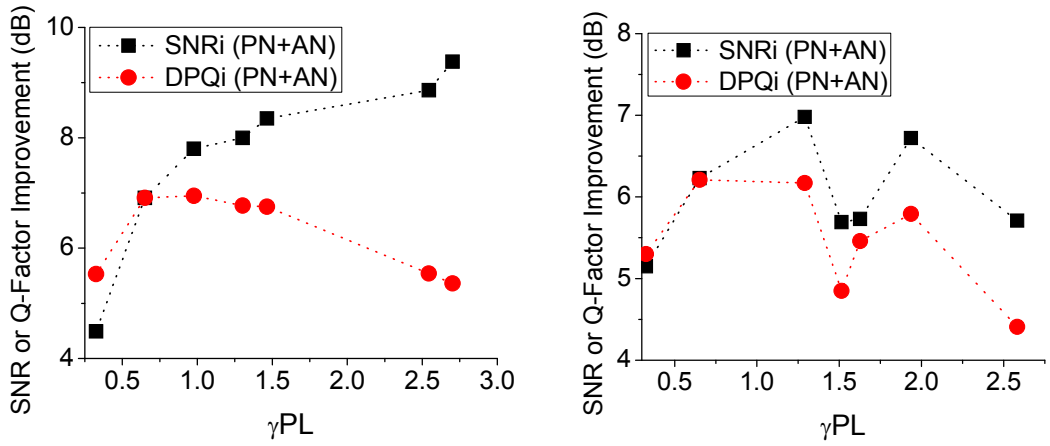

Figure 6.38: SNR and differential phase Q-factor improvement against nonlinear phase shift. Left: 2 nm wavelength shift; right: 5 nm wavelength shift.

Figure 6.38 summarizes behavior of the PR-WC process for both 2 and 5 nm wavelength shifts (from signal to idler 4). For both results the initial improvement of the phase is obscured by noise at detection, resulting in optima at small pumping powers. For the 2 nm wavelength shift, the phase degrades continuously while the SNR increases, due to limiting amplification in the depleted pump regime. A SNR improvement approaching 10 dB was achieved at the highest pumping power, which coincided with positive conversion efficiency (the output idler power was greater than the signal launch power). Figure 6.39(a-c) shows constellations with the SNR values for the input signal, the idler with best phase statistics, and the idler at maximum conversion efficiency. The latter diagram clearly shows localization of the amplitudes and phases. Overall, the standard deviation of differential phase increased from 6.25 degrees (for the output with best phase statistics) to 8.4 degrees (for the largest conversion

efficiency). The corresponding degradation of the differential phase Q-factor was approximately 1.23 dB between the two cases.

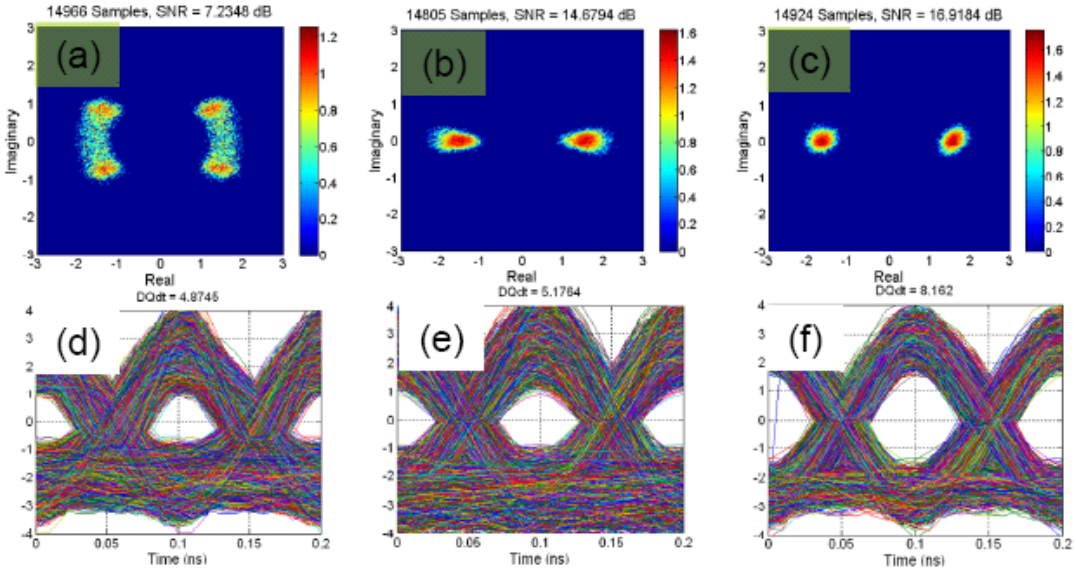

Figure 6.39: Constellations (a-c) and eye diagrams (d-f) for input signal (a,d), output idler with best phase statistics (b,e) and for maximum conversion (c,f). 2 nm wavelength shift.

Eye diagrams for the input and two outputs are given in Figure 6.39(d-f). For each case, the decision threshold Q-factors were calculated after differential demodulation in software domain. An increase of 4.3 dB was obtained for the output in the depleted pump regime, indicating the substantial improvement of overall signal quality.

Equivalent regenerative behavior was not obtained for the larger wavelength shift because the same polarization factors affecting 5 nm WC of noiseless inputs were present in this experiment. However reduction of amplitude and phase noise through wavelength conversion, with a commensurate increase

of both SNR and decision-threshold Q-factor, were obtained. Figure 6.38 showed performance of PR-WC for a 5 nm wavelength shift initially improved with pump power but then degraded. For the initial results polarization effects were minimized and the behavior was closer to the 2 nm case. Data for larger pumping powers were taken under different conditions where polarization modulation was more prominent. Figure 6.40 shows the input and output constellations and eye diagrams. It is also evident the input signal was further degraded for this case, which will mainly allow amplitude noise to persist (phase regeneration is largely independent of the input phase noise distribution). For comparison, the minimum phase noise standard deviation measured was 6.92 degrees, which is quite close to the minimum for the 2 nm case which had slightly smaller input noise. However this value increased to 10.6 degrees at the maximum pump power for 5 nm wavelength shift. The best output was obtained for a total pumping power of 448 mW ($\gamma PL = 1.25$), although the results in Figure 6.40(c, f), corresponding to maximum conversion to the idler wavelength, still indicate SNR improvement.

Optical spectra for maximum conversion to the idler wavelength are shown for both cases in Figure 6.41. Shorter (longer) wavelength arrows indicate the input signal (output idler 4) in each case. Substantial cascaded FWM is observed in both results around the signal and idler wavelengths. In principle the higher order idlers are also PR-WC copies of the primary idlers and could be used to extend the wavelength conversion range. However these were found to exhibit excess noise compared to the primary outputs and were not studied further.

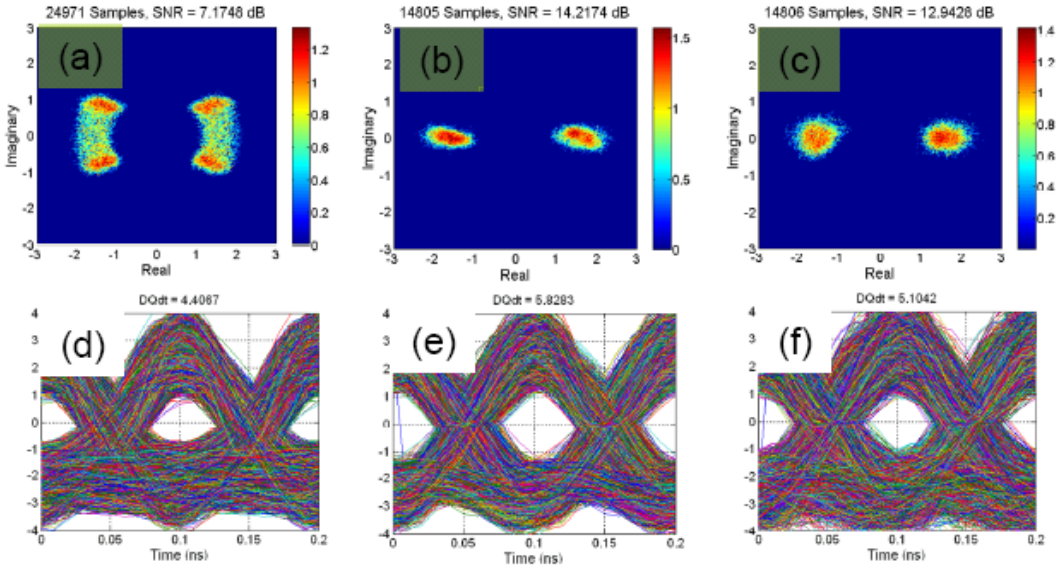

Figure 6.40: Consetllations (a-c) and eye diagrams (d-f) for input signal (a,d), output idler with best phase statistics (b,e) and for maximum conversion (c,f). 5 nm wavelength shift.

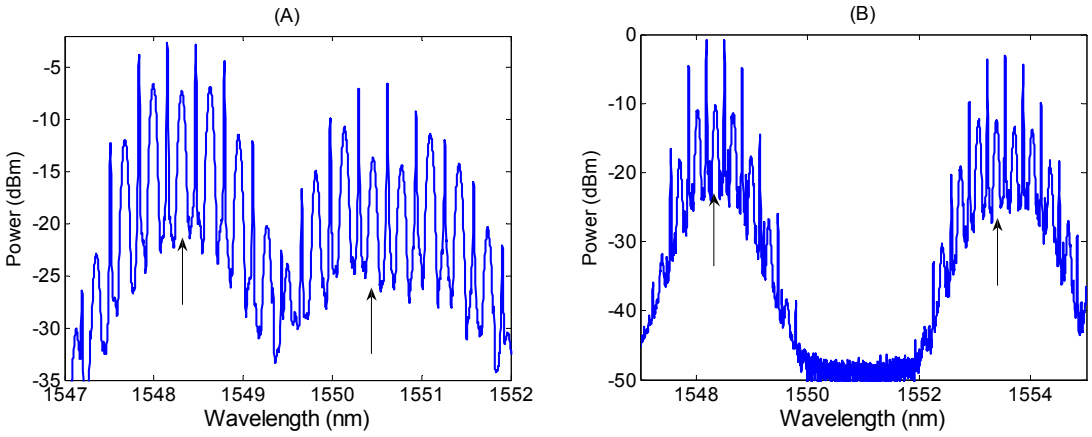

Figure 6.41: Spectrum of PR-WC for maximum pumping powers. (a, b): 2, 5 nm wavelength shift.

CHAPTER SEVEN: TECHNIQUES FOR PHASE REGENERATION OF QUADRATURE PHASE-SHIFT KEYED SIGNALS

7.1. Introduction

Recently quadrature phase-shift keying (QPSK) has been studied for transmission with increased spectral efficiency. The robustness of QPSK towards fiber nonlinearities and dispersion comes at the price of increased complexity at both the transmitter and receiver. QPSK can be detected differentially using essentially twice the number of components required for DPSK, or using coherent detection with a phase-locked local oscillator or digital signal processing. Figure 7.1 shows the QPSK constellation with an example coding scheme and a schematic for differential detection (coherent detection follows a scheme similar to that used in experiments of Chapters 4 and 5). It is intuitively clear that a QPSK signal will be less tolerant to phase noise than a DPSK signal.

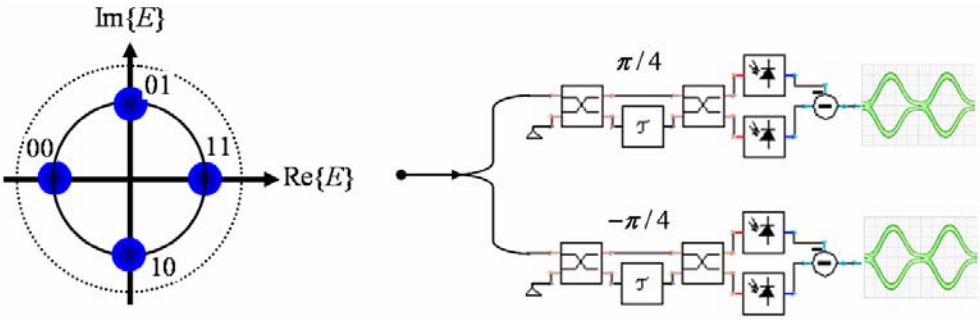

Figure 7.1: QPSK constellation and differential-detection receiver implementation.

Although many of the functionalities for all-optical networking developed for OOK and DPSK signals can be adapted to handle QPSK signals, optical regeneration will be considerably more complex. Phase-sensitive amplification as

discussed to this point can not process QPSK signals because two encoded phases will be de-amplified. The following sections discuss two methods for applying PSA techniques to regenerate QPSK signals.

7.2. Parallel Processing with Phase-Sensitive Amplifiers

QPSK regeneration was previously demonstrated for GHz signals in the microwave domain [148]. A schematic for the device is shown in Figure 7.2. A pump and noisy QPSK signal are divided evenly between two identical PSAs. A phase shifter adjusts the input phases for one PSA so that each device amplifies the input signal in a different manner (detailed below). The outputs are then combined to recover the (regenerated) input signal.

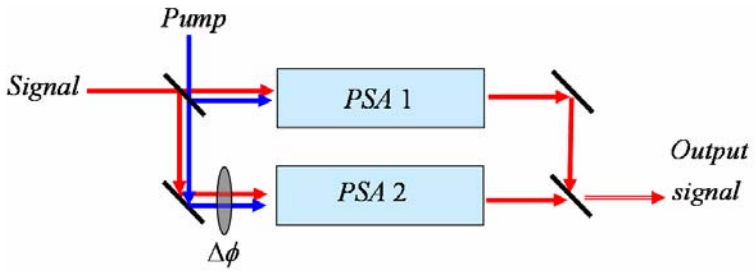

Figure 7.2: Schematic for parallel-PSA implementation of QPSK regeneration.

The pump phases are chosen so that the maximum gain occurs for an input phase that lies halfway between two of the QPSK states as depicted in Figure 7.3(a, b). According to Figure 7.3(a) the gain for all four phases is equalized (but not maximized) so that all inputs are amplified, rather than attenuated. This inherently destroys phase information: as shown in Figure 7.3(a-c) the four signal input phases are projected onto two axes, defined by the pump

phases. Figure 7.3(b) shows the phase axes corresponding to maximum signal gain for two values of input pump phase, assuming the signal constellation input to each PSA is the same. Signal phase distributions are assumed to be centered at values of (45, 135, 225 and 315 degrees) relative to the carrier phase. After amplification by the PSA two regenerated combinations of phases are formed as shown in Figure 7.3(a). The phase information carried by the input signal is recovered by combining the two PSA outputs as shown in Figure 7.3(d). Figure 7.4 shows the coding scheme explicitly.

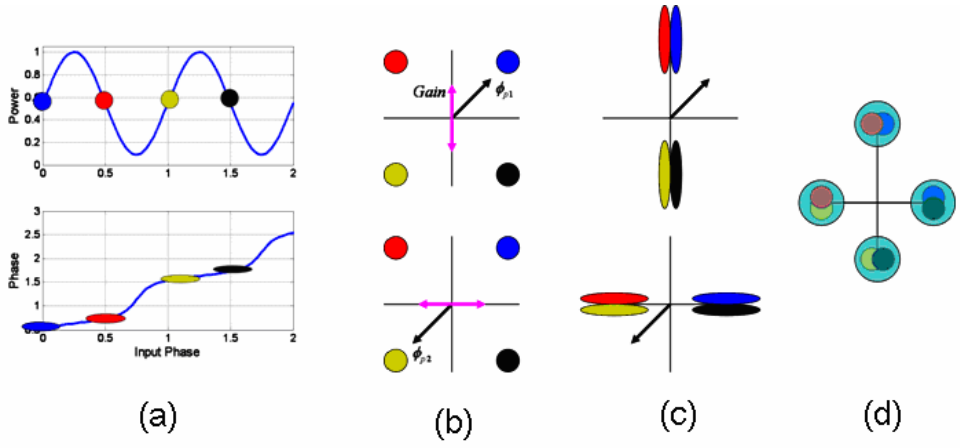

Figure 7.3. (a) Depiction of PSA operation with pump phase adjusted to amplify all four states equally. (b) Orientation of the pump phase and axes for maximum gain for PSA 1 (upper) and PSA 2 (lower). (c) Projection of four phases down to two different combinations defined by the pump phases in each PSA. (d) Regenerated signal after recombination of the two tributary signals.

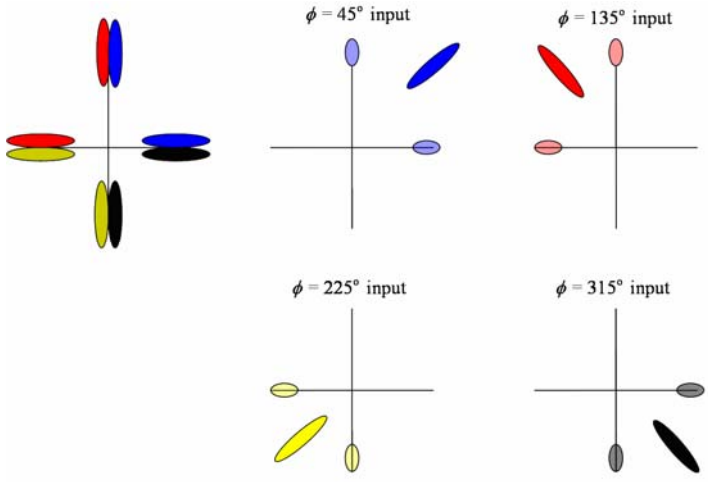

Figure 7.4: Coding scheme explicitly showing recovery of the input phase information.

To clarify how phase regeneration occurs and establish the requirements for individual PSAs the process was analyzed theoretically and through numerical simulations. The most logical choice for each implementation of PSA is to use the degenerate PC process, because of its advanced performance characteristics. However the small-signal solution (Equation 5.2) does not facilitate an exact analysis of the phase regeneration process. Beginning with that equation, and choosing the sum of the pump phases $\phi_1 + \phi_2 = 0$ and $\phi_1 + \phi_2 = \pi$ in the upper and lower PSAs, respectively, the recombined output field can be written

$$B_s(z \to L) = \cosh(\kappa L)\cdot B_s(0) + i\cdot\sinh(\kappa L)\cdot B_s^*(0) + \cosh(\kappa L)\cdot B_s(0)\ldots \\ -i\cdot\sinh(\kappa L)\cdot B_s^*(0) + i2\delta/\kappa\cdot\sinh(\kappa L) \qquad (7.1)$$

In the small-signal analysis the phase-conjugate contributions vanish and the output signal takes the form $B_s(L) = 2\cosh(\kappa L)\cdot B_s(0) + i2\delta/\kappa \cdot \sinh(\kappa L)$: even though the individual PSAs provide phase projection and regeneration, the final output is not phase-regenerated. This establishes the condition that each PSA must operate in the depleted pump regime, and therefore no small-signal, phase-only regeneration is possible. An analytical solution for the SP-PSA in the depleted-pump regime is not available; however the NOLM-PSA can be analyzed without changing the conclusions. Neglecting fiber losses the analytical solution for the output signal in the depleted pump regime is

$$E_{s,out} = e^{i\cdot\phi_o}\cdot i\cdot\left[Ap(0)\cdot e^{i\cdot\phi_{po}}\cdot\sin(\phi_{nl}) + As(0)\cdot e^{i\cdot\phi_{so}}\cdot\cos(\phi_{nl})\right] \tag{7.2}$$

where the previously defined nonlinear phase shifts were $\phi_o = \gamma\cdot z\cdot\left(Pp(0)+Ps(0)\right)/2$ and $\phi_{nl} = \gamma\cdot z\cdot\sqrt{Pp(0)\cdot Ps(0)}\cdot\sin\left(\phi_{po}-\phi_{so}\right)$. A phase-sensitive nonlinear phase shift can be defined for each PSA due to the differing input pump phases, $\phi_{nl1,2} = \gamma\cdot z\cdot\sqrt{Pp(0)\cdot Ps(0)}\cdot\sin\left(\phi_{po1,2}-\phi_{so}\right)$. Figure 7.3(b) shows that to form the proper phase projections the phase axes for maximum gain should be rotated by π/2 between the two PSAs. For the NOLM-PSA this corresponds to a rotation of pump phase by π/2 (rather than π for the SP-PSA). As a result the two phase-sensitive nonlinear phase shifts take the form

$$\phi_{nl1} = \gamma \cdot z \cdot \sqrt{Pp(0) \cdot Ps(0)} \cdot \sin\left(\phi_{po} - \phi_{so}\right) \text{ and } \phi_{nl2} = \gamma \cdot z \cdot \sqrt{Pp(0) \cdot Ps(0)} \cdot \cos\left(\phi_{po} - \phi_{so}\right)$$

(7.3)

Intuitively one expects the amplifier parameters (length, nonlinearity and pump and signal launch powers) must be equalized between the individual PSAs. Under this condition the output signal after recombination of the two tributaries is

$$E_{s,out} = e^{i \cdot \phi_o} \cdot i \cdot \begin{bmatrix} Ep(0) \cdot \sin\left(g \cdot \sin(\delta)\right) + Es(0) \cdot \cos\left(g \cdot \sin(\delta)\right) \ldots \\ i \cdot Ep(0) \cdot \sin\left(g \cdot \cos(\delta)\right) + Es(0) \cdot \cos\left(g \cdot \cos(\delta)\right) \end{bmatrix} \quad (7.4)$$

where $g = \gamma \cdot z \cdot \sqrt{Pp(0) \cdot Ps(0)}$ is the magnitude of the phase-sensitive nonlinear phase shift and δ is the pump-signal phase difference. For processing of DPSK signals with a single NOLM-PSA the condition g = π/2 is required to implement phase and amplitude regeneration simultaneously. The PSA is configured so that the average values of the signal phase distributions are at the points for maximum gain. In the present case the gain for each phase distribution is reduced so that gain for all four phases can be equalized. To retain depletion of the pumps the nonlinear phase shift coefficient must therefore be increased.

The two pump terms in equation (7.4) define the signal output phase quadrant, while the signal terms introduce phase perturbations. For phase regeneration to occur, the magnitudes of the pump contributions should be

equalized while the signal contributions should be minimized. Simultaneously the sensitivity of each term to signal phase fluctuations should be minimal. Noting that for a noisy signal phases are distributed around the values π/4 (+mπ/2, m = 1, 2, 3) relative to the reference pump phase of $\phi_o = 0$, the signal terms vanish exactly when the products $g \cdot \sin(\delta) = g \cdot \cos(\delta) = \pm\pi/2$. This occurs for $g = 1/\sqrt{2}$ when $\delta = \phi_o - \phi_{so} = -\pi/4 - m\pi/2$, which applies to a noiseless signal. The output field reduces to

$$E_{s,out} \approx e^{i\cdot\phi_o} \cdot i \cdot \left[Ep(0) \cdot \sin\left(g \cdot \sin(\delta)\right) + i \cdot Ep(0) \cdot \sin\left(g \cdot \cos(\delta)\right) \right] \tag{7.5}$$

which maps the input phase set {45 135 225 315} degrees to the output set {135 225 315 45} degrees. The output constellation is rotated by 90 degrees, which impacts neither differentially detected nor coherently detected QPSK signals. The pump contributions are equalized for the same value of g, when the input signal is noiseless. It is straightforward to calculate the sensitivity of each pump and signal term in equation (7.9) to changes in input signal phase. For example,

$$\frac{d}{d\phi_s} \sin\left(g \cdot \sin(-\phi_s)\right) = -g \cdot \cos\left(\phi_s\right) \cdot \cos\left(g \cdot \sin\left(\phi_s\right)\right) \tag{7.6a}$$

$$\frac{d}{d\phi_s} \sin\left(g \cdot \cos(-\phi_s)\right) = -g \cdot \sin\left(\phi_s\right) \cdot \cos\left(g \cdot \cos\left(\phi_s\right)\right) \tag{7.6b}$$

Both terms are zero simultaneously only for parameters $\phi_s = \pi/4$ and $g = 1/\sqrt{2}$. Thus the nonlinear phase shift required for phase regeneration is ~0.707π. These conditions establish that the average signal phase (taking the exemplary value of π/4) and power are sufficient to deplete the pump in each PSA, and that the output powers of the individual PSAs are equalized, necessarily resulting in simultaneous amplitude regeneration.

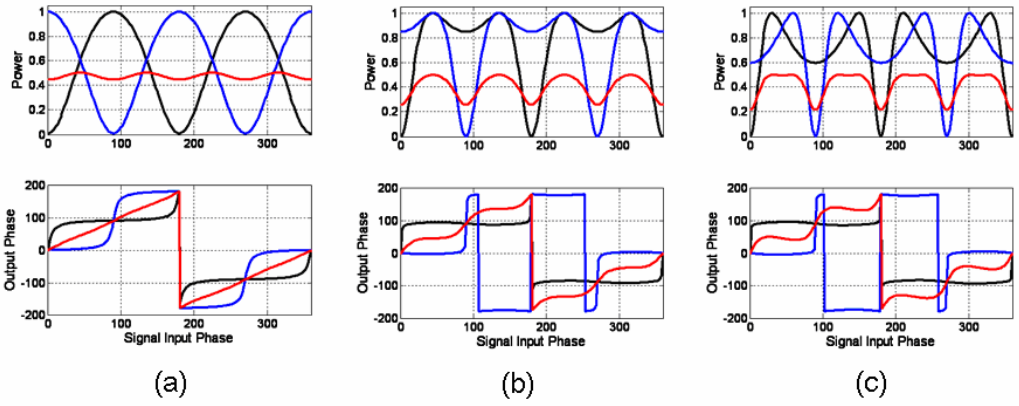

Figure 7.5: Output power and phase for individual PSAs (black and blue lines) and the recombined output (red lines). (a) PSAs 1, 2 operate in the small-signal regime, providing phase projection and regeneration. (b) PSAs are optimized for phase and amplitude regeneration: signal inputs with phases π/4 +mπ/2 deplete the pump. (c) PSAs 1, 2 are operated slightly beyond the depleted-pump regime.

The range of signal phase for which these conditions are maintained is determined by correlation of the signal power-phase response from each PSA. This correlation is maximized when the coefficient $g = 1/\sqrt{2}$ and the signal average phases are $\phi_{so} = \pi/4 + m\pi/2$ relative to the carrier phase. Figure 7.5 depicts the outputs from individual PSAs and the final output after recombination of the two tributaries. Black traces correspond to the output of PSA 1 (zero pump

phase) while blue traces correspond to PSA 2 (π phase shift for a SP-PSA or π/2 shift for a NOLM-PSA). The red traces show the output power and output phase after field recombination. Figure 7.5(a) confirms 2-level phase regeneration of the two tributary signals does not guarantee 4-level phase regeneration at the output. For noiseless inputs it is obvious the gain is equalized between PSAs; however for surrounding phases output power from one PSA exceeds that of the other. According to equation (7.4), the differing amplitudes disrupt 4-level phase regeneration. Figure 7.5(b) corresponds to $g = 1/\sqrt{2}$. Examination of this case reveals that for phases surrounding the average values of $\phi_{so} = \pi/4 + m\pi/2$ the output powers from each PSA remain equalized. This allows 4-level phase regeneration as shown in the lower plots. Figure 7.5(c) corresponds to $g > 1/\sqrt{2}$. In this case phase regeneration begins to degrade as the output powers again differ; however depending on the symmetry of each output power with respect to that obtained for $\phi_{so} = \pi/4 + m\pi/2$, some phase regeneration is retained.

Numerical simulations were carried out to verify QPSK regeneration with parallel PSAs. Simulations were implemented using PSAs based on degenerate FWM. Use of a PSA based on NOLM is not appropriate because of its inherent conversion between amplitude and phase noise, which limits the output phase noise variance to higher values than what can be obtained using an SP-PSA.

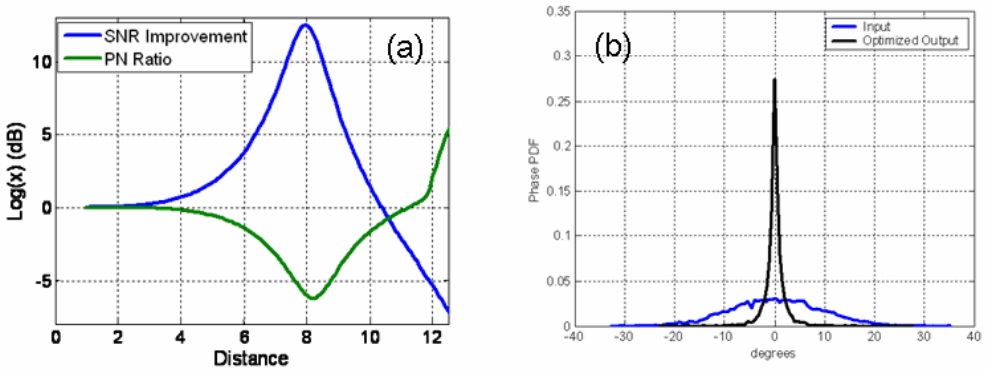

Figure 7.6. (a) SNR improvement and phase noise variance reduction in dB against distance. (b) Input (blue line) and output (black line) phase distributions after all phases are rotated towards zero-phase axis. Output corresponds to optimal case from part (a).

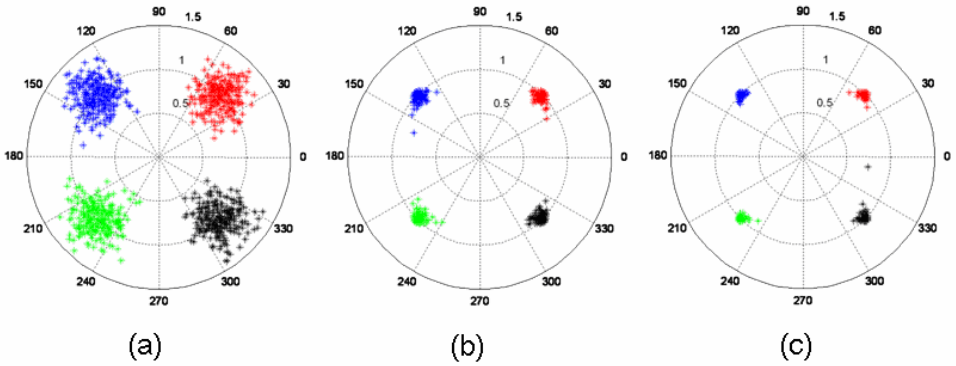

Figure 7.7: QPSK polar plots. (a) Input with SNR = 13 dB. (b) After regeneration with signal power 7 dB below pump (SNR = 25.5 dB). (c) After regeneration with signal power 15 dB below pump (SNR = 27 dB).

An input QPSK signal was generated and degraded by addition of random ASE-type noise. The signal quality was characterized by calculation of signal to noise ratio and the standard deviation of the complete phase distribution: $SNR = 10 \cdot \log_{10}\left(\left\langle P_{sig} \right\rangle / \mathrm{var}\left(E'_{sig}\right)\right)$ where E'_{sig} is obtained by rotating the individual samples by their reference (originally encoded) phase values. This projects all

four QPSK states onto the zero-phase axis. The phase distribution of the rotated field is used to quantify the overall phase noise of the signal, rather than calculating values for each state individually. The signal power was reduced 7-15 dB below that of a 1 W pump which had a 35 dB SNR to allow for degradation of the results by a noisy pump. Figure 7.6 shows improvement of output SNR and phase noise reduction (defined as $R_{pn} = 10 \cdot \log_{10}\left(\sigma_{out} / \sigma_{in}\right)$) for increasing distance. The SNR and phase variance are optimized for slightly different distance values, requiring a small trade-off between optimization of phase or amplitude statistics. Figure 7.6(b) shows an example of the input and output phase distributions at optimum performance. Polar plots of the input and output signals are shown in Figure 7.7. The input signal was degraded to an SNR of 13 dB and regeneration was tested using different pump to signal input power ratios, maintaining the same pump SNR of 35 dB. Results in Figure 7.7(b,c) for ratios of 7 and 15 dB respectively indicate substantial improvement of the signal quality using this technique. The output SNR values were 25.5 and 27 dB respectively.

The results of Figure 7.6 and Figure 7.7 indicate substantial signal quality improvement could be obtained using phase projection and regeneration with parallel PSAs. The process is theoretically sound but difficult practically. The requirement for identical PSA operation can not be circumvented simply through control of the relative output powers (e.g. through attenuation of one output): the characteristics of the signal power-phase response must be equalized between the two devices to maintain the regenerative properties. The scheme also requires considerable phase stabilization that is difficult in the optical domain.

7.3. Cascaded Four-Wave Mixing in Fiber

7.3.1. Principle of Operation

A novel form of phase-sensitive amplification suitable for processing QPSK signals is derived from cascading two FWM processes: phase-conjugation followed by degenerate FWM (called SP-PSA). The first stage is used to prepare pump waves for the second stage that have anti-correlated phase shifts with respect to the signal. This effectively provides phase-coding of the PSA pumps, allowing these to serve as dynamic reference phases for the signal. If precise anti-correlation between pump and signal phase shifts can be achieved, the end result provides substantial QPSK phase and amplitude regeneration.

For reference recall the degenerate FWM process outlined in Chapter 5 in which $\partial_z A_S = i2\gamma A_1 A_2 A_S^* e^{-i\beta z}$, $\partial_z I_S = -4\gamma\sqrt{I_1 I_2 I_S{}^2}\cdot\sin(\theta)$ and $\partial_z A_{1,2} = i\gamma A^*_{2,1} A_S{}^2 e^{i\beta z}$. The total relative phase $\theta = \phi_1 + \phi_2 - 2\phi_s - \beta(z)$ allows for 2nd order phase-sensitive gain (amplification of 2-level PSK signals). The same process provides 4th order phase-sensitive gain if each pump phase $\phi_{1,2} = \phi_{1,2}(0) - \phi_s$: the pumps should be phase-conjugate images of the signal, so that the total relative phase reads $\theta = \phi_1(0) + \phi_2(0) - 4\phi_s - \beta(z)$. $\phi_{1,2}(0)$ represent constant phase shifts of the pump waves relative to the signal carrier phase. The signal frequency remains at the degeneracy point $\omega_s = (\omega_1 + \omega_2)/2$. Therefore, the PC pumps should be provided by using waves derived from modulation of the signal carrier to generate new symmetrically spaced pumps.

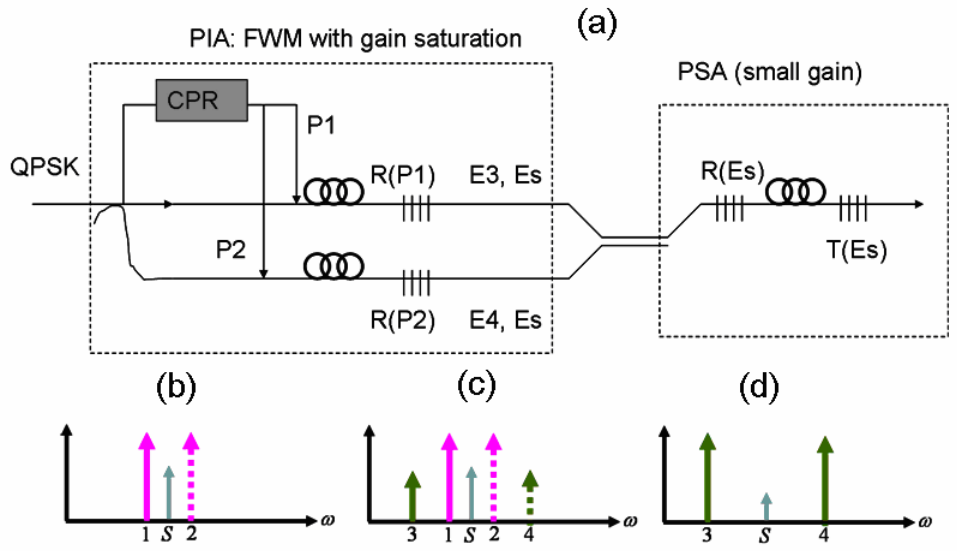

Figure 7.8: Schematic of FWM-based QPSK regeneration and frequency allocations. (a) CPR: carrier phase and polarization recovery. PIA: phase-insensitive amplification, stage 1. R(E) denotes reflection or filtering of a wave while T(E) denotes transmission. Spectrum at input (b) and output (c) of PIA stage and at input to PSA stage (d). Dotted lines indicate waves present only in the lower path while for (b, c) solid lines indicate waves present in upper path (the signal "S" is present in both paths).

The complete process and frequencies of waves involved are outlined in Figure 7.8. A QPSK signal is divided into two paths for generation of pumps and for optical processing. After carrier phase and polarization recovery an initial set of symmetrically spaced pumps is derived by modulating the optical carrier, for example using CSRZ modulation. The degraded QPSK signal is combined with pump 1 in the upper path (pump 2 is rejected using a narrowband optical filter) and with pump 2 in the lower path. Pumps 3 and 4 are generated in the upper and lower paths respectively by the single-pump PC process in high-confinement fibers, and a second set of filters at the output rejects residual light from pumps 1 and 2. These interactions are phase-insensitive: phase locking of waves 1 and 2

to the signal is not required. Pumps 3 and 4 are then launched together with the QPSK signal into a final HCF, producing the 4th order PSA interaction necessary to regenerate the phase.

Pumps 3 and 4 are generated using the single pump PC processes

$$\partial_z A_{3,4} = i\gamma {A_{1,2}}^2 A_S^* e^{-i\beta z} + i2\gamma \left|A_{1,2}\right|^2 A_{3,4} \qquad \text{(7.7a,b)}$$

$$\partial_z A_{1,2} = i2\gamma A^*_{1,2} A_S A_{3,4} e^{i\beta z} + i\gamma \left|A_{1,2}\right|^2 A_{1,2} \qquad \text{(7.7c,d)}$$

$$\partial_z A_S = i\gamma A^2_{1,2} A^*_{3,4} e^{-i\beta z} + i2\gamma \left|A_{1,2}\right|^2 A_{1,2} \qquad \text{(7.7e,f)}$$

where in the small-signal regime only CPM of weaker waves (1, 2 and the signal) by the pumps is considered in addition to the primary FWM processes. The initial phases of waves 3 and 4 produced in the first stage are determined by the phases of pumps 1 and 2 and the signal phase: $\phi_{3,4} = \pi/2 + 2\phi_{1,2} - \phi_S$. Analytical solutions to equations (7.7), including the effects of CPM, read

$$A_{3,4}(z) = \frac{i\gamma \left|A_{1,2}\right|^2 A_S^*(0)}{2\Gamma_{3,4}} \sinh\left(\Gamma_{3,4} z\right) e^{i\cdot\theta_{3,4}\cdot z} \qquad \text{(7.8a,b)}$$

The gain coefficient $\Gamma_{3,4} = \sqrt{\gamma^2 {P_{1,2}}^2 - {\Delta_{3,4}}^2 / 4}$, $\Delta_{3,4} = 2\gamma P_{1,2} + \beta_{3,4}$ is the net wave-vector mismatch and $\theta_{3,4} = 3\gamma P_{1,2} + \beta_{3,4} / 2 + 2\phi_{1,2}$ accounts for the pump input phase and the linear and nonlinear phase shifts. The linear wave-vector mismatch is $\beta_{3,4} = k_s + k_{3,4} - 2k_{1,2}$. In the ideal case $P_1 = P_2$ and the frequencies of waves 1 and 2 are similar (spaced by 40 – 160 GHz) which eliminates the need for the subscripts 3, 4 in both the gain coefficient and wave-vector mismatch. In that case waves 3 and 4 should evolve in a similar manner provided the fiber nonlinear coefficients, loss and dispersion are similar. The signal output from either path is

$$A_s(z) = \left(A_S(0) \cdot \cosh(\Gamma z) + i A_S(0) \frac{\Delta}{2\Gamma} \sinh(\Gamma z) \right) e^{i \cdot \theta_s \cdot z} \tag{7.9}$$

These outputs result from phase-insensitive amplification of the signal, which produces PC waves 3 and 4 that exhibit the (conjugated) data phases of the signal itself. A critical feature of the overall QPSK phase regeneration process is the absence of phase regeneration in the first stage, which would destroy phase information.

According to Figure 7.8, original pumps 1 and 2 are discarded after the first stage. Pumps 3 and 4 are amplified, the signal is attenuated and the total relative phase is adjusted between the PI stage and the final PSA stage. This adjustment is required to orient the two squeezing axes properly for amplification

and regeneration of the QPSK data phases in the PSA stage. It is straightforward to show that the required phase rotation is $\Delta = \pi / 2$, which can be applied either to pump 3 or pump 4. Because original pumps 1 and 2 exhibit the signal carrier phase, pumps 3 and 4 do as well, simplifying the phase locking process. In principle it is only necessary to control the phase of one of the new pumps to maintain the proper total phase difference between the inputs to the PSA stage.

PSA of the signal in stage two proceeds as usual with waves 3 and 4 acting as pumps. The signal input-output relationship takes the usual form of a squeezing transformation described previously. For z' > L (L is the length of stage 1):

$$B_s(z) = \mu(z') \cdot B_s(L) + \nu(z') \cdot B_s^*(L) \tag{7.10}$$

with the amplitude $A_s(z') = B_s(z') \cdot \exp\left(-i\beta z'/2 + i3\gamma(P_3 + P_4)z'/2\right)$, and the auxiliary functions

$$\mu(z') = \cosh(\kappa z') + \frac{i\delta}{\kappa}\sinh(\kappa z') \tag{7.11}$$

$$\nu(z') = i\frac{\Gamma}{\kappa}\sinh(\kappa z') \tag{7.12}$$

The gain coefficient $\kappa = \sqrt{|\Gamma|^2 - \delta^2}$ where $\Gamma = 2\gamma A_3 A_4$ and $\delta = \beta/2 + \gamma(P_3 + P_4)/2$. The phase difference between the first and second terms in (7.10) has the dependence (but not the exact form) $\theta = 2(\langle\phi_3\rangle + \langle\phi_4\rangle) - 4\phi_S$. It is straightforward to plot the signal input-output phase and output power from Equation (7.10). A result of this calculation is shown in Figure 7.9.

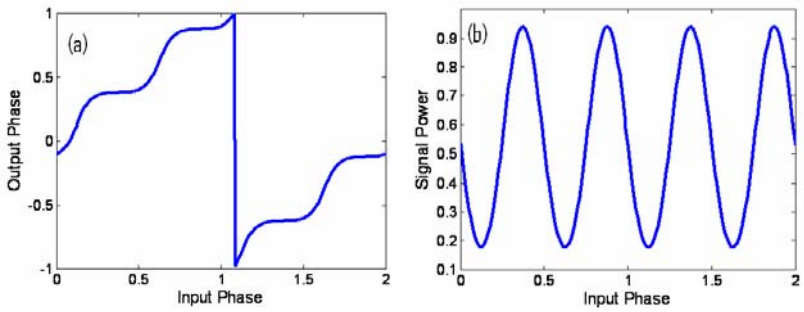

Figure 7.9: Numerically calculated output phase (left) and normalized power (right) for the cascaded FWM process.

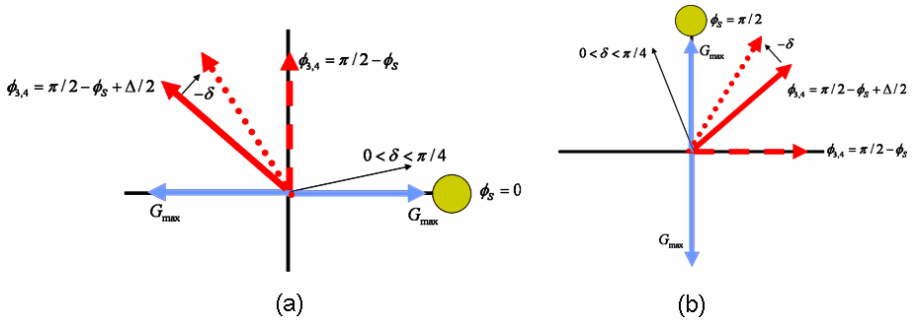

Figure 7.10: Orientation of phases for PSA stage of QPSK regeneration. (a) Signal input phase of 0. Red dashed line: initial pump phases 3 and 4 from phase-insensitive stage. Solid line: after rotation to properly orient maximum gain axes. Dotted line: pump phases when the signal exhibits a phase error δ. (b) Corresponding phase orientations for a signal input phase of π/2.

The phase relationships required for the overall process are depicted in Figure 7.10 for two values of signal input phase: 0 and π/2. Pump phases for the other signal input phases follow in a similar manner. The original pump phases 1 and 2 are taken to be zero. For the zero-phase input signal, pumps 3 and 4 are initially phased at π/2 and are rotated to lie in the third quadrant, which produces maximum gain along the 0, π input phase axis. The sum of the pump phases $\phi_3 + \phi_4 = 3\pi/2$. For the π/2 phase input the pumps shift to the first quadrant, the maximal-gain axis is oriented along $\pm\pi/2$ and $\phi_3 + \phi_4 = \pi/2$. This agrees with the earlier statement that for a SP-PSA the total pump phase must shift by π radians in order to rotate the squeezing axis by π/2 radians. A signal with a phase error δ is also represented. The corresponding pump phases (3, 4) move by –δ. These fast and anti-phase fluctuations of the pump and signal are the source of 4th order PSA by the overall process. Intrinsically, the range of input phase variation per QPSK-state that can be regenerated is ½ that achieved for DPSK regeneration.

7.3.2. Regenerative Performance

Initially QPSK phase regeneration was studied for input signals degraded only by phase noise. This illustrated that phase regeneration could be obtained based on operation of both the PI and PSA stages in the un-depleted pump regime. Figure 7.11 shows an input signal degraded by phase noise, the signal after the first and second stages, and the phase distributions before and after regeneration. Samples are color-coded according to their originally encoded

(noiseless) phase values to verify that information is preserved after regeneration.

In general QPSK signals acquire both amplitude and phase noise, and the amplitude noise may not be removed by other regenerators in the system. According to equations (7.8) signal power fluctuations are transferred directly to waves 3 and 4, which serve as strong pumps during the PSA stage. The presence of pump power fluctuations during PSA will strongly degrade phase regeneration results, through introduction of nonlinear phase noise, as well as increase signal amplitude noise due to gain modulation. The un-depleted pump processes outlined above are therefore insufficient for treating general QPSK signals that exhibit both amplitude and phase noise.

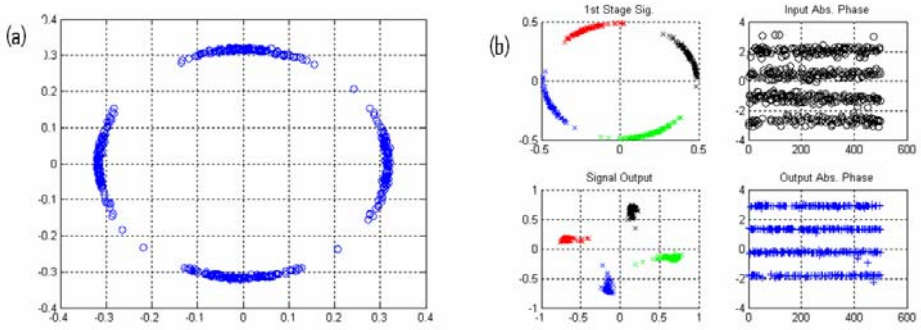

Figure 7.11: Phase regeneration of a 4-level PSK signal degraded only by phase noise. (a) Input QPSK signal. (b) Signal after PIA (top) and PSA (bottom) stages. (c) Absolute phase per sample before (top) and after (bottom) phase regeneration.

The potential for simultaneous phase and amplitude regeneration for QPSK was studied by considering general solutions for both the PIA and PSA

stages. Stage 1 of the process is phase-insensitive amplification of a signal by pumps 1 and 2 to produce idlers (new pumps) 3 and 4:

$$\partial_z A_{3,4} = i\gamma {A_{1,2}}^2 A_S^* e^{-i\beta z} + i\gamma \left(2\left|A_{1,2}\right|^2 + 2\left|A_S\right|^2 + \left|A_{3,4}\right|^2 \right) A_{3,4} \qquad (7.13a,b)$$

$$\partial_z A_{1,2} = i2\gamma {A^*}_{1,2} A_S A_{3,4} e^{i\beta z} + i\gamma \left(\left|A_{1,2}\right|^2 + 2\left|A_{3,4}\right|^2 + 2\left|A_S\right|^2 \right) A_{1,2} \qquad (7.13c,d)$$

$$\partial_z A_S = i\gamma {A^2}_{1,2} {A^*}_{3,4} e^{-i\beta z} + i\gamma \left(2\left|A_{1,2}\right|^2 + 2\left|A_{3,4}\right|^2 + \left|A_S\right|^2 \right) A_S \qquad (7.13e,f)$$

In the depleted-pump case all SPM and CPM processes are taken into account. In principle the amplitudes of waves 3 and 4, and of the signal itself, can be regenerated in this single-pump PC process. If the phase correlations between waves 3 and 4 are well-preserved, pumps with small power fluctuations can be provided for the PSA stage. Equations (7.13) were solved numerically for up to 2000 signal inputs with random amplitude and phase to simulate the degraded QPSK signal. The interaction length was determined by minimizing amplitude fluctuations of waves 3 and 4 at the output, which are idlers in the process. Note this does not automatically minimize signal amplitude fluctuations. The signal and idler are regenerated for the same interaction length only when the input signal average power is substantially smaller than the pump (e.g. 15-20 dB).

Amplitude-regenerated outputs 3 and 4 from stage 1 were amplified, the signal was attenuated and constant (over all samples) phase rotation was applied to one pump to orient the axes for maximum signal gain in stage 2. The coupled-mode equations for the PSA stage read

$$\partial_z A_{3,4} = i\gamma A_{4,3}{}^{*} A_S{}^{2} e^{i\beta z} + i\gamma \left(2\left|A_S\right|^2 + 2\left|A_{4,3}\right|^2 + \left|A_{3,4}\right|^2 \right) A_{3,4} \qquad \text{(7.14a,b)}$$

$$\partial_z A_S = i2\gamma A_3 A_4 A^{*}{}_S e^{-i\beta z} + i\gamma \left(2\left|A_3\right|^2 + 2\left|A_4\right|^2 + \left|A_S\right|^2 \right) A_S \qquad \text{(7.14c)}$$

Figure 7.12 shows an example of results obtained when amplitude regeneration is provided in stage 1. Pumps 1 and 2 were chosen with initial phases that produced the optimal SNR of the final output signal. The original signal exhibits four phase states with additive ASE-type noise; the approximate SNR was 13 dB. Pumps 3 and 4 are shown after amplitude regeneration in the PIA stage and have phase distributions similar to the signal after stage 1. Finally the output signal after the PSA stage is shown, revealing that it is possible to substantially reduce both amplitude and phase fluctuations. The SNR was improved to approximately 20 dB while the overall PN variance was reduced by a factor ~1/9.

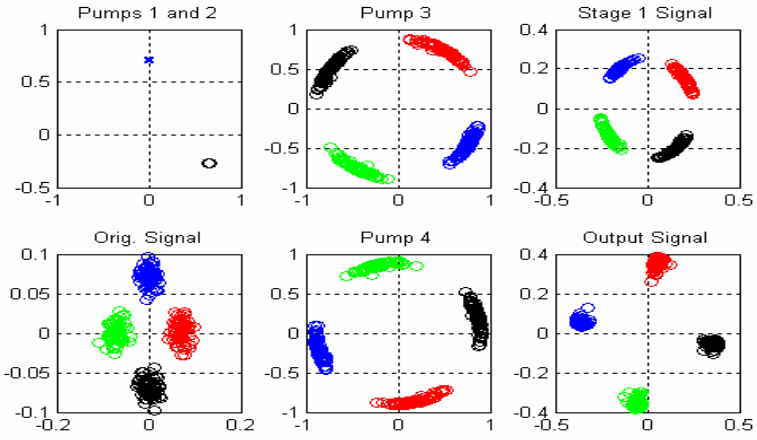

Figure 7.12: Phase regeneration of a 4-level PSK signal degraded only by phase and amplitude noise. (a) Top: orientation of pumps 1 and 2. Bottom: input QPSK signal. (b) Pumps 3 (top) and 4 (bottom) after amplitude regeneration. (c) Signal after amplitude regeneration in PIA stage (top) and after phase regeneration in PSA stage (bottom).

The dynamics of the two-stage QPSK regeneration process were studied to understand the conditions for obtaining phase and amplitude noise reduction. A key feature of the process is the precise anti-correlation of signal and pump phase shifts relative to carrier phase, produced in the first (phase-insensitive) stage. If the signal exhibits a phase error δ, each pump 3, 4 should exhibit the error –δ due to phase conjugation. This condition is disrupted by cumulative SPM and CPM induced phase shifts of the signal and idler, which both depend on signal initial power. Analysis shows that to achieve the required phase correlations, the initial signal should be ~15 dB below the PI-stage pump.

7.4. Summary

Two schemes were evaluated as candidates for practical QPSK regeneration. The first implementation relies on phase projection and regeneration using

parallel PSAs, with use of the SP-PSA most appropriate due to its enhanced performance. Depleted-pump operation is required but the method is sound theoretically. One of the technical challenges is a requirement for three instances of phase-locking with ambiguous conditions for proper phase alignment. The main challenge is the need to equalize not the average PSA output powers, but the exact response of the power to input phase (and amplitude) between PSAs. They must essentially be identical in terms of length, dispersive properties and launching powers. Although such a scheme was implemented for GHz signals, its use at optical frequencies remains dubious.

In the second scheme cascaded FWM processes are used to provide a novel (4-level) PSA directly in fiber. Because the PSA stage pumps are produced directly from the signal they must be amplitude-regenerated in the first stage through gain saturation. Phase correlation of the pumps and signal is maintained for slow saturation of FWM gain, at reasonable power ratios. Because all the pumps share the same carrier phase, their synchronization is simplified. Phase-locking is only required in the second stage, offering advantage over the previous technique. The main technical challenge to this scheme is a need for similar materials (two HNLFs) for the first stage interaction.

CHAPTER EIGHT: CONCLUSIONS

In this research analytical and experimental investigations of regenerative signal processing techniques for binary- and quadrature-phase-shift keyed signals were conducted.

Experimental investigations of phase-preserving amplitude regeneration based on single-pump FWM in optical fibers clarified performance characteristics for inputs with differing noise distributions. Regeneration of signals suffering only ASE additive noise performed well over a limited range of input SNR. Results for larger noise levels were degraded due to introduction of amplified quantum noise, ASE beating noise (from ASE around the pump wavelength) and weakly induced nonlinear phase noise. When the signal exhibits intensity pattern effects, as arise from dispersion or FWM during transmission, the strength of induced nonlinear phase noise during regeneration can be prohibitive.

Phase regeneration was proposed and demonstrated for the first time for differential phase-shift keyed signals, based on phase-sensitive amplification. Two implementations of PSA were studied experimentally. In the first implementation, a frequency and polarization-degenerate pump and signal exchange energy through a nonlinear interferometer, due to unbalanced SPM of the combined, counter-propagating fields. The device produced the first successful result of combined phase and amplitude noise reduction for a DPSK signal. The dependence on SPM to produce differing nonlinear phase shifts leads to an intrinsic conversion between amplitude and phase noise at the initial combination of pump and signal that can not be suppressed by the phase-

sensitivity of the signal gain. The impact of this contribution is reduced for lower signal input powers, which require correspondingly higher pumps. This in turn renders performance more susceptible to pump wave imperfections, which are prominent when the pumps are phase-modulated to suppress stimulated Brillouin scattering. Use of novel highly nonlinear materials with enhanced SBS thresholds can alleviate these performance restrictions.

The second PSA implementation is based on FWM in fiber directly, which occurs when two pumps are symmetric around an input signal. The usual two-pump phase-conjugation process becomes phase-sensitive because the signal and PC idler share the same frequency. The traveling-wave geometry of this implementation suppresses conversion between signal amplitude and phase noise, leading to improved performance over the NI-based PSA. Signal gain is also exponential, compared to quadratic in the former case, improving the prospect for simultaneous amplification and regeneration.

Both PSA implementations allowed simultaneous noise (amplitude and phase) reduction. While the NI-PSA suffered from the requirement to phase modulate the pump wave, the SP-PSA was limited by the presence of a residual carrier left over from generation of the pumps. The presence of this wave set the available pump-to-signal power ratio to avoid strong PSA gain of the carrier. In principle this restriction is simple to overcome, requiring only a grating with stronger reflectivity. It is also necessary to have significantly tighter ASE filtering around the pump wavelengths, for both low-noise amplification of signals and for regeneration. Both PSA architectures require carrier phase and polarization

recovery prior to implementation; for the SP-PSA this is followed by modulation to provide the pumps. Experiments and calculations suggest spacing pumps farther apart will have advantages. Among these are better phase-matching, discrimination against cascaded FWM (under normal dispersion), and better signal filtering tolerance.

Phase-regenerative wavelength conversion was demonstrated using parallel FWM processes: phase-conjugation and Bragg-scattering (also called frequency conversion). Previous research suggested a two-stage implementation could produce PSA of an idler at a new wavelength; however such a scheme offers little advantage compared to the serial implementation of PSA followed by wavelength conversion. Analysis of the two-stage scheme revealed strict requirements for energy exchanged during each stage and synchronization of the phases of all waves in the second stage, which is difficult to realize with independent source lasers. In the parallel implementation these restrictions are removed: ideal (perfectly binary) phase regeneration can be obtained for the idlers without regeneration of the signal, and the phase of the pump providing wavelength conversion is independent of the phases of the other waves. Small-signal analysis showed that ideal behavior could be maintained over the entire interaction length (for which the small-signal approximations were valid) by tuning the power of the WC pump, at the expense of variable conversion efficiency as the WC range is increased. The latter effect can be partially mitigated by adjusting the powers of the other two pumps, although the solution is complex. Numerical analysis showed that single-stage PR-WC performed well for any

interaction length due to evolution of the BS and PC phase-matching parameters as energy is exchanged between waves. In the depleted-pump regime (where the idlers deplete the WC pump), PR-WC provides amplitude regeneration as well as phase-regeneration, similar to other PSAs. Experiments confirmed the features predicted by theory for wavelength shifts of 2 and 5 nm from the signal to one idler. For input signals with minimal ASE noise, PR-WC generally produces slight reductions of the signal-to-noise ratio. This arises mainly from excessive amplifier noise that was not removed by filtering, particularly surrounding the WC pump. For inputs that were intentionally degraded, conversion efficiencies in excess of -2 dB for idlers with simultaneously reduced phase and amplitude noise were demonstrated.

In situations where only phase-regeneration is of interest, PR-WC offers the possibility of ideal regeneration for ultra-low interaction lengths or pumping powers. The initially generated, perfectly-binary-phased idlers need only be suitably amplified to appropriate power levels, possibly through PSA. However their characteristics should not degrade significantly even if parametric amplifiers or laser amplifiers are used.

A brief analysis was conducted of schemes for phase regeneration of QPSK signals. Two implementations, one based on parallel binary phase regeneration and another designed to process QPSK signals directly, were analyzed. The former scheme could be made practical if suitable integrated, highly nonlinear materials were developed, to simply phase synchronization. It lacks fundamentally the ability to operate in the small-signal regime (regenerating

the phase without simultaneous removal of amplitude noise). The latter was developed for the first time in this research and also suffers from complexity. However, any QPSK regeneration can be expected to be more complicated than DPSK regeneration. To this point analysis suggested amplitude regeneration is also required in this scheme, to avoid introduction of nonlinear phase noise during the second-stage (PSA) interaction. However given the ability of PSAs based on FWM to suppress this type of noise conversion, a more thorough analysis is warranted, to ascertain the impact of pump amplitude fluctuations on signal phase during PSA. Ultimately, study of these techniques provides a basis for continued work towards realization of QPSK phase regeneration.

REFERENCES

[1] F. P. Kapron, D. B. Keck, and R. D. Maurer, "RADIATION LOSSES IN GLASS OPTICAL WAVEGUIDES," *Applied Physics Letters*, vol. 17, pp. 423-425, 1970.

[2] I. Hayashi, M. B. Panish, P. W. Foy, and S. Sumski, "JUNCTION LASERS WHICH OPERATE CONTINUOUSLY AT ROOM TEMPERATURE," *Applied Physics Letters*, vol. 17, pp. 109-111, 1970.

[3] E. A. E. Willner, *IEEE Journal of Selected Topics in Quantum Electronics*, vol. 6, pp. 827, 2000.

[4] J. I. Yamada, S. Machida, and T. Kimura, "2 Gbit/s optical transmission experiments at 1.3 Â¿m with 44 km single-mode fibre," *Electronics Letters*, vol. 17, pp. 479-480, 1981.

[5] T. Miya, Y. Terunuma, T. Hosaka, and T. Miyashita, "Ultimate low-loss single-mode fibre at 1.55 Â¿m," *Electronics Letters*, vol. 15, pp. 106-108, 1979.

[6] K. Nakagawa, *Trans. IECE Jpn. Pt. J*, vol. 78B, pp. 713, 1995.

[7] G. P. Agrawal, *Fiber Optic Communications Systems*, 3rd ed: Wiley-Interscience, 2001.

[8] K. Fukuchi, T. Kasamatsu, M. Morie, R. Ohhira, t. Ito, K. Sekiya, D. Ogasahara, and T. Ono, presented at Conference on Optical Fiber Communications (OFC), Washington, DC, 2001.

[9] J. P. Turkiewicz, E. Tangdiongga, G. D. Khoe, and H. d. Waardt, "Clock recovery and demultiplexing performance of 160-gb/s OTDM field experiments," *Photonics Technology Letters, IEEE*, vol. 16, pp. 1555-1557, 2004.

[10] A. I. Siahlo, J. Seoane, A. T. Clausen, L. K. Oxenlowe, and P. Jeppensen, "320 Gb/s Single-polarization OTDM Transmission over 80 km Standard Transmission Fiber," presented at OFC, 2005, OFF3.

[11] P. S. Cho, G. Harston, C. J. Kerr, A. S. Greenblatt, A. Kaplan, Y. Achiam, G. Levy-Yurista, M. Margalit, Y. Gross, and J. B. Khurgin, "Investigation of 2-b/s/Hz 40-gb/s DWDM transmission over 4/spl times/100 km SMF-28 fiber using RZ-DQPSK and polarization multiplexing," *Photonics Technology Letters, IEEE*, vol. 16, pp. 656-658, 2004.

[12] C. Kim, G. Goldfarb, Y. Han, Z. Li, X. Li, and G. Li, "WDM Transmission over 320 km EDFA-Amplified SSMF Using 30 Gb/s Return-to-Zero Optical Differential 8-Level Phase-Shift Keying (OD8PSK)," *Opt. Express*, vol. 13, pp. 4044-4049, 2005.

[13] C. Kim and G. Li, "Direct-detection optical differential 8-level phase-shift keying (OD8PSK) for spectrally efficient transmission," *Opt. Express*, vol. 12, pp. 3415-3421, 2004.

[14] D. Chowdhury, "Polarization mode dispersion in optical communication systems," presented at Optical Fiber Communication Conference and Exhibit, 2001. OFC 2001, 2001.

[15] H. F. Haunstein, S.-G. Wolfgang, A. Dittrich, K. Sticht, and R. Urbansky, "Principles for electronic equalization of polarization-mode dispersion," *Lightwave Technology, Journal of*, vol. 22, pp. 1169-1182, 2004.
[16] A. H. Gnauck and P. J. Winzer, "Optical phase-shift-keyed transmission," *Lightwave Technology, Journal of*, vol. 23, pp. 115-130, 2005.
[17] F. Forghieri, R. W. Tkach, and A. R. Chraplyvy, "Fiber nonlinearities and their impact on transmission systems," in *Optical Fiber Telecommunications*, vol. IIIA. San Diego, CA: Academic Press, 1997, pp. 196-264.
[18] J. P. Gordon and L. F. Mollenauer, "Phase noise in photonic communications systems using linear amplifiers," *Opt. Lett.*, vol. 15, pp. 1351, 1990.
[19] C. J. McKinstrie and C. Xie, "Phase jitter in single-channel soliton systems with constant dispersion," *Selected Topics in Quantum Electronics, IEEE Journal of*, vol. 8, pp. 616-625, 2002.
[20] C. J. McKinstrie, C. Xie, and T. I. Lakoba, "Efficient modeling of phase jitter in dispersion-managed soliton systems," *Opt. Lett.*, vol. 27, pp. 1887-1889, 2002.
[21] K. Hoon, "Cross-phase-modulation-induced nonlinear phase noise in WDM direct-detection DPSK systems," *Lightwave Technology, Journal of*, vol. 21, pp. 1770-1774, 2003.
[22] C. J. McKinstrie, C. Xie, and C. Xu, "Effects of cross-phase modulation on phase jitter in soliton systems with constant dispersion," *Optics Letters*, vol. 28, pp. 604-606, 2003.
[23] H. Keang-Po, "Error probability of DPSK signals with cross-phase modulation induced nonlinear phase noise," *Selected Topics in Quantum Electronics, IEEE Journal of*, vol. 10, pp. 421-427, 2004.
[24] M. Rohde, C. Caspar, N. Heimes, M. Konitzer, E. J. Bachus, and N. Hanik, "Robustness of DPSK direct detection transmission format in standard fibre WDM systems," *Electronics Letters*, vol. 36, pp. 1483-1484, 2000.
[25] R. June-Koo, D. Chowdhury, C. Kwok Sing, and U. Gliese, "DPSK 32×10 Gb/s transmission modeling on 5×90 km terrestrial system," *Photonics Technology Letters, IEEE*, vol. 12, pp. 1627-1629, 2000.
[26] T. Miyano, M. Fukutoku, K. Hattori, and H. Ono, "Suppression of degradation induced by SPM/XPM+GVD in WDM transmission using a bit-synchronous intensity modulated DPSK signal," presented at OECC, Chiba, Japan, 2000.
[27] J. Leibrich, C. Wree, and W. Rosenkranz, "CF-RZ-DPSK for suppression of XPM on dispersion-managed long-haul optical WDM transmission on standard single-mode fiber," *Photonics Technology Letters, IEEE*, vol. 14, pp. 155-157, 2002.

[28] C. Xu, X. Liu, and L. Mollenauer, "Comparison of return-to-zero phase shift keying and on-off keying in long haul dispersion managed transmissions," presented at OFC, Atlanta, GA, 2003.
[29] J.-X. Cai, D. G. Foursa, C. R. Davidson, Y. Cai, G. Domagala, H. Li, L. Liu, W. W. Patterson, A. N. pilipetskii, M. Nissov, and N. S. Bergano, "A DWDM demonstration of 3.73 Tb/s over 11,000 km using 373 RZ-DPSK channels at 10 Gb/s," presented at OFC, Atlanta, GA, 2003.
[30] R. J. Essiambre, G. Raybon, and B. Mikkelsen, "Pseudo-linear transmission of high speed TDM signals: 40 and 160 Gb/s," in *Optical Fiber Telecommunications*, vol. IVB, I. P. K. a. T. Li, Ed. San Diego, CA: Academic Press, 2002, pp. 232-304.
[31] X. Liu, C. Xu, and X. Wei, "Nonlinear phase noise in pulse-overlapped transmission based on return-to-zero differential phase-shift keying," presented at ECOC, Copenhagen, Denmark, 2002.
[32] X. Wei and X. Liu, "Analysis of intrachannel four-wave mixing in differential phase-shift keying transmission with large dispersion," *Opt. Lett.*, vol. 28, pp. 2300-2302, 2003.
[33] A. H. Gnauck, X. Liu, X. Wei, D. M. Gill, and E. C. Burrows, "Comparison of modulation formats for 42.7-gb/s single-channel transmission through 1980 km of SSMF," *Photonics Technology Letters, IEEE*, vol. 16, pp. 909-911, 2004.
[34] J. Leuthold, "All-optical cross connects in transparent networks," presented at Photonic Devices and Algorithms for Computing V, San Diego, CA, USA, 2003.
[35] T. von Lerber, S. Honkanen, and F. Kueppers, "Roadmap for low-cost optical regeneration," presented at Optical Transmission Systems and Equipment for Networking VI, Boston, MA, USA, 2007.
[36] O. Leclerc, B. Lavigne, E. Balmefrezol, P. Brindel, L. Pierre, D. Rouvillain, and F. Seguineau, "Optical regeneration at 40 Gb/s and beyond," *Lightwave Technology, Journal of*, vol. 21, pp. 2779-2790, 2003.
[37] A. Poustie, "SOA-based all-optical processing," presented at OFC (Invited tutorial OWF1), 2007.
[38] C. Bornholdt, S. Bauer, M. Mohrle, H. P. Nolting, and B. Sartorius, "All optical clock recovery at 80 GHz and beyond," presented at Optical Communication, 2001. ECOC '01. 27th European Conference on, 2001.
[39] K. Inwoong, K. Cheolhwan, P. L. LiKamWa, and L. Guifang, "Dynamics of all-optical clock recovery using two-section index- and gain-coupled DFB lasers," *Lightwave Technology, Journal of*, vol. 23, pp. 1704-1712, 2005.
[40] L. Yuhua and L. Guifang, "80 Gbit/s all-optical clock recovery using two-section gain-coupled DFB laser," *Electronics Letters*, vol. 38, pp. 892-893, 2002.
[41] F. Ohman, S. Bischoff, B. Tromborg, and J. Mork, "Semiconductor devices for all-optical regeneration," presented at Transparent Optical Networks, 2003. Proceedings of 2003 5th International Conference on, 2003.

[42] B. Sartorius, "3R All-optical signal regeneration," presented at Optical Communication, 2001. ECOC '01. 27th European Conference on, 2001.
[43] D. Wolfson, A. Kloch, T. Fjelde, C. Janz, B. Dagens, and M. Renaud, "40-Gb/s all-optical wavelength conversion, regeneration, and demultiplexing in an SOA-based all-active Mach-Zehnder interferometer," *Photonics Technology Letters, IEEE*, vol. 12, pp. 332-334, 2000.
[44] Z. Zuqing, M. Funabashi, P. Zhong, L. Paraschis, and S. J. B. Yoo, "10 000-hop cascaded in-line all-optical 3R regeneration to achieve 1 250 000-km 10-Gb/s transmission," *Photonics Technology Letters, IEEE*, vol. 18, pp. 718-720, 2006.
[45] R. Salem, M. A. Foster, A. C. Turner, D. F. Geraghty, M. Lipson, and A. L. Gaeta, "All-optical regeneration on a silicon chip," *Opt. Express*, vol. 15, pp. 7802-7809, 2007.
[46] S. Bigo, O. Leclerc, and E. Desurvire, "All-optical fiber signal processing and regeneration for soliton communications," *Selected Topics in Quantum Electronics, IEEE Journal of*, vol. 3, pp. 1208-1223, 1997.
[47] A. D. Ellis, K. Smith, and D. M. Patrick, "All optical clock recovery at bit rates up to 40 Gbit/s," *Electronics Letters*, vol. 29, pp. 1323-1324, 1993.
[48] C. Johnson, K. Demarest, C. Allen, R. Hui, K. V. Peddanarappagari, and B. Zhu, "Multiwavelength all-optical clock recovery," *Photonics Technology Letters, IEEE*, vol. 11, pp. 895-897, 1999.
[49] C. Kouloumentas, N. Pleros, P. Zakynthinos, D. Petrantonakis, D. Apostolopoulos, O. Zouraraki, A. Tzanakaki, H. Avramopoulos, and I. Tomkos, "Packet clock recovery using a bismuth oxide fiber-based optical power limiter," *Opt. Express*, vol. 15, pp. 9948-9953, 2007.
[50] H. K. Lee, C. H. Lee, S. B. Kang, M. Y. Jeon, K. H. Kim, J. T. Ahn, and E. H. Lee, "All-fibre-optic clock recovery from non-return-to-zero format data," *Electronics Letters*, vol. 34, pp. 478-480, 1998.
[51] W. Lijun, S. Yikai, A. Agarwal, and P. Kumar, "Polarization insensitive widely tunable all-optical clock recovery based on AM mode-locking of a fiber ring laser," *Photonics Technology Letters, IEEE*, vol. 12, pp. 211-213, 2000.
[52] Y. Su, L. Wang, A. Agarwal, and P. Kumar, "Wavelength-tunable all-optical clock recovery using a fiber-optic parametric oscillator," *Optics Communications*, vol. 184, pp. 151-156, 2000.
[53] E. Tangdiongga, J. P. Turkiewicz, G. D. Khoe, and H. d. Waardt, "Clock recovery by a fiber ring laser employing a linear optical amplifier," *Photonics Technology Letters, IEEE*, vol. 16, pp. 611-613, 2004.
[54] K. Inoue, "Suppression of level fluctuation without extinction ratio degradation based on output saturation in higher order optical parametric interaction in fiber," *Photonics Technology Letters, IEEE*, vol. 13, pp. 338-340, 2001.
[55] K. Inoue, "Optical level equalisation based on gain saturation in fibre optical parametric amplifier," *Electronics Letters*, vol. 36, pp. 1016-1017, 2000.

[56] E. Ciaramella and S. Trillo, "All-optical signal reshaping via four-wave mixing in optical fibers," *Photonics Technology Letters, IEEE*, vol. 12, pp. 849-851, 2000.
[57] S. Radic and C. J. McKinstrie, "Optical Amplification and Signal Processing in Highly Nonlinear Optical Fiber," *IEICE Trans Electron*, vol. E88-C, pp. 859-869, 2005.
[58] S. Radic, C. J. McKinstrie, R. M. Jopson, J. C. Centanni, and A. R. Chraplyvy, "All-optical regeneration in one- and two-pump parametric amplifiers using highly nonlinear optical fiber," *Photonics Technology Letters, IEEE*, vol. 15, pp. 957-959, 2003.
[59] G. M. Tosi-Beleffi, F. Curti, D. M. Forin, F. Matera, and M. Guglielmucci, "10 Gbit/s all-optical 2R fiber based regeneration," *Optics Communications*, vol. 236, pp. 323-327, 2004.
[60] Y. Su, L. Wang, A. Agarwal, and P. Kumar, "Simultaneous 3R regeneration and wavelength conversion using a fiber-parametric limiting amplifier," presented at Optical Fiber Communication Conference and Exhibit, 2001. OFC 2001, 2001.
[61] L. Yuhua, K. Croussore, K. Cheolhwan, and L. Guifang, "All-optical 2R regeneration using data-pumped fibre parametric amplification," *Electronics Letters*, vol. 39, pp. 1263-1264, 2003.
[62] Y. Li and G. Li, "2R regeneration and simultaneous wavelength conversion using a fiber parametric amplifier and a semiconductor optical amplifier," presented at Optical Fiber Communications Conference, 2003. OFC 2003, 2003.
[63] A. Bogris, H. Simos, D. Alexandropoulos, and D. Syvridis, "All-optical regeneration based on pump-depletion effect in fiber parametric amplification," presented at Optical Components and Materials III, San Jose, CA, USA, 2006.
[64] P. V. Mamyshev, "All-optical data regeneration based on self-phase modulation effect," presented at Optical Communication, 1998. 24th European Conference on, 1998.
[65] X. Liu, C. Xu, W. H. Knox, and M. F. Man, "Characteristics of all-optical 2R regenerators based on self-phase modulation in high-nonlinear fibers," presented at Lasers and Electro-Optics, 2002. CLEO '02. Technical Digest. Summaries of Papers Presented at the, 2002.
[66] M. Matsumoto, "Analysis of a 2R optical regenerator utilizing self-phase modulation in a highly nonlinear fiber," presented at Lasers and Electro-Optics, 2002. CLEO '02. Technical Digest. Summaries of Papers Presented at the, 2002.
[67] M. Matsumoto and O. Leclerc, "Analysis of 2R optical regenerator utilising self-phase modulation in highly nonlinear fibre," *Electronics Letters*, vol. 38, pp. 576-577, 2002.
[68] H. Tsing-Hua, G. Raybon, and C. Headley, "Optimization of pulse regeneration at 40 Gb/s based on spectral filtering of self-phase

modulation in fiber," *Photonics Technology Letters, IEEE*, vol. 16, pp. 200-202, 2004.
[69] B. Cuenot and A. D. Ellis, "WDM signal regeneration using a single alloptical device," *Opt. Express*, vol. 15, pp. 11492-11499, 2007.
[70] M. Vasilyev and T. I. Lakoba, "All-optical multichannel 2R regeneration in a fiber-based device," *Opt. Lett.*, vol. 30, pp. 1458-1460, 2005.
[71] I. Tomkos, C. Kouloumentas, and S. Tsolakidis, "Performance Studies of Multi-Wavelength All-Optical 2R Regeneration Subsystems Based on Highly Non-Linear Fibers," presented at Transparent Optical Networks, 2007. ICTON '07. 9th International Conference on, 2007.
[72] M. Matsumoto, "Efficient all-optical 2R regeneration using self-phase modulation in bidirectional fiber configuration," *Opt. Express*, vol. 14, pp. 11018-11023, 2006.
[73] M. Daikoku, N. Yoshikane, T. Otani, and H. Tanaka, "Optical 40-gb/s 3R regenerator with a combination of the SPM and XAM effects for all-optical networks," *Lightwave Technology, Journal of*, vol. 24, pp. 1142-1148, 2006.
[74] M. Pantouvaki, M. J. Fice, R. Feced, E. P. Burr, R. Gwilliam, A. B. Krysa, J. S. Roberts, and A. J. Seeds, "10-Gb/s all-optical 2R regeneration using an MQW Fabry-Perot saturable absorber and a nonlinear fiber," *Photonics Technology Letters, IEEE*, vol. 16, pp. 617-619, 2004.
[75] C. Schubert, R. Ludwig, S. Watanabe, E. Futami, C. Schmidt, J. Berger, C. Boerner, S. Ferber, and H. G. Weber, "160 Gbit/s wavelength converter with 3R-regenerating capability," *Electronics Letters*, vol. 38, pp. 903-904, 2002.
[76] J. Suzuki, T. Tanemura, and K. Kikuchi, "All-optical regenerator based on XPM-induced wavelength shift in highly-nonlinear fiber at 40 Gb/s," presented at Lasers and Electro-Optics, 2005. (CLEO). Conference on, 2005.
[77] A. Bogoni, P. Ghelfi, M. Scaffardi, and L. Poti, "All-optical regeneration and demultiplexing for 160-gb/s transmission systems using a NOLM-based three-stage scheme," *Selected Topics in Quantum Electronics, IEEE Journal of*, vol. 10, pp. 192-196, 2004.
[78] F. Seguineau, B. Lavigne, D. Rouvillain, P. Brindel, P. Pierre, L. Pierre, and O. Leclerc, "Experimental demonstration of simple NOLM-based 2R regenerator for 42.66 Gbit/s WDM long-haul transmissions," presented at Optical Fiber Communication Conference, 2004. OFC 2004, 2004.
[79] C. Xu, X. Liu, and X. Wei, "Differential phase shift keying for high spectral efficiency optical transmissions," *IEEE Journal of Selected Topics in Quantum Electronics*, vol. 10, pp. 281-293, 2004.
[80] C. Pare, A. Villeneuve, P. A. Belanger, and N. J. Doran, "Compensating for dispersion and the nonlinear Kerr effect without phase conjugation," *Opt. Lett.*, vol. 21, pp. 459, 1996.
[81] I. R. Gabitov and P. M. Lushnikov, "Nonlinearity management in a dispersion managed system," *Optics Letters*, vol. 27, pp. 113-115, 2002.

[82] C. J. McKinstrie, S. Radic, and C. Xie, "Reduction of soliton phase jitter by in-line phase conjugation," *Opt. Lett.*, vol. 28, pp. 1519-1521, 2003.
[83] S. L. Jansen, D. van den Borne, G. D. Khoe, H. de Waardt, C. C. Monsalve, S. Spalter, and P. M. Krummrich, "Reduction of phase noise by mid-link spectral inversion in a DPSK based transmission system," presented at Optical Fiber Communication Conference, 2005. Technical Digest. OFC/NFOEC, 2005.
[84] C. Xu and X. Liu, "Postnonlinearity compensation with data-driven phase modulators in phase-shift keying transmission," *Opt. Lett.*, vol. 27, pp. 1619-1621, 2002.
[85] C. Xu, L. Mollenauer, and L. Xiang, "Compensation of nonlinear self-phase modulation with phase modulators," *Electronics Letters*, vol. 38, pp. 1578-1579, 2002.
[86] X. Liu, X. Wei, R. E. Slusher, and C. J. McKinstrie, "Improving transmission performance in differential phase-shift-keyed systems by use of lumped nonlinear phase-shift compensation," *Opt. Lett.*, vol. 27, pp. 1616-1618, 2002.
[87] J. Hansryd, J. v. Howe, and C. Xu, "Experimental demonstration of nonlinear phase jitter compensation in DPSK modulated fiber links," *Photonics Technology Letters, IEEE*, vol. 17, pp. 232-234, 2005.
[88] V. S. Grigoryan, M. Shin, P. Devgan, J. Lasri, and P. Kumar, "SOA-based regenerative amplification of phase-noise-degraded DPSK signals: dynamic analysis and demonstration," *Lightwave Technology, Journal of*, vol. 24, pp. 135-142, 2006.
[89] M. Shin, P. S. Devgan, V. S. Grigoryan, and P. Kumar, "SNR Improvement of DPSK signals in a semiconductor optical regenerative amplifier," *IEEE Photonics Technology Letters*, vol. 18, pp. 49-51, 2006.
[90] P. Johannisson, G. Adolfsson, and M. Karlsson, "Suppression of phase error in differential phase-shift keying data by amplitude regeneration," *Opt. Lett.*, vol. 31, pp. 1385-1387, 2006.
[91] C. C. Wei and J. Chen, "Convergence of phase noise in DPSK transmission systems by novel phase noise averagers," *Opt. Express*, vol. 14, pp. 9584-9593, 2006.
[92] M. Matsumoto, "A fiber-based all-optical 3R regenerator for DPSK signals," presented at Optical Transmission, Switching, and Subsystems IV, Gwangju, South Korea, 2006.
[93] M. Matsumoto, "Phase-preservation capability of all-optical amplitude regenerators using fiber nonlinearity," presented at Optical Fiber Communications (OFC), 2006.
[94] M. Matsumoto, "Regeneration of RZ-DPSK signals by fiber-based all-optical regenerators," *Photonics Technology Letters, IEEE*, vol. 17, pp. 1055-1057, 2005.
[95] M. Matsumoto, "Performance improvement of DPSK signal transmission by means of optical limiters using FWM in fibers," *IEEE Journal of Lightwave Technology*, vol. 23, pp. 2696-2701, 2005.

[96] M. Matsumoto, "Nonlinear phase noise reduction of DPSK signals by an all-optical amplitude limiter using FWM in a fiber," presented at European Conference on Optical Communications (ECOC), 2006.
[97] M. Matsumoto, "Simultaneous reshaping of OOK and DPSK signals by a fiber-based all-optical regenerator," *Opt. Express*, vol. 14, pp. 1430-1438, 2006.
[98] S. Boscolo, R. Bhamber, and S. K. Turitsyn, "Design of Raman-based NOLM for optical 2R regeneration of RZ-DPSK transmission," presented at Optical Fiber Communication Conference, 2006 and the 2006 National Fiber Optic Engineers Conference. OFC 2006, 2006.
[99] A. Striegler, M. Meissner, K. Cvecek, K. Sponsel, G. Leuchs, and B. Schmauss, "NOLM-based RZ-DPSK signal regeneration," *IEEE Photonics Technology Letters*, vol. 17, pp. 639-641, 2005.
[100] K. Croussore and G. Li, "Amplitude regeneration of RZ-DPSK signals based on four-wave mixing in fibre," *Electronics Letters*, vol. 43, pp. 177-178, 2007.
[101] K. Croussore, C. Kim, and G. Li, "All-optical regeneration of differential phase-shift keying signals based on phase-sensitive amplification," *Optics Letters*, vol. 29, pp. 2357-2359, 2004.
[102] K. Croussore, I. Kim, C. Kim, Y. Han, and G. Li, "Phase-and-amplitude regeneration of differential phase-shift keyed signals using a phase-sensitive amplifier," *Opt. Express*, vol. 14, pp. 2085-2094, 2006.
[103] K. Croussore and G. Li, "Phase Regeneration of NRZ-DPSK Signals Based on Symmetric-Pump Phase-Sensitive Amplification," *Photonics Technology Letters, IEEE*, vol. 19, pp. 864-866, 2007.
[104] K. Croussore, I. Kim, Y. Han, C. Kim, and G. Li, "Demonstration of phase regeneration of DPSK signals based on phase-sensitive amplification," *Optics Express*, vol. 13, pp. 3945-3950, 2005.
[105] G. P. Agrawal, "Modulation instability induced by cross-phase modulation," *Physical Review Letters*, vol. 59, pp. 880, 1987.
[106] R. Loudon, *The Quantum Theory of Light*, 3rd ed: Oxford Science Publications, 2000.
[107] S. M. Barnett and C. R. Gilson, "Photon-number fluctuations in phase-sensitive linear amplifiers," *Physical Review A*, vol. 40, pp. 6314, 1989.
[108] N. Bloembergen, *Nonlinear Optics*: W. A. Benjamin, Inc., 1965.
[109] D. F. Walls, in *Nature (London)*, vol. 306, 1983, pp. 141.
[110] L.-A. Wu, H. J. Kimble, J. L. Hall, and H. Wu, "Generation of Squeezed States by Parametric Down Conversion," *Physical Review Letters*, vol. 57, pp. 2520, 1986.
[111] R. E. Slusher, L. W. Hollberg, B. Yurke, J. C. Mertz, and J. F. Valley, "Observation of squeezed states generated by four-wave mixing in an optical cavity," *Physical Review Letters*, vol. 22, pp. 2409-2412, 1985.
[112] P. Kumar and J. H. Shapiro, "Squeezed-state generation via forward degenerate four-wave mixing," *Physical Review A*, vol. 30, pp. 1568, 1984.

[113] M. Shirasaki and H. A. Haus, "Squeezing of pulses in a nonlinear interferometer," *J. Opt. Soc. Am. B*, vol. 7, pp. 30, 1990.
[114] M. Marhic and C. Hsia, "Optical amplification and squeezed light generation in fibre interferometers performing degenerate four-wave mixing," *Quantum Optics*, vol. 3, pp. 341-357, 1991.
[115] M. E. Marhic, C. H. Hsia, and J. M. Jeong, "Optical Amplification in a nonlinear fiber interferometer," *Electronics Letters*, vol. 27, pp. 210-211, 1991.
[116] C. M. Caves, "Quantum limits on noise in linear amplifiers," *Physical Review D*, vol. 26, pp. 1817, 1982.
[117] H. P. Yuen, "Reduction of quantum fluctuation and suppression of the Gordon - Haus effect with phase-sensitive linear amplifiers," *Opt. Lett.*, vol. 17, pp. 73, 1992.
[118] W. Imajuku, A. Takada, and Y. Yamabayashi, "Low-noise amplification under the 3-dB noise figure in high-gain phase-sensitive amplifier," *Electronics Letters*, vol. 35, pp. 1954-1955, 1999.
[119] A. Takada and W. Imajuku, "Amplitude noise suppression using a high gain phase sensitive amplifier as a limiting amplifier," *Electronics Letters*, vol. 32, pp. 677-679, 1996.
[120] R. Li, P. Kumar, and W. L. Kath, "Dispersion compensation with phase-sensitive optical amplifiers," *IEEE Journal of Lightwave Technology*, vol. 12, pp. 541-549, 1994.
[121] C. J. McKinstrie and S. Radic, "Phase-sensitive amplification in a fiber," *Optics Express*, vol. 20, pp. 4973-4979, 2004.
[122] M. Vasilyev, "Distributed phase-sensitive amplification," *Optics Express*, vol. 13, pp. 7563-7571, 2005.
[123] R. Tang, P. Devgan, P. L. Voss, V. S. Grigoryan, and P. Kumar, "In-line frequency non-degenerate phase-sensitive fiber optical parametric amplifier," *IEEE Photonics Technology Letters*, vol. 17, pp. 1845-1847, 2005.
[124] Y. Mu and C. M. Savage, "Parametric amplifiers in phase-noise-limited optical communications," *J. Opt. Soc. Am. B*, vol. 9, pp. 65, 1992.
[125] W. Imajuku, A. Takada, and Y. Yamabayashi, "Inline coherent optical amplifier with a noise figure lower than 3 dB quantum limit," *Electronics Letters*, vol. 36, 2000.
[126] W. Imajuku and A. Takada, "In-line phase-sensitive amplifier with optical-PLL-controlled internal pump light source," *Electronics Letters*, vol. 33, pp. 2155-2156, 1997.
[127] W. Imajuku and A. Takada, "Optical phase-sensitive amplification using two phase-locked light sources," *Electronics Letters*, vol. 33, pp. 1403-1404, 1997.
[128] A. Takada and W. Imajuku, "In-line optical phase-sensitive amplifier employing pump laser injection-locked to input signal light," *Electronics Letters*, vol. 34, pp. 274-276, 1998.

[129] S. Norimatsu, K. Iwashita, and K. Noguchi, "An 8 Gb/s QPSK optical homodyne detection experiment using external-cavity laser diodes," *IEEE Photonics Technology Letters*, vol. 4, pp. 765-767, 1992.
[130] I. Kim, K. Croussore, X. Li, and G. Li, "All-Optical Carrier Synchronization Using a Phase-Sensitive Oscillator," *Photonics Technology Letters, IEEE*, vol. 19, pp. 987-989, 2007.
[131] I. Kim, K. Croussore, X. Li, G. Li, T. Hasegawa, and N. Sugimoto, "All-optical carrier phase and polarization recovery using a phase-sensitive oscillator," presented at Optical Fiber Communications (OFC), 2007.
[132] C. Dorrer, "Complete characterization of periodic optical sources by use of sampled test-plus-reference interferometry," *Optics Letters*, vol. 30, pp. 2022-2024, 2005.
[133] C. Dorrer, C. R. Doerr, I. Kang, R. Ryf, J. Leuthold, and P. J. Winzer, "Measurement of eye diagrams and constellation diagrams of optical sources using linear optics and waveguide technology," *IEEE Journal of Lightwave Technology*, vol. 23, pp. 178-186, 2005.
[134] I. Kim, C. Kim, and G. Li, "Requirements for the sampling source in coherent linear sampling," *Optics Express*, vol. 12, pp. 2723-2730, 2004.
[135] C. J. McKinstrie and M. G. Raymer, "Four-wave-mixing cascades near the zero-dispersion frequency," *Opt. Express*, vol. 14, pp. 9600-9610, 2006.
[136] C. J. McKinstrie, S. Radic, M. G. Raymer, and L. Schenato, "Unimpaired phase-sensitive amplification by vector four-wave mixing near the zero-dispersion frequency," *Opt. Express*, vol. 15, pp. 2178-2189, 2007.
[137] P. A. Andersen, T. Tokle, G. Yan, C. Peucheret, and P. Jeppesen, "Wavelength conversion of a 40-Gb/s RZ-DPSK signal using four-wave mixing in a dispersion-flattened highly nonlinear photonic crystal fiber," *Photonics Technology Letters, IEEE*, vol. 17, pp. 1908-1910, 2005.
[138] P. Devgan, R. Tang, V. S. Grigoryan, and P. Kumar, "Highly Efficient Multichannel Wavelength Conversion of DPSK Signals," *J. Lightwave Technol.*, vol. 24, pp. 3677-3682, 2006.
[139] L. Zhihong, D. Yi, M. Jinyu, W. Yixin, and L. Chao, "Cascaded all-optical wavelength conversion for RZ-DPSK signal based on four-wave mixing in semiconductor optical amplifier," *Photonics Technology Letters, IEEE*, vol. 16, pp. 1685-1687, 2004.
[140] C. McKinstrie, S. Radic, and M. Raymer, "Quantum noise properties of parametric amplifiers driven by two pump waves," *Opt. Express*, vol. 12, pp. 5037-5066, 2004.
[141] C. J. McKinstrie, S. Radic, and A. R. Chraplyvy, "Parametric amplifiers driven by two pump waves," *Selected Topics in Quantum Electronics, IEEE Journal of*, vol. 8, pp. 538-547, 2002.
[142] A. H. Gnauck, R. M. Jopson, C. J. McKinstrie, J. C. Centanni, and S. Radic, "Demonstration of Low-Noise Frequency Conversion by Bragg Scattering in a Fiber," *Opt. Express*, vol. 14, pp. 8989-8994, 2006.

[143] K. Inoue and T. Mukai, "Experimental study on noise characteristics of a gain-saturated fiber optical parametric amplifier," *Lightwave Technology, Journal of*, vol. 20, pp. 969-974, 2002.
[144] P. Vorreau, A. Marculescu, J. Wang, G. Bottger, B. Sartorius, C. Bornholdt, J. Slovak, M. Schlak, C. Schmidt, S. Tsadka, W. Freude, and J. Leuthold, "Cascadability and Regenerative Properties of SOA All-Optical DPSK Wavelength Converters," *Photonics Technology Letters, IEEE*, vol. 18, pp. 1970-1972, 2006.
[145] B. Sartorius, C. Bornholdt, J. Slovak, M. Schlak, C. Schmidt, A. Marculescu, P. Vorreau, S. Tsadka, W. Freude, and J. Leuthold, "All-optical DPSK wavelength converter based on MZI with integrated SOAs and phase shifters," presented at Optical Fiber Communication Conference, 2006 and the 2006 National Fiber Optic Engineers Conference. OFC 2006, 2006.
[146] I. Kang, C. Dorrer, L. Zhang, M. Rasras, L. Buhl, A. Bhardwaj, S. Cabot, M. Dinu, X. Liu, M. Cappuzzo, L. Gomez, A. Wong-Foy, Y. F. Chen, S. Patel, D. T. Neilson, J. Jacques, and C. R. Giles, "Regenerative all optical wavelength conversion of 40-Gb/s DPSK signals using a semiconductor optical amplifier Mach-Zehnder interferometer," *IEE Conference Publications*, vol. 2005, pp. v6-29-v6-29, 2005.
[147] C. J. McKinstrie, M. G. Raymer, S. Radic, and M. V. Vasilyev, "Quantum mechanics of phase-sensitive amplification in a fiber," *Optics Communications*, vol. 257, pp. 146-163, 2006.
[148] S. Komaki, A. Akeyama, and O. Kurita, "Direct phase regeneration of a 400 Mbit/s QPSK signal at 1.7 GHz," *IEEE Transactions on Communications*, vol. 27, pp. 1829-1836, 1979.